8-2014

Mineralized microbialites as archives of environmental evolution of a hypersaline lake basin: Laguna Negra, Catamarca Province, Argentina

Joy Buongiorno
University of Tennessee - Knoxville, jbuongio@utk.edu

To the Graduate Council:

I am submitting herewith a thesis written by Joy Buongiorno entitled "Mineralized microbialites as archives of environmental evolution of a hypersaline lake basin: Laguna Negra, Catamarca Province, Argentina." I have examined the final electronic copy of this thesis for form and content and recommend that it be accepted in partial fulfillment of the requirements for the degree of Master of Science, with a major in Geology.

Linda C. Kah, Major Professor

We have read this thesis and recommend its acceptance:

Annette S. Engel, Colin D. Sumrall

Accepted for the Council:
Carolyn R. Hodges

Vice Provost and Dean of the Graduate School

(Original signatures are on file with official student records.)

Mineralized microbialites as archives of environmental evolution of a hypersaline lake basin: Laguna Negra, Catamarca Province, Argentina

A Thesis Presented for the

Master of Science

Degree

The University of Tennessee, Knoxville

Joy Buongiorno

August 2014

Dedication

For our beloved Nala, the most beautiful princess of a kitty there ever was. Rest in peace in the land of milk and honey ham, Nalabear.

Acknowledgements

I would like to express my immense appreciation to my thesis advisor, Linda Kah, for the boundless encouragement, thoughtfulness, and dedication.

I also owe a great debt to my lab mates and fellow graduate students who helped me through this process in countless ways.

Most of all, I am sincerely grateful to Michael Altom for his endless support and love.

Abstract

Environmental fluctuations related to climate, biological productivity, and evaporation can be recorded by sedimentary archives within lacustrine depositional systems. Sediments within terminal, closed-basin lakes are amongst the most sensitive paleoenvironmental indicators, and have great potential for permitting detailed reconstruction of environmental conditions via a variety of geochemical and isotopic proxies. Microbialites, however, have been largely overlooked as repositories of paleoenvironmental data. Here, we investigate mineralized microbialites within Laguna Negra, a high-altitude (4100 meters above sea level) hypersaline, closed-basin lake in the Argentinian Puna region and explore the potential recovery of environmental signals from these unique sedimentary archives. Mineralized microbialites within Laguna Negra preserve complex layering composed of three distinct carbonate fabrics—isopachous cement phases, botryoidal precipitates, and microbially-associated micrite. These phases are interpreted to reflect differential physical and biological influences on carbonate nucleation and growth. Detailed preservation of successive laminae within these microbialites provides the opportunity for time-wise reconstruction of geochemical signatures.

Geochemical analysis of Laguna Negra microbialites shows overall range of δ^{13}[delta-13]C_{carb}[carbonate carbon] is from +5.75‰ [permil] to +18.25‰ and from -2.04‰ to +7.36‰ for δ^{18}[delta-18]O_{carb}[carbonate oxygen]. Long-term signals preserved within successive laminae of lighter $\delta^{13}C_{carb}$ and $\delta^{18}O_{carb}$ through time suggests increased input water contribution since the beginning of microbialite deposition. General hydrological evolution of Laguna Negra is

reconstructed via integration of observed oxygen isotopes signatures with published water balance models, and is consistent with regional records from other lacustrine systems. Examination of paired $\delta^{13}C_{carb}$ and δ^{13}[delta-13]C_{org}[organic carbon] permits interpretation of the relative effects of evaporation and biotic activity in the evolution of Laguna Negra, and reveals that extrinsic parameters, such as CO_2 [carbon dioxide] degassing and evaporation are the primary control on isotopic evolution.

Geochemical and petrographic differences between microbialites across a spatial gradient, however, suggest that Laguna Negra microbialites also preserve signals that represent both heterogeneous evolution of environments within the lake and influence of biogenic activity. Ultimately, understanding of the relative effects of environmental and biotic parameters on the evolution of lacustrine deposits will enhance our understanding of both paleoenvironmental change and its potential relationship to microbialite mineralization.

Table of Contents

List of Tables

List of Figures

Section 1: Introduction

The Andean Altiplano is located between the modern tropical and extratropical rainfall belts and is extremely sensitive to climatic change. Fluctuation in hydrological regime during the late Pleistocene and Holocene have been preserved by a variety of paleoclimatic records, including ice cores (Thompson *et al*., 2000), tree rings (Christie *et al*., 2011), and lake sediment cores (Valero-Garcés *et al*., 1996; Schwalb *et al*., 1999; Valero-Garcés *et al*., 2000; Abbott *et al*., 2003). Despite a large number of studies dedicated to paleoclimate reconstruction, inconsistencies among proxy data suggest that different sedimentary archives record distinct scales of hydrological interaction. For example, regional groundwater bodies and paleosols of the Atacama Desert are slow in responding to climate change, and therefore, proxies that sample these repositories provide robust data on timescales of centuries to millennia (Grosjean *et al*., 2003). By contrast, proxies such as pollen and rodent middens provide information that results from climatic variability on seasonal to inter-annual scales (Grosjean *et al*., 2003). As a result of the inherent variability regarding the scale to which proxies can be applied, sound paleoenvironmental reconstruction requires detailed understanding of the limitations of different sedimentary archives.

Lacustrine sediments offer multiple avenues of proxy information through which paleoenvironments may be reconstructed. Specifically, sediments within lakes and salars can record decadal to centennial climate variability (Grosjean *et al*., 2003) via inorganic carbon and

oxygen isotopes (Grosjean, 1994; Schwalb *et al*., 1999), organic elemental ratios and carbon isotopes (Pueyo *et al*., 2011), and trace metal concentrations within carbonate (Chivas *et al*., 1993; Valero-Garcés *et al*., 1996). Preservation of high-resolution records also permits interpretation of a range of environmental conditions that may reflect a combination of abiotic and biotic drivers. For example, ecological conditions related to periods of enhanced biological productivity can be reflected in the isotopic composition of organic carbon (Meyers & Horie, 1993; Meyers & Lallier-vergés, 1999). Productivity, however, is often dependent upon rates of evaporation and precipitation within the basin (Valero-Garcés *et al*., 2000; Grosjean, 2001), which in turn, can be reconstructed via oxygen isotopes and trace elements (cf. Frantz *et al*., 2012; De Cort *et al*., 2013;).

Hydrologically closed basins, in which water export occurs only through evaporation—and, in particular, hypersaline lakes within these closed basins—are unusually sensitive to climate change, and serve as critical paleoenvironmental sensors (Valero-Garcés *et al*., 1996; Grosjean *et al*., 1997). Laguna Negra, Catamarca Province, Argentina (27°38'S, 68°32' W) is a terminal hypersaline lake within the Laguna Verde closed basin system. In order to better understand the history of environmental fluctuations in climate and water balance—as well as the nature and degree to which these physical agents have driven changes in productivity within Laguna Negra since the Late Holocene—we present a multi-proxy analysis of lake sediments. Whereas limnogeological studies most commonly examine lake sediment cores, here we examine mineralogical and geochemical records preserved within laminated, mineralized microbialites. Laguna Negra microbialites consist of concentrically laminated structures (Gomez

et al., *in press*). We systematically examine successive laminae for petrographic textures, mineralogy, isotopic composition of carbonate (oxygen and carbon) and organic constituents, and elemental compositions of carbonate phases. Combining geochemical data and hydrological models, we build a time-wise reconstruction of paleohydrological variation within Laguna Negra. Comparison of observed and modeled records from Laguna Negra with those of other regional lake records (Grosjean *et al*., 1997; Valero-Garcés *et al*., 2000) will test whether mineralized microbialites within Laguna Negra provide an effective archive of paleoenvironmental change.

Section 2: Geological Setting

The Andean Altiplano is a volcanic plateau with an average elevation of 4,000 meters above sea level, with volcanic peaks reaching up to 6,000 meters in elevation (Fig. 1). Block faulting during Cenozoic uplift resulted in several large, topographically isolated basins that are filled with extensive siliciclastic, evaporite, and carbonate deposits (Strecker *et al*., 1989; Alonso *et al*., 1991; Valero-Garcés *et al*., 2000; Carrapa *et al*., 2005; Bissig & Riquelme, 2010). These closed basins occur within a region of northwestern Argentina where the Subandean, Interandean, and Eastern Cordillera mountain ranges effectively block of moisture from both the Amazon basin and the Atlantic, resulting in less than 200 mm/year of precipitation, most of which is in the form of snowfall (Vuille & Ammann, 1997; Strecker *et al*., 2007; Garreaud *et al*., 2009). Additionally, subtropical high-pressures across the region provide an atmospheric structure that results in stable, extremely arid conditions (Bookhagen *et al*., 2001). Across the region, sedimentary records reflect the presence of a long-term, strongly negative water balance (Valero-Garcés *et al*., 1996; Grosjean *et al*., 1997; Schwalb *et al*., 1999; Valero-Garcés *et al*., 2000).

Laguna Negra

Laguna Negra is the southernmost lake within the Laguna Verde Complex (LVC), which is a series of hypersaline lakes within the southernmost Puna region, Catamarca Province,

Argentina (Fig. 1a). Unlike extensively studied salars of the Chilean Atacama (Grosjean, 1994; Valero-Garcés *et al*., 1996; Grosjean *et al*., 1997), the paleoenvironmental information within the LVC remains relatively unstudied. Laguna Negra is shallow (<2 m deep) and has a current area of ~8.6 km^2 (Fig. 1c). The lake contains no surface outflow and is isolated from the other lakes in the LVC by an extensive salt flat that covers more than half of the lake basin. Terrestrially-sourced input waters enter at the southwestern margin of the lake, and correspond to the primary location of open water within the basin.

Mineralized microbialites (Fig. 2) are located exclusively along the southwestern margin of the lake. As with other hypersaline lake basins within the Altiplano, eukaryotic growth is severely restricted by severe aridity, extreme daily and seasonal temperature fluctuations, and intense UV radiation (Ordoñez, 2009). Within Laguna Negra, a single species of salt marsh grass (*Spartina* sp.) occurs along southwest lake margin, at the point of freshwater input. Organic matter (OM) production is dominated by microbial mats, containing a consortia of cyanobacteria and pennate and centric diatoms (*Surirella*) in the upper 1-3 mm of the mat, an undermat containing purple and green sulfur bacteria, and a thick black horizon dominated by microbial sulfur reduction (Gomez *et al*., *in press*). Such consortia are similar to other high-elevation Andean lake (Ordoñez, 2009). These mats are restricted to the southern margin of the lake, and are spatially associated with microbial carbonate (Fig. 2). Throughout most of the lake, the substrate consists of unconsolidated immature silt, sand, and volcanic lithic components (Gomez *et al*., *in press*).

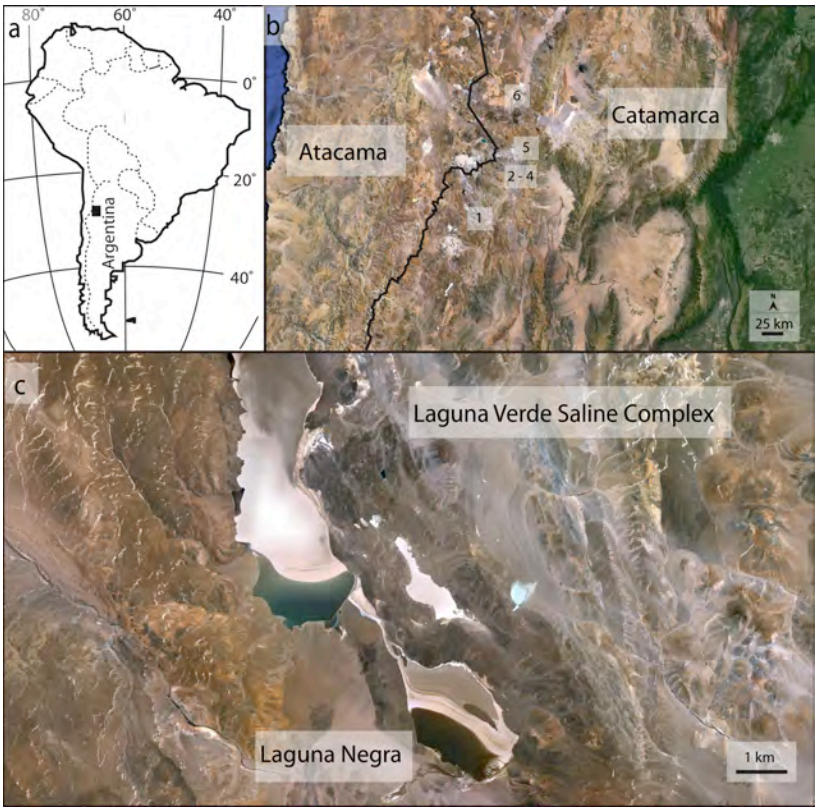

Figure 1: (a) Catamarca province, NW Argentina, where the Laguna Verde Saline Complex (LVC) is located. (b) Locations of other lake complexes in the Puna of Argentina, including (1) Laguna Negra (this study), (2) San Francisco Basin (Valero-Garcés et al., 2000; 2001), (3) Laguna Miscanti (Valero-Garcés et al., 1996), (4) Lake Lejia (Grosjean, 1994), (5) Las Peladas (Valero-Garcés et al., 2001), and (6) and El Peindo (Valero-Garcés et al 2000; 2001). (c) Detail of the LVC. Laguna Negra is the southernmost lake within the LVC and is separated from the other lakes within the complex by halite deposits. Regional geology consists of andesitic to balsaltic volcanic rocks as well as numerous closed-basin lakes containing siliciclastic, carbonate, and evaporite lithologies.

Lake Chemistry

Measurements of lake water chemistry reveal that lake waters within Laguna Negra consist of a Ca-, Na-, and Cl-rich brine (Gomez *et al*., *in press*). Salinity is as high as 309‰, alkalinity, expressed as Total Alkalinity (carbonate, bicarbonate, and hydroxide alkalinity) is approximately 833 mg/L, and [CO_2] [the concentration of carbon dioxide] is 3002 ppmv as determined through titration with sodium hydroxide to the phenolphthalein end-point in 100 mL samples (Table 1). These values are in stark contrast to brackish inlet waters that reflects their origin from glacial snowmelt, with an average salinity of 18 ‰, alkalinity of 270 mg/L, and [CO_2] of 216 mg/L. The measured concentration of calcium within lake waters is elevated compared to theoretical ionic concentrations (Gomez *et al*., *in press*), suggesting a possible contribution from calcium-rich regional deep ground waters that circulate within Ordovician limestone (cf. Risacher, 2003). These elevated calcium ion concentrations are responsible for the relatively low molar Mg/Ca ratios of both lake (0.41) and mixing zone (0.78) waters relative to other closed, saline basins in the Altiplano region of Chile and Northwestern Argentina, which typically range from 3.2 to ≥10 (Valero-Garcés *et al*., 1996; Risacher *et al*., 1999; Valero-Garcés *et al*., 1999; Valero-Garcés *et al*., 2000; Pueyo *et al*., 2011).

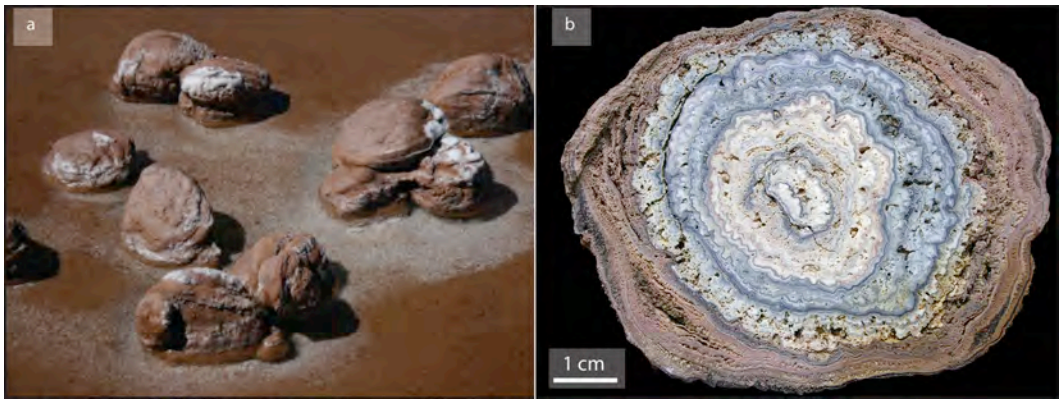

Figure 2: (a) Microbialites of Laguna Negra (b) Slab section showing concentric, millimeter-scale lamination.

Table 1: Hydrochemical measurements made in 2009 on inlet, lake, and mixing zone waters (Gomez et al., in press).

Sample	Water type	pH	CO_2	Temp	Salinity	Hard-ness	Alkalinity	Na^+	K^+	Mg^{2+}	Ca^{2+}	Cl^-	SO_4^{2-}
			mg/L	C	ppt	mg/L	mg/L	mg/L	mg/L	mg/L	mg/L	mg/L	mg/L
1	Lake	5.7	2886	18.5	325	10900	880	61921	3998	5180	14650	196100	82
2	Lake	5.6	3520	15.7	317	n.d.	930	61562	5320	7180	14650	204800	95
3	Mixing Zone	7.7	231	21.7	16	12800	550	2969	293	400	330	75200	128
4	Mixing Zone	6.5	982	20.8	120	38100	300	28894	1328	2150	6120	68800	176
6	Inlet Water	7.8	214	20.8	15	5300	290	2845	158	450	820	9450	31
7	Inlet Water	7.8	218	20.0	9	2000	430	876	146	260	460	5630	21.7
8	Inlet Water	7.4	288	22.8	27	6600	200	6638	379	1230	2630	19990	495
9	Inlet Water	7.5	285	23.1	22	5300	160	4154	178	970	1910	13780	322
10	Lake	5.8	2601	6.8	286	90000	690	90922	7420	7680	19280	198100	108
11	Inlet Water	5.7	2562	31.1	316	83900	330	14372 6	6216	6640	19210	208400	104
12	Inlet Water	6.8	423	31.6	63	24000	40	6902	258	1590	5740	38830	506
Avg.	Lake	5.7	3002	13.6	309	50450	833	71468	5579	6680	16193	199666	95
Avg.	Mixing Zone	7.2	665	24.9	27	21183	241	27523	1222	1856	5128	49346	246
Avg.	Inlet	7.1	606	21.3	68	25450	425	15931	810	1275	3225	72000	152

In addition to broad differences between lake and inlet waters, initial water chemistry measurements show persistent chemical zones along the southern edge of Laguna Negra (Gomez *et al*., *in press*). This shallow water margin reflects the northward progradation of alluvial fan deposits and corresponds to the region of microbialite mineralization. Zone 1 is located at the southernmost margin of the lake and contains the source of fresh inlet water. Its location is marked by nearshore salt marsh grass, *Spartina* sp. (Figs. 3a, b). Zone 2 is an intermediate zone between fresh waters of Zone 1 and more brackish waters and contains ponds with active microbial growth (Figs. 3a, c). Zone 3 reflects a zone of mixing between inlet and lake waters, and represents the exclusive region of microbialite mineralization (Figs. 3a, d-f).

Microbial carbonate deposition is restricted to Zone 3, and is referred to as the stromatolite belt (Gomez *et al*., 2012). Initial data suggests that the stromatolite belt, itself, contains heterogeneous hydrochemistry inferred to result from a combination of spatial differences in the extent of mixing and evaporation (Gomez *et al*., *in press*). Within these zones, laminar mineralized crusts are located primarily within Zone 3A (Fig. 3d); Zone 3B is dominated by centimeter-scale carbonate gravels (Fig. 3e); and Zone 3C contains the most extensive accumulations of microbial oncolites (Fig. 4f). Samples for this study were collected from Zone 3A and Zone 3C.

Figure 3: Geochemical zones of Laguna Negra. (a) Map view of zonation, modified from Gomez et al., in press. (b) Zone 1 characterized by freshwater inlet and salt marsh grass. (c) Microbial mats within Zone 2. (d) Laminar microbialite crusts in Zone 3A, the zone farthest from fresh water source. (e) Carbonate gravels within Zone 3B. (f) Spheroidal to discoidal microbialites within Zone 3C.

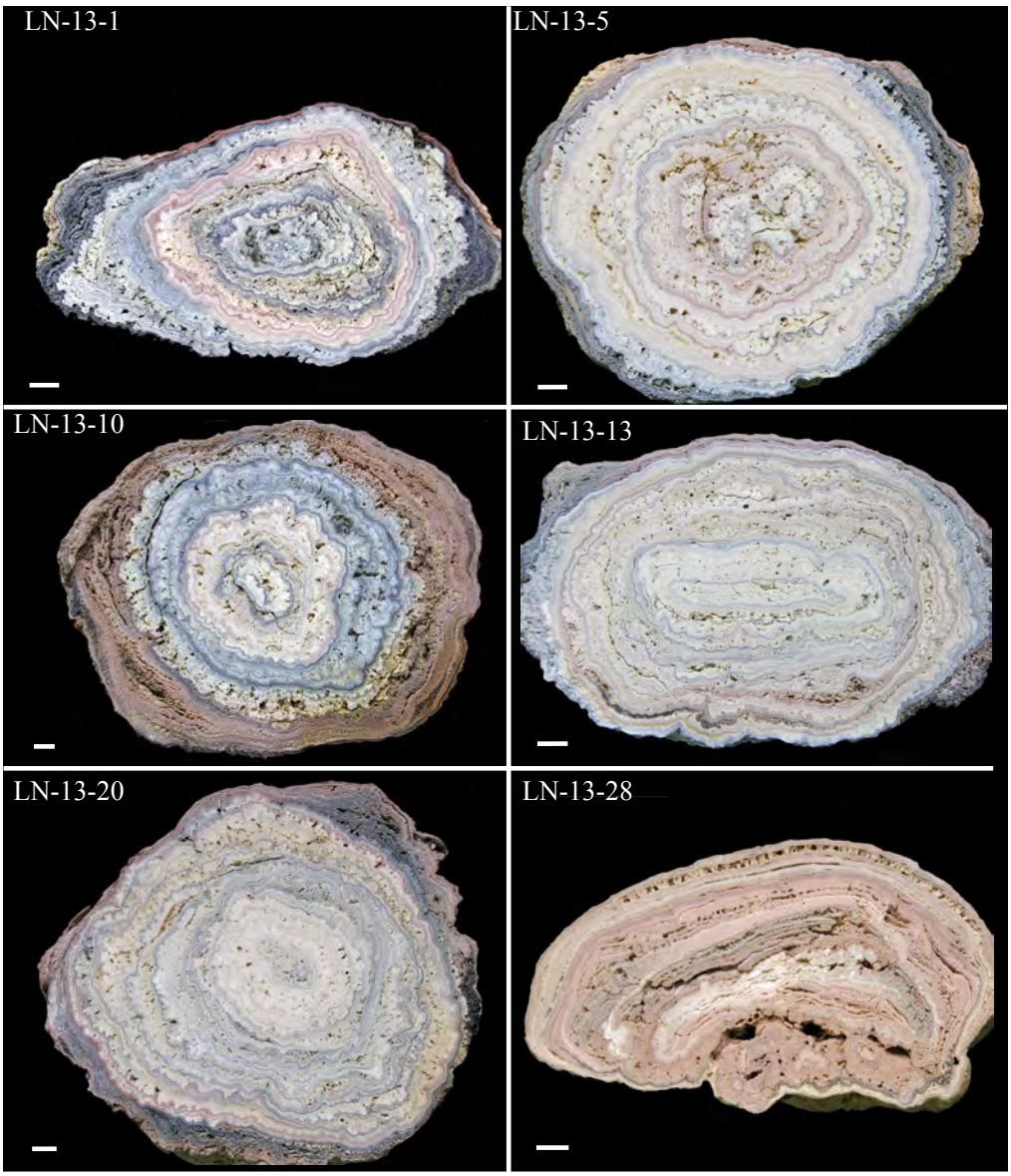

Figure 4: Microbialites used in this study. Samples LN-13-1 through LN-13-20 are interpreted as "microbially-mediated", whereas sample LN-13-28 is interpreted as "chemically precipitated". Scale bars are 1 cm.

Section 3: Microbialites as Paleoenvironmental Archives

Microbialites are organosedimentary structures (Burne & Moore, 1987) that contain lamination that result from the complex interplay of extrinsic (environmental) and intrinsic (ecological) factors (Riding, 2011; Bosak *et al*., 2013). Lamination can result from a combination of trapping and binding of detrital material (cf. coarse-grained microbialites; Riding *et al*., 1991; Reid *et al*., 2003; Dupraz *et al*., 2013), and the *in situ* precipitation of carbonate minerals (cf. micrite and cement-dominated microbialites; Riding, 2008). The inherent dependence of lamina formation on the environmental conditions—e.g., the supply of detrital sediment or the ambient saturation state of carbonate minerals—combined with the successive accretion of laminae through time suggest that lacustrine microbialites, in particular, may prove to be critical repositories of paleoenvironmental information.

Although broadly underutilized as detailed environmental archives, microbialites have been employed in combination with isotope proxies to reconstruct elements of lake hydrology (Arp *et al*., 2005; Last *et al*., 2010; Kaźmierczak *et al*., 2011; Frantz *et al*., 2012; Ghinassi *et al*., 2012). A growing concern, however, involves the degree to which microbial processes may overprint environmental records preserved in microbialite lamination. Specifically, diverse microbial communities that comprise microbial mats can both evolve in response to changing environmental conditions and can alter regional to microscale environments through metabolic activity (Visscher *et al*., 2000; Dupraz & Visscher, 2005; Braissant *et al*., 2007; Dupraz *et al*.,

2009; Meister, 2013). Additionally, microbial activity can affect local carbonate saturation by increasing local pH through CO_2 fixation, heterotrophic respiration (e.g. sulfate reduction), and degradation of extracellular polymeric substance (EPS; Dupraz *et al*., 2009 *for review*).

Laguna Negra microbialites

Mineralized microbialites within Laguna Negra occur as laminar crusts and spheroidal to discoidal concentrically laminated oncoids that range from a few centimeters to ~30 cm in diameter (Fig 2). Platy crusts and oncoids are distributed across Zone 3 (Fig. 3f), where they occur both as subaerially exposed accumulations and as discrete bodies within the sediment subsurface (Gomez *et al*., *in press*). Although the morphology of microbialites varies across exposure area, laminar crusts (sample LN-13-28) are most common in Zone 3A and spheroidal oncolite forms (samples LN-13-1, LN-13-5; LN-13-10; LN-13-13; LN-13-20) are more common in Zone 3C (Fig. 4). Spatial variation in morphology may reflect, in part, water depth, which is typically shallower in Zone 3A. Many oncoids show discrete external ridges that represent outward growth at the air-water interface, potentially, associated with evaporation-driven mineral precipitation.

Oncolite growth occurs through the accretion of broadly concentric, smooth to irregular laminae, which vary in color from white to red to green. Coloration changes are potentially reflective of vertical stratification of microbial communities containing characteristic pigmentation. Whereas upper surfaces exposed above the sediment-water interface are typically

orange in color, which are speculated to result from cyanobacterial UV-attenuating pigments, carotenoid and scytonemin (Proteau *et al*., 1993), portions of oncoids that occur at or beneath the sediment-water interface are commonly dark green to black in color, suggesting a transition from photoautotrophic groups (green and purple bacteria) to heterotrophic groups (sulfate reducing bacteria; SRB; Gomez *et al*., *in press*).

At present, there is little constraint as to the rate of lamina accretion in Laguna Negra oncolites. Microbial lamination has been suggested, in various cases, to represent diurnal (Golubic & Focke, 1978; Bissett *et al*., 2008), seasonal (Konhauser *et al*., 2001), or even annual or perennial (Grotzinger & Knoll, 1999; Petryshyn *et al*., 2012) deposition. Constraining the frequency with which laminae are accreted within Laguna Negra microbialites would enhance our ability to correlate geochemical changes across microbialites through space and time. Uncertainty in the time represented by successive laminae may be the greatest hindrance to using mineralized microbialites as paleoenvironmental proxies; yet, despite this uncertainty, microbialites of Laguna Negra record time-series within successive laminae, allowing reconstruction of time-wise changes in the lake environment based upon superposition of layers and relative age within individual microbialites. It is also important to note that discontinuities are also present within microbialites, with discrete laminae sometimes pinching out. Lack of complex organic matter precludes the use of C^{14} age dating of Laguna Negra microbialites, however, preliminary U-Th dating provides an age of 2443 ± 252 for the innermost laminae and 1057 ± 283 for the outermost laminae (Gomez *et al*., *in press*), which indicates deposition beginning during the Late Holocene with laminae accretion on decadal time scales.

Section 4: Analytical Methods

Sample collection

Microbialites were collected within Laguna Negra from chemical zones 3A and 3C during austral Fall 2013. Individual samples were sawed in half with water and photographed; samples with the potential for longest time series (i.e., the greatest number of consecutive laminae) were prepared for petrographic and geochemical analyses. For each sample, one half was impregnated with epoxy for thin sectioning, while the matching face was left free of secondary treatment and prepared for biogeochemical analyses (inorganic and organic isotopes, elemental abundances, mineralogy, total carbon). Laminae were identified and traced in photographic images, and identified in terms of their petrographic expressions. Geochemical analyses were conducted on splits of sample powder that were drilled from discrete laminae using a microdrill press fitted with carbide drill bits measuring 0.25 to 1 mm in diameter.

Mineralogical identification

Mineralogical identification was conducted on multiple samples using standard powder X-ray diffraction (XRD) analyses with a Rigaku Ultima IV at The University of Tennessee, Knoxville. Eleven laminae across 5 samples were analyzed. Counts were taken from 4° to 70°

(2-theta) at a rate of 2°/minute, with 40 kilovolts and 30 milliamperes. Resulting spectra were analyzed via PDXL software.

Isotopic composition of carbonate phases

Carbon and oxygen isotopic values of carbonate phases utilized approximately 150 μg of sample powder. Sample was reacted with 100% orthophosphoric acid (H_3PO_4) in an He-flushed, sealed tube. Liberated CO_2 was sampled with a Finnigan Gas Bench II, and isotopic ratios were measured with a Thermo Fischer Delta V Advantage Isotope Ratio Mass Spectrometer at Washington University, St. Louis, Missouri. Results are expressed in standard delta notation (δ) as the per mil (‰) difference relative to in-house standards calibrated to the Vienna Pee Dee Belemnite (VPDB) marine carbonate standard for oxygen and carbon:

$$\delta‰ = [(R_{sample\text{-}} - R_{standard}/R_{standard})] - 1) * 1000 \qquad (1)$$

where R is the ratio (^{13}C:^{12}C) for carbon and (^{18}O:^{16}O) for oxygen. Sample heterogeneity contributes to overall uncertainty, which is based upon duplicate analyses of standards. Results are better than 0.2 ‰ for both $\delta^{13}C$ and $\delta^{18}O$. Conversion of PDB values to SMOW (standard mean ocean water) was carried out according to:

$$\delta^{18}O_{SMOW} = 1.03091(\delta^{18}O_{PDB}) + 30.91 \text{ (2) (Friedman \& O'Neil, 1977)}$$

Elemental compositions of carbonate phases

Major, minor and trace element abundances were determined using a Perkin-Elmer Inductively Coupled Plasma Optical Emission Spectroscopy (ICP-OES) at the University of Tennessee, Knoxville. Approximately 1.5 mg of sample power was dissolved in 10 mL 2% nitric acid. Insoluble material was pelleted by centrifugation and the supernatant was decanted into clean sample tubes. Samples were analyzed for Ca, Mg, Fe, Sr, and Mn and spectra were calibrated to a series of gravimetrically determined standards. Reproducibility was better than ± 4 ppm for calcium, ± 2 ppm for magnesium, ± 0.004 ppm for iron, ± 0.005 ppm for strontium, and ± 0.004 ppm for manganese based upon replicate measurements of standard solutions.

Organic carbon analyses

In order to determine the quantity of material required for organic carbon analysis, total carbon (TC) and total inorganic carbon (TIC) were measured with a CM5015 CO_2 coulometer with a manual acidification module and high temperature furnace at the University of Tennessee. TOC was calculated as the difference between TC and TIC:

$$\% \text{ TOC} = \text{TC} - \text{TIC} \qquad (3)$$

For both TC and TIC, ~5 mg of sample powder was used. Percentage of TC is reported from photodetection of percent transmittance after sample powder was combusted in a ceramic

boat at 900°C in pure O_2 for 12 minutes. TIC is recorded via titration CO_2 liberated though reaction with 2N hydrochloric acid. Analytical errors were ± 0.4% for TIC and ± 0.7% for TC based upon replicate of powder samples.

Powders from several laminae were combined to isolate enough material for organic matter analyses, resulting in a substantially coarser resolution than single lamina analysis. Successive laminae were grouped together according to similarity in isotopic value and color in hand sample. Sample powders were combined and acidified to completion with 10% acetic acid and rinsed with deionized water. Carbon and nitrogen content of organic matter and isotopic composition of organic carbon was determined using a Delta V Plus mass-spectrometer at Washington University. Standards for organic carbon isotopes included graphite, sucrose, and IAEA-CH-3. Duplicate analyses of standards show results are ±0.4‰.

Statistics

Tukey Test

Statistically significant differences in observed isotopic compositions between the center-most and outer-most laminae were determined through Tukey range testing. Testing was conducted on pseudo-replicates in lieu of standard replicate data, which would require a large number of samples. Our pseudo-replicates included four successive laminae in each microbialite as replicates used for statistical testing. It is crucial to note, however, that use of this technique with pseudo-replicates carries the connotation of a genetic relationship between grouped

laminae, which is not necessarily the case. The Tukey method is a single-step statistical test that compares means through a combination of ANOVA and pair-wise comparison of means. Tukey testing was applied as an additional means to corroborate the qualitatively observed trend in isotope data with a quantitative approach.

Principal Component Analysis (PCA)

Multivariate principal component analysis was conducted in PAST (Paleontological Statistic Software; Hammer *et al*., 2001) on samples separated by fabric type (isopachous, micritic, botryoidal) and their respective measured strontium concentrations, magnesium to calcium ratios, oxygen and carbon isotopes of carbonate, and mineralogy.

Section 5: Results and Interpretation

Petrographic components

Petrographic analysis reveals that Laguna Negra microbialite laminae are composed of three discrete microfabric types: isopachous, botryoidal, and micritic (Fig. 5; see also Gomez *et al*., *in press*). XRD was performed on 11 discrete laminae, representing multiple samples of each lamina type. Microbialites contain both aragonite and calcite in each lamina type, although higher abundances of aragonite occur in sample LN-13-28 from Zone 3A, which are dominated by isopachous laminae. Despite confirmation of aragonite mineralogies, all samples have mole % $MgCO_3 < 5.27\%$, reflecting low Mg/Ca ratios of lake waters. Isopachous laminae are typically continuous, uniform in thickness (50–100 μm thick), and exhibit a high degree of inheritance. Combined, these features result in smooth surface morphologies that typify this fabric type (e.g. LN-13-28). Isopachous laminae consist of acicular carbonate that displays both competitive and syntaxial growth, with competitive growth fabrics making initiation of isopachous growth over other laminae types. Isopachous bands do not contain morphologically identifiable microbial or algal elements. UV fluorescence, however, reveals rhythmic microbands within laminae, suggesting variation in the amount of OM incorporated during growth. High degree of inheritance during laminae accretion, coupled with uniform thickness throughout the trace of individual laminae, suggests that isopachous laminae represent primarily abiotic, or chemically, induced changes in carbonate saturation and calcite precipitation, which is speculated to occur

during mixing of lake waters with inlet waters and degassing of CO_2 (Gomez *et al*., *in press*). Although isopachous laminae are present in all samples, it is the dominant fabric type in oncoids collected within Zone 3A (cf. LN-13-28).

Botryoidal layers are composed of clear, radially-oriented carbonate crystals of both aragonite and calcite. Individual botryoids average ~230 μm tall and ~320 μm wide, although larger botryoids occur in oncolites collected from Zone 3A (cf. LN-13-28). Inheritance from underlying layers is irregular and thickness is variable both within and between botryoidal laminae. Botryoidal fabrics occur primarily as individual botryoids surrounding micritic nuclei, or as stacked botryoids that fringe micritic clumps, creating more laterally continuous laminae. In most cases, botryoidal fabrics encompass diatom (primarily pennate and centric) remains. Abundance of associated diatoms and elevated fluorescence of sedimentary organic matter at botryoid centers leads to the speculation of organic materials to aid in carbonate nucleation. For example, diatom extracellular polymeric substance (EPS) has been suggested to serve as an organic template for carbonate mineralization as well as provide ions, such as Ca^{2+}, that can contribute to calcium carbonate formation during organic matter degradation (Dupraz *et al*., 2009).

Micritic laminae are irregular in thickness (45–650 μm thick) and are a dominant component of Laguna Negra microbialites. Micritic laminae contribute substantially to the irregular surface morphology of the microbialites, with highly variable inheritance. Micritic

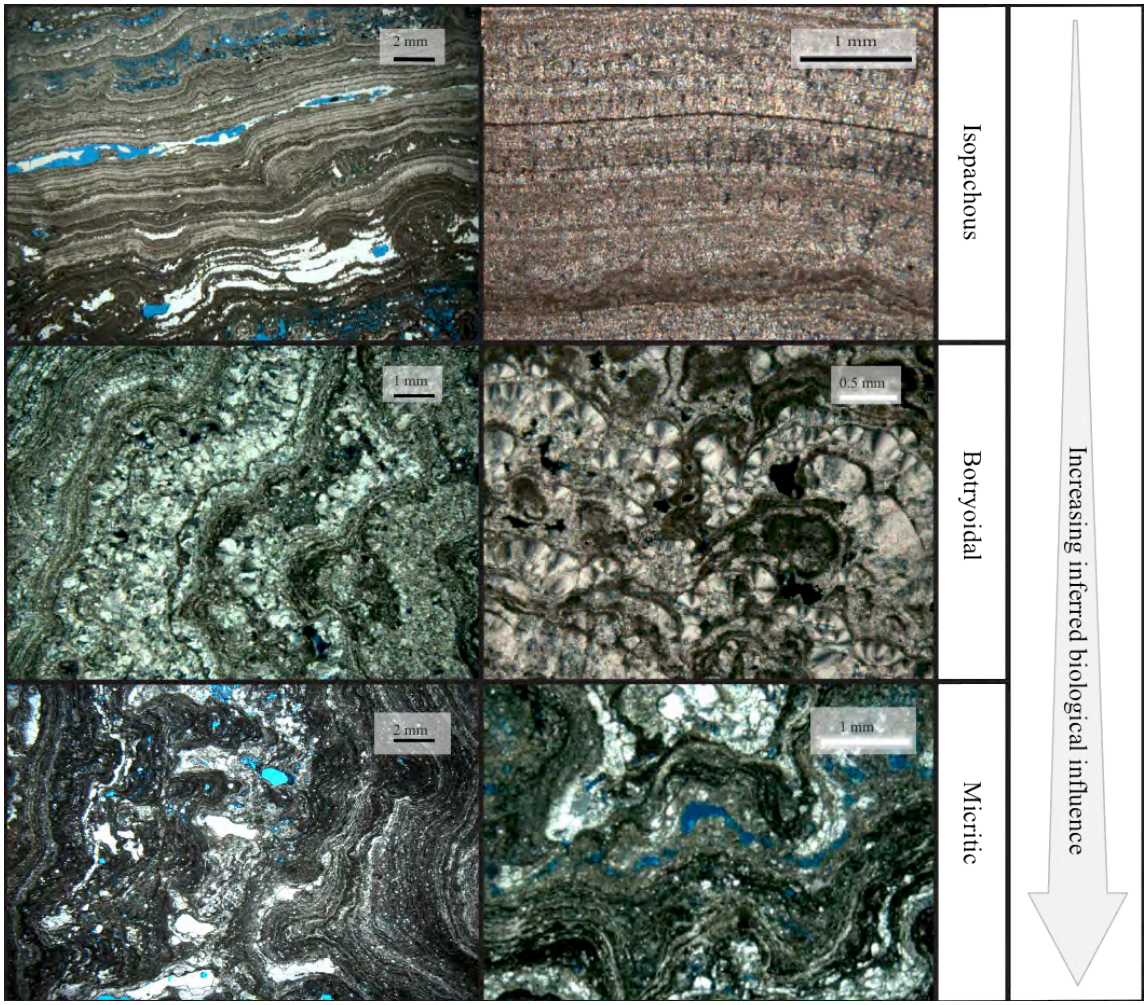

Figure 5: Microfabric types within microbialites, with an inferred increase in the degree of biological influence in microfabric formation from top (isopachous) to bottom (micritic). All images are under cross-polarized light.

laminae display heterogeneous banding of dark, micritic, and organic-rich layers and brighter regions dominated by microspar suggestive of differential amounts of effects of biological influence on microfabric evolution (Fig. 5). Pristine to compacted *Rivularia*-like filaments (Mlewski *et al*., 2014) and diatoms (pennate and centric, *Surirella* and *Navicula* spp; Boidi *et al*., 2014) identified with confocal microscopy and scanning electron microscopy have been found to occur within both dark and light bands of micritic laminae. Association of micritic fabrics with microbial elements suggests precipitation intimately associated with microbial activity. Micritic laminae are present in all oncoids, but are the dominant fabric in Zone 3C (Samples LN-13-1, LN-13-5, LN-13-10, LN-13-13, LN-13-20).

Interpretation of petrographic microfabrics

The relative proportions of each microfabric type is responsible for the mesoscale morphology of the microbialites, with samples composed of botryoidal and micritic fabric types displaying great irregularity in lamina thickness and synoptic relief (Samples LN-13-1, LN-13-5, LN-13-10, LN-13-13, LN-13-20; Fig. 4). Samples of this type are interpreted as microbially-mediated and are from Zone 3C. By contrast, a high relative abundance of isopachous microfabric produces a microbialite with a relatively smooth surface morphology (Sample LN-13-28; Fig. 4). The regular nature of lamination on both the centimeter and micrometer scales within LN-13-28 of Zone 3A suggests precipitation without the overriding influence of biological activity, and is here classified as chemically-precipitated.

In light of petrographic fabrics that suggest variable participation of biological activity, it is critical to determine in what way biological activity may potentially influence preservation of geochemical signals. Micritic laminae, and to a lesser degree botryoidal laminae, are inferred to reflect biological influence on formation of calcium carbonate. Biologically induced mineralization is the process by which precipitation of minerals takes place as a result of secondary biogeochemical reactions (Mann, 2001), which can reflect a multitude of microenvironmental alterations induced by bacterial metabolisms (Ehrlich, 1981, 1998; Reid *et al*., 2003; Dupraz & Visscher, 2005; Dupraz *et al*., 2013). Within microbial mats, the diverse assemblage of bacterial metabolisms causes changes in microenvironmental conditions through anabolic and catabolic reactions, the combined result of which is the potential for carbonate precipitation (Ehrlich, 1996; Dupraz *et al*., 2009, 2013). Ehrlich (1981) characterized several of the essential biochemical reactions that promote the growth of calcium carbonate. These include the release of CO_2 and NH_3 as products of OM oxidation, microbial reduction of SO_4^{2+}, photosynthetic drawdown of CO_2, and hydrolysis of urea. Increased pH associated with photosynthesis (Pentecost & Riding, 1986; Riding, 2000; Bissett *et al*., 2008), heterotrophic respiration (Visscher *et al*., 1998, 2000; Braissant *et al*., 2007) and degradation of low-molecular weight organics and EPS (Dupraz *et al*., 2009; Gallagher *et al*., 2010) are well established mechanisms of precipitation within mats and are likely reflected in micritic laminae within Laguna Negra microbialites. The formation of characteristic microbialite laminae has been suggested to arise through complex physiochemical forcing induced by biological community succession within microbial mats (Reid *et al*., 2000; Dupraz *et al*., 2013), and although not constrained at present, the relative role of metabolic processes is currently being investigated via

a combination of metagenomic analysis, confocal microscopy, and microRaman spectroscopy (cf. Gomez, *personal communication*).

The contribution of cyanobacterial photosynthesis and CO_2 drawdown at the mat surface to overall microenvironmental change has been controversial (Pentecost & Riding, 1986; Pentecost & Bauld, 1988; Ludwig *et al*., 2005; Bisset *et al*., 2008). Laguna Negra microbialites, however, contain clear evidence for mineralization at the microbialite surface, in the form of isopachous and botryoidal cements, suggesting the potential for carbonate formation via changes in calcite saturation state induced by biological drawdown of CO_2. Microbial oxidation of OM, such as cyanobacteria, diatoms, and their EPS cannot be discounted as a potential driver of calcite nucleation. Botryoidal laminae, for instance, are clearly associated with clumps of degraded OM. Botryoidal laminae are the main constituent of microbialite centers, suggesting that the initiation of microbialite formation and subsequent laminae accretion may be related to the deposition of particulate OM in the form of diatoms, dead cyanobacteria, and the associated accumulation of organic-rich EPS. Within subsequent laminae, the precipitation of calcite coupled with continuous metabolic activity during crystal growth potentially induced fluctuation in nucleation to growth ratios of calcium carbonate crystals (Bissett *et al*., 2008), resulting in the development of micritic layers. Enhancement in the size of botryoids in Zone 3A, in association with abundant isopachous laminae, suggest a predominant influence of extrinsic chemical conditions.

Isotopic compositions of carbonate phases

The carbon and oxygen isotope compositions of carbonate phases can be found in Tables 2-7, and are shown in Figs. 6 and 7. Carbon isotope values range from +5.75 to +18.25 ‰ (vs. VPDB) and oxygen isotopic values range from -2.04 to +7.36 ‰ (vs. VPDB; Fig. 8a), although the range of both carbon and oxygen isotope values observed in any single microbialite is typically smaller, averaging 5 ‰. Within discrete microbialites, carbon isotopes record distinct trends from heavier to lighter isotopic values (Fig. 6), with oxygen isotopes showing a similar, although more variable trend (Fig. 7). Pair-wise comparisons combined with ANOVA testing show that there is a statistically significant progression of mean values from the innermost laminae, outward toward the rim in all samples examined.

Interpretation of isotopic compositions

Hydrological balance within closed basin lake systems is most frequently interpreted by examination of oxygen and carbon isotope covariance (Fig. 8), with an R^2 value ≥ 0.7 most commonly associated with closed-basin lakes (Talbot, 1990). Such covariance reflects the overall coupling between isotopic evolution and hydrological balance, wherein freshwater input supplies isotopically light carbon and oxygen, and kinetic fractionation during evaporation leaves both carbon and oxygen isotope reservoirs enriched with respect to the heavier isotopes, ^{13}C and ^{18}O (Li & Ku, 1997). Although Laguna Negra is a hydrologically closed system, covariance of the complete isotopic dataset—which provides an overall R^2 value of 0.024—is substantially

weaker than in many closed basin lakes (Fig. 8a). Covariance is substantially stronger when individual oncolites are examined individually (providing R^2 values of 0.07 to 0.71), and when covariance is determined for 4-point running averages of are considered (providing R^2 values of 0.24 to 0.83) (Fig. 8b).

Absence of strong covariation between carbon and oxygen isotopes within Laguna Negra oncolites suggests that parameters other than simple hydrologic balance are at play in Laguna Negra. Sample LN-13-28, for instance, which is represented by dominantly chemical precipitation (Zone 3A), records the most strongly covariant carbon and oxygen isotope covariance ($R^2 = 0.71$). Samples LN-13-1 and LN-13-5, which consist of dominantly microbially mediated fabrics, were collected from Zone 3C approximately 55 meters from inlet waters and record moderately covariant isotopic compositions ($R^2 = 0.63, 0.54$, respectively). By contrast, samples LN-13-10, LN-13-13, and LN-13-20 are microbially mediated samples collected within 25 meters of the fresh water input source in Zone 3C. These samples preserve the weakest covariance ($R^2 = 0.28, 0.35$, and 0.074, respectively). When observed in this context, weakest covariance occurs in samples that were collected closest to the source of fresh water input, which is also reflected in light average $\delta^{18}O$ values (0.94, 0.57, and 0.94‰, respectively) and most variable $\delta^{18}O$ between adjacent laminae (Fig. 7). Samples that were collected further from the source of fresh water input record substantially more covariant signals. These observations suggest that degree of covariance in Laguna Negra oncolites may directly reflect precipitation of carbonate within a zone of active mixing, across which fresh water influx is variable. Similarly, that strongest covariance is recorded in samples petrographically inferred to record least amount

of biological influence suggests that relatively weak covariance in many samples may also reflect spatial variability in the extent of influence played by biological activity. Such variability demonstrates sensitivity of signals related to spatial and temporal position within Laguna Negra, and suggests that extraction of high-resolution paleoenvironmental data may be difficult in the absence of a broader geochemical framework.

Despite spatial variation in isotopic composition, and our current inability to distinctly correlate laminae between individual oncolites, all samples record general trend of heavier to lighter isotopic composition (in both $\delta^{13}C$ and $\delta^{18}O$), suggesting that oncolites record, on the whole, growth during a time of greater input water contribution. Complexity of the isotopic signals is, furthermore, not dissimilar to that recorded in other saline, closed lakes in the region (Fig. 8b). For example, isotopic data from El Peinado (26° 29' 59" S, 68° 05' 32"W, 3,820 m a.s.l), Las Peladas (27° 05' 83" S, 68° 04' 85" W, 3,860 m a.s.l.), and San Francisco (26° 56' S, 68° 08' W, 3,900 m a.s.l) basins (Valero-Garcés *et al*., 2000; Valero-Garcés *et al*., 2001) within Northwestern Argentina (cf. Fig. 1) are comparable to those recorded within carbonates of Laguna Negra. Each of these saline basins record $\delta^{18}O$ values substantially heavier than the isotopic composition of regional input waters (-10 ‰ vs. SMOW; Risacher, 2003), highlighting the overall negative water balance of the region. O-isotope compositions, however, vary dramatically through the region. Within the San Francisco basin, for instance, isotopic analysis showed systematically increasing values from the margin to the center of the lake (Valero-Garcés *et al*., 2000). Isotopically light samples from Las Peladas have been interpreted to reflect

Table 2: Inorganic and organic isotopic and elemental compositions of laminae within microbialite LN-13-1.

Lamina #	Sample No.	Lamina type	δ^{13}Ccarb (‰ vs. VPDB)	δ^{18}O (‰ vs. VPDB)	Mg/Ca	Sr (ppm)	TOC %	C/N	δ^{13}Corg (‰ vs. VPDB)
1	1-TOR-1	Isopachous	8.09	0.29	0.02	2371			
2	1-TOR-2	Isopachous	6.45	-1.10	0.01	2121	1.12	10.28	-16.13
3	1-TOR-3	Isopachous	7.77	-0.74	0.01	2425			
4	1-1-1	Micrite	5.75	-0.85	0.01	2182			
5	1-1-2	Mixed micrite/Microspar	7.96	-2.04	0.01	2485	0.40	9.71	-23.22
6	1-2	Mixed microspar/micrite	6.52	-0.86	0.01	2189			
7	1-3-W	Isopachous	8.34	-0.71	0.03	2680			
8	1-3-1	Isopachous	9.21	-0.85	0.02	2557			
9	1-3-2	Isopachous	9.15	-1.33	0.02	2572			
10	1-3-3	Botryoidal	9.55	0.09	0.10	2496			
11	1-4-1	Isopachous	9.41	-0.38	0.01	2950	1.18	9.94	-21.43
12	1-4-2	Isopachous	9.80	2.16	0.02	2611			
13	1-5	Mixed botryoid/micrite	11.35	1.76	0.02	2851			
14	1-6-1	Mixed botryoid/micrite	9.37	0.80	0.02	2436			
15	1-6-2	Mixed micrite/Microspar	9.80	0.40	0.01	2624			
16	1-7	Micrite	8.93	-0.53	0.02	2368			
17	1-8-1	Micrite	9.90	0.23	0.01	2592			
18	1-8-2	Mixed botryoid/micrite	9.15	0.35	0.01	2253	1.22	12.07	-26.45
19	1-9	Micrite	10.43	0.49	0.01	2238			

Table 2 con't

Lamina #	Sample No.	Lamina type	δ^{13}Ccarb (‰ vs. VPDB)	δ^{18}O (‰ vs. VPDB)	Mg/Ca	Sr (ppm)	TOC %	C/N	δ^{13}Corg (‰ vs. VPDB)
20	1-10-1	Mixed micrite/Microspar	11.72	0.94	0.01	2283			
21	1-10-2	Mixed micrite/Microspar	11.72	0.94	0.01	2642	1.22	12.07	-26.45
22	1-11	Mixed micrite/Microspar	11.02	0.73	0.01	2313			
23	1-12	Mixed micrite/Microspar	12.32	1.60	0.02	2371			
24	1-13	Mixed micrite/Microspar	10.97	1.56	0.01	2221			
25	1-14	Mixed micrite/Microspar	10.34	0.98	0.01	2173			
26	1-15	Mixed micrite/Microspar	9.62	1.43	0.02	1751	1.81	15.17	-25.68
27	1-16	Mixed micrite/Microspar	10.17	1.33	0.02	1993			
28	1-17	Mixed micrite/Microspar	10.80	1.40	0.02	2276			
29	1-18	Mixed micrite/Microspar	12.70	2.51	0.01	3796			
30	1-19-1	Mixed micrite/Microspar	10.97	1.69	0.01	2357			
31	1-19-2	Mixed micrite/Microspar	10.90	2.08	0.01	2344	0.96	-	-
32	1-20-1	Mixed micrite/Microspar	12.12	1.34	0.01	2401			
33	1-20-2	Mixed micrite/Microspar	11.80	1.45	0.03	2507			

Table 2 con't

Lamina #	Sample No.	Lamina type	δ^{13}Ccarb (‰ vs. VPDB)	δ^{18}O (‰ vs. VPDB)	Mg/Ca	Sr (ppm)	TOC %	C/N	δ^{13}Corg (‰ vs. VPDB)
34	1-21-1	Mixed micrite/Microspar	11.21	1.07	0.01	2633	0.96	-	-
35	1-21-2	Mixed micrite/Microspar	12.32	0.82	0.01	3002			
36	1-22-1	Mixed micrite/Microspar	12.97	1.34	0.02	4192	3.87	7.14	-20.07
37	1-22-2	Mixed micrite/botryoid	12.40	2.36	0.02	3556			
38	1-23-1	Mixed botryoid/micrite	12.51	0.99	0.01	3220	0.92	10.16	-21.96
39	1-23-2	Mixed botryoid/micrite	11.95	1.50	0.03	2860			
40	1-24	Mixed botryoid/micrite	14.43	1.78	0.02	4387			
41	1-25	Mixed botryoid/micrite	12.28	3.58	0.02	2731			
42	1-26-1	Mixed microspar/micrite	11.86	1.34	0.02	3448			
43	1-26-2	Mixed microspar/micrite	12.31	1.57	0.02	3785			
44	1-27	Micrite	12.65	1.66	-	-			
45	1-28	Mixed micrite/botryoid	13.68	2.09	0.03	5670			
46	1-29	Mixed micrite/botryoid	14.25	2.39	0.01	7285			

Table 3: Inorganic and organic isotopic and elemental compositions of laminae within microbialite LN-13-5. Dashes indicate either insufficient sample powder for analysis.

Lamina #	Sample No.	Lamina type	δ^{13}Ccarb (‰ vs. VPDB)	δ^{18}O (‰ vs. VPDB)	Mg/Ca	Sr (ppm)	TOC %	C/N	δ^{13}Corg (‰ vs. VPDB)
1	5-1	Mixed microspar/micrite	6.55	-0.17	0.02	2218	0.37	-	-
2	5-2	Mixed microspar/micrite	6.66	-0.42	0.01	2102			
3	5-3-1	Mixed micrite/botryoidal	8.95	-0.25	0.01	2292	1.47	11.04	-17.29
4	5-3-2	Mixed micrite/botryoidal	8.22	-0.17	0.02	2448			
5	5-4	Micrite	8.18	-0.27	0.01	2313	1.75	8.81	-18.47
6	5-5-1	Mixed botryoid/micrite	8.79	-0.45	0.01	2299			
7	5-5-2	Micrite	8.58	-0.18	0.02	2303			
8	5-6	Mixed botryoid/micrite	9.18	0.46	0.01	2360			
9	5-7-1	Mixed microspar/micrite	9.27	0.20	0.02	2426			
10	5-7-2	Botryoidal	-	-	0.02	2113			
11	5-8-1	Micrite	8.27	0.18	0.02	2477			
12	5-8-2	Micrite	8.52	0.85	0.02	2239			
13	5-9	Mixed microspar/micrite	7.78	1.32	0.02	2168	1.60	7.59	-19.71
14	5-10-1	Mixed microspar/micrite	7.87	0.90	0.02	2085			
15	5-10-2	Isopachous	8.30	0.30	0.02	2272			

Table 3 con't

Lamina #	Sample No.	Lamina type	δ^{13}Ccarb (‰ vs. VPDB)	δ^{18}O (‰ vs. VPDB)	Mg/Ca	Sr (ppm)	TOC %	C/N	δ^{13}Corg (‰ vs. VPDB)
16	5-11	Isopachous	9.35	0.77	0.02	2159			
17	5-12	Mixed botryoid/micrite	10.61	0.84	0.02	2248	1.29	1.5	-18.9
18	5-13	Mixed botryoid/micrite	9.73	0.51	0.01	2314			
19	5-14-1	Mixed botryoid/micrite	9.39	0.96	0.01	1796			
20	5-14-2	Mixed botryoid/micrite	9.24	0.20	0.01	2060	1.64	-	-
21	5-15-1	Mixed botryoid/micrite	10.73	0.76	0.01	2316			
22	5-15-2	Mixed microspar/micrite	-	-	0.02	2317			
23	5-16	Mixed microspar/micrite	10.34	0.30	0.02	2180			
24	5-17	Isopachous	10.29	0.82	0.02	2046	0.89	16.22	-21.76
25	5-18-1	Isopachous	10.23	0.76	0.02	1927			
26	5-18-2	Mixed microspar/micrite	10.73	1.34	0.02	2103			
27	5-19	Mixed microspar/micrite	12.33	2.74	0.02	2350			
28	5-20	Mixed microspar/micrite	11.47	1.48	0.02	2222			
29	5-21	Mixed microspar/micrite	9.68	1.20	0.02	1973	0.00	-	-
30	5-22	Mixed microspar/micrite	13.24	1.80	0.02	2881			
31	5-23	Mixed microspar/micrite	11.79	1.27	0.03	2288	0.74	9.34	-20.16
32	5-24	Mixed botryoid/micrite	11.02	0.72	0.02	2315			
33	5-25-1	Mixed botryoid/micrite	12.26	1.35	0.03	2319	-	-	-
34	5-25-2	Mixed botryoid/micrite	13.58	1.50	0.01	3015			

Table 4: Inorganic and organic isotopic and elemental compositions of laminae within microbialite LN-13-10.

Lamina #	Sample No.	Lamina type	δ^{13}Ccarb (‰ vs. VPDB)	δ^{18}O (‰ vs. VPDB)	Mg/Ca	Sr (ppm)	TOC %	C/N	δ^{13}Corg (‰ vs. VPDB)
1	10-1	Isopachous	8.35	-0.07	0.02	2237			
2	10-2	Mixed micrite/botryoidal	9.90	2.09	0.02	1757	1.38	11.84	-21.64
3	10-3	Micrite	10.29	2.63	0.02	1729			
4	10-4	Botryoidal	10.23	1.85	0.02	2128			
5	10-5	Mixed micrite/botryoidal	8.73	0.58	0.03	2103			
6	10-6	Mixed micrite/botryoidal	9.67	0.99	0.03	2113			
7	10-7-1	Mixed micrite/microspar	11.27	1.08	0.01	2419			
8	10-7-2	Mixed micrite/microspar	10.86	1.19	0.02	2269			
9	10-8	Mixed micrite/microspar	8.32	0.36	0.02	2153			
10	10-9	Botryoidal	8.35	0.45	0.03	2284	1.04	13.18	-26.93
11	10-10	Isopachous	10.99	0.53	0.01	2501			
12	10-11	Isopachous	9.31	-0.10	0.03	2322			
13	10-12	Isopachous	9.68	1.14	0.03	2351			
14	10-13	Micrite	9.37	-0.03	0.02	2458			
15	10-14	Micrite	9.61	1.24	0.03	2474			
16	10-15	Micrite	11.15	0.86	0.01	2764			
17	10-16-1	Mixed micrite/microspar	9.52	0.50	0.02	2695			
18	10-16-2	Mixed micrite/microspar	9.20	-0.16	0.02	2494			
19	10-17	Botryoidal	9.88	0.19	0.02	2489			

Table 4 con't

Lamina #	Sample No.	Lamina type	δ^{13}Ccarb (‰ vs. VPDB)	δ^{18}O (‰ vs. VPDB)	Mg/Ca	Sr (ppm)	TOC %	C/N	δ^{13}Corg (‰ vs. VPDB)
20	10-18	Micrite	9.07	0.29	0.02	2214			
21	10-19	Mixed micrite/botryoidal	10.31	0.27	0.01	2304			
22	10-20	Botryoidal	10.31	1.69	0.02	1922			
23	10-21	Mixed micrite/botryoidal	10.91	1.79	0.03	2209	0.66	-	-
24	10-22	Micrite	10.61	2.17	0.02	2379			
25	10-23-1	Mixed micrite/botryoidal	10.30	0.66	0.01	2021			
26	10-23-2	Mixed micrite/botryoidal	9.79	0.87	0.03	2069			
27	10-24	Mixed micrite/botryoidal	10.56	0.95	0.01	2176	1.26	8.07	-21.29
28	10-25	Micrite	10.31	1.04	0.02	2041			
29	10-26	Mixed micrite/botryoidal	11.61	1.22	0.02	2918			
30	10-27	Mixed micrite/botryoidal	11.80	1.43	0.03	2255			
31	10-28	Micrite	11.55	1.53	0.03	2440			

Table 5: Inorganic and organic isotopic and elemental compositions of laminae within microbialite LN-13-13.

Lamina #	Sample No.	Lamina type	δ^{13}Ccarb (‰ vs. VPDB)	δ^{18}O (‰ vs. VPDB)	Mg/Ca	Sr (ppm)	TOC %	C/N	δ^{13}Corg (‰ vs. VPDB)
1	13-TOR	Micrite	6.34	-0.39	0.02	2402	0.74	19.02	-25.41
2	13-1	Micrite	5.95	-0.90	0.02	2248			
3	13-2	Micrite	6.22	-0.74	0.02	2267			
4	13-3	Botryoidal	8.46	-1.31	0.03	2385	1.10	23.34*	-24.28
5	13-4	Mixed micrite/botryoidal	9.47	-0.65	0.03	2499			
6	13-5-1	Micrite	8.66	-0.09	0.03	2195			
7	13-5-2	Mixed micrite/botryoidal	8.63	0.50	0.03	2370			
8	13-6	Botryoidal	8.49	0.83	0.03	2357			
9	13-7	Isopachous	7.27	-0.88	0.02	2170	0.99	10.50	-20.48
10	13-8-1	Botryoidal	8.15	-0.71	0.03	2146			
11	13-8-2	Isopachous	8.73	0.35	0.02	2305			
12	13-9	Mixed micrite/botryoidal	7.68	1.02	0.02	2028	0.91	-	-
13	13-10-1	Micrite	8.07	0.07	0.03	2183	0.88	-	-
14	13-10-2	Micrite	7.76	-0.88	0.02	2197			
15	13-11-1	Botryoidal	8.54	-0.26	0.03	2209			
16	13-11-2	Isopachous	8.83	-0.25	0.02	2243			
17	13-12-1	Mixed micrite/botryoidal	10.08	0.31	0.03	2477			

Table 5 con't

Lamina #	Sample No.	Lamina type	δ^{13}Ccarb (‰ vs. VPDB)	δ^{18}O (‰ vs. VPDB)	Mg/Ca	Sr (ppm)	TOC %	C/N	δ^{13}Corg (‰ vs. VPDB)
18	13-12-2	Mixed micrite/botryoidal	9.03	0.60	0.02	2329			
19	13-13-1	Mixed micrite/botryoidal	8.28	1.20	0.02	2036			
20	13-13-2	Mixed micrite/microspar	7.92	1.52	0.02	2081			
21	13-13-3	Mixed micrite/microspar	9.24	1.69	0.02	2088	2.33	26.26	-24.72
22	13-14	Micrite	8.78	-0.04	0.02	2117			
23	13-15	Mixed micrite/botryoidal	8.83	0.48	0.03	2178			
24	13-16	Micrite	9.89	0.95	0.03	1963			
25	13-17-1	Micrite	9.41	1.64	0.03	1929			
26	13-17-2	Mixed micrite/microspar	10.80	1.13	0.03	2122			
27	13-18	Botryoidal	9.83	0.50	0.03	2264			
28	13-19-1	Micrite	10.66	0.75	0.02	2225			
29	13-19-2	Mixed micrite/botryoidal	9.70	1.62	0.03	2179			
30	13-20	Micrite	9.96	0.39	0.02	2274			
31	13-21	Mixed micrite/microspar	10.98	2.14	0.03	2341			
32	13-22-1	Mixed micrite/microspar	10.09	1.04	0.02	2423			
33	13-22-2	Micrite	10.90	0.97	0.00	2786			
34	13-22-3	Botryoidal	10.19	1.38	0.02	2478			
35	13-23-1	Micrite	10.65	1.23	0.03	2026	1.68	9.09	-19.77

Table 5 con't

Lamina #	Sample No.	Lamina type	δ^{13}Ccarb (‰ vs. VPDB)	δ^{18}O (‰ vs. VPDB)	Mg/Ca	Sr (ppm)	TOC %	C/N	δ^{13}Corg (‰ vs. VPDB)
36	13-23-2	Mixed micrite/botryoidal	10.93	0.36	0.06	4224			
37	13-23-3	Mixed micrite/botryoidal	11.04	1.48	0.00	3568			
38	13-24	Botryoidal	9.57	0.76	0.02	2245	1.68	9.09	-19.77
39	13-25-1	Mixed micrite/microspar	9.94	0.06	0.03	2759			
40	13-25-2	Mixed micrite/microspar	10.64	1.15	0.03	3117			
41	13-26	Botryoidal	10.12	2.16	0.03	2802			
42	13-27	Botryoidal	9.44	1.78	0.03	2301			
43	13-28	Mixed micrite/botryoidal	8.63	0.63	0.03	2557			
44	13-29	Mixed micrite/botryoidal	8.89	1.37	0.03	5811	0.65	-	-

*N just at detection limits.

Table 6: Inorganic and organic isotopic and elemental compositions of laminae within microbialite LN-13-20.

Lamina #	Sample No.	Lamina type	δ^{13}Ccarb (‰ vs. VPDB)	δ^{18}O (‰ vs. VPDB)	Mg/Ca	Sr (ppm)	TOC %	C/N	δ^{13}Corg (‰ vs. VPDB)
1	20-1	Botryoidal	8.23	1.52	0.04	2145	1.03	38.11	-26.89
2	20-2	Botryoidal	8.15	2.47	0.04	1244			
3	20-3	Botryoidal	8.44	1.93	0.03	1090			
4	20-4	Micritic	8.36	0.22	0.03	2155	0.77	16.3*	-23.3*
5	20-5	Mixed micritic/botryoidal	7.50	0.67	0.02	2218	0.43	9.12	-21.39
6	20-6	Micritic	7.93	0.51	0.02	2263			
7	20-7-1	Micritic	8.53	-1.05	0.03	2247			
8	20-7-2	Mixed micritic/botryoidal	9.61	0.10	0.04	2369			
9	20-7-3	Mixed micritic/botryoidal	8.64	-0.25	0.03	2271			
10	20-8-1	Micitic	8.16	-0.05	0.02	2134			
11	20-8-2	Mixed micritic/botryoidal	9.51	0.18	0.03	2550			
12	20-8-3	Mixed micritic/botryoidal	8.60	0.33	0.04	1496			
13	20-9	Micritic	8.49	0.55	0.05	2512			
14	20-10	Mixed micritic/microspar	9.70	0.82	0.03	2507			
15	20-11	Mixed micritic/microspar	8.48	0.88	0.03	2316			
16	20-12	Micritic	9.91	0.55	0.03	2387			

Table 6 con't

Lamina #	Sample No.	Lamina type	δ^{13}Ccarb (‰ vs. VPDB)	δ^{18}O (‰ vs. VPDB)	Mg/Ca	Sr (ppm)	TOC %	C/N	δ^{13}Corg (‰ vs. VPDB)
17	20-13	Mixed micritic/microspar	9.16	1.10	0.04	1787			
18	20-14	Micritic	10.36	0.62	0.03	2324			
19	20-15	Mixed micritic/microspar	9.04	1.37	0.03	2252			
20	20-16	Botryoidal	9.03	0.07	0.02	2741			
21	20-17	Micritic	8.62	1.54	0.04	1549			
22	20-18	Mixed micritic/microspar	11.52	1.63	0.03	2182			
23	20-19-1	Micitic	9.33	1.37	0.03	2543			
24	20-19-2	Botryoidal	10.62	1.56	0.05	1633			
25	20-20-1	Micritic	9.41	1.75	0.05	2366			
26	20-20-2	Mixed micritic/botryoidal	9.46	1.45	0.04	1751			
27	20-21	Mixed micritic/microspar	11.21	1.08	0.03	3171	1.75	-	-
28	20-22	Mixed micritic/microspar	-	-	0.04	1691			
29	20-23	Micritic	10.42	0.65	0.03	2352			
30	10-24	Mixed micritic/microspar	10.26	1.53	0.03	2559			
31	20-25	Mixed micritic/microspar	10.98	0.92	0.03	2794			
32	20-26-1	Mixed micritic/botryoidal	9.93	0.04	0.03	2386			
33	20-26-2	Micrite	10.65	1.90	0.04	2519			
34	20-26-3	Mixed micritic/microspar	-	-	0.05	1710			

Table 6 con't

Lamina #	Sample No.	Lamina type	δ^{13}Ccarb (‰ vs. VPDB)	δ^{18}O (‰ vs. VPDB)	Mg/Ca	Sr (ppm)	TOC %	C/N	δ^{13}Corg (‰ vs. VPDB)
35	20-27	Micrite	11.27	1.00	0.02	3021			
36	20-28	Botryoidal	12.08	0.65	0.03	3621			
37	20-29	Micricit	10.84	1.46	0.04	2769			
38	20-30	Mixed micritic/botryoidal	11.20	1.46	0.02	2662			
39	20-31	Mixed micritic/botryoidal	10.72	1.99	0.02	2480			
40	20-32-1	Micritic	10.48	1.44	0.02	2396			
41	20-32-2	Mixed micritic/botryoidal	10.28	0.71	0.03	2443			
42	20-33	Mixed micritic/botryoidal	9.92	1.01	0.03	2443	1.21	15.52	-20.61
43	20-34	Mixed micritic/botryoidal	10.39	1.04	0.03	2412			
44	20-35	Mixed micritic/botryoidal	9.14	1.08	0.04	1444			
45	20-36	Mixed micritic/botryoidal	8.09	-0.01	0.03	2307			
46	20-37	Mixed micritic/microspar	9.30	1.34	0.04	1328			
47	20-38	Mixed micritic/microspar	9.42	1.18	0.04	4024			

*Peaks outside of ideal range

Table 7: Inorganic and organic isotopic and elemental compositions of microbialite LN-13-28.

Lamina #	Sample No.	Lamina type	δ^{13}Ccarb (‰ vs. VPDB)	δ^{18}O (‰ vs. VPDB)	Mg/Ca	Sr (ppm)	TOC %	C/N	δ^{13}Corg (‰ vs. VPDB)
1	28-1-1	Isopachous	9.11	3.37	0.06	2367	0.66	-	-
2	28-1-2	Isopachous	9.35	3.78	0.02	2343			
3	28-2	Micritic	8.28	2.21	0.02	2701	0.25	-	-
4	28-3	Isopachous	10.76	5.08	0.03	2204	0.00	-	-
5	28-4	Isopachous	10.66	4.19	0.03	2394			
6	28-5	Isopachous	9.04	3.00	0.03	2250			
7	28-6-1	Micrite	8.62	2.41	0.02	2221			
8	28-6-2	Mixed micritic/botryoidal	8.22	4.30	0.03	2245	0.70	-	-
9	28-7	Mixed micritic/botryoidal	10.49	2.63	0.03	2170			
10	28-7-R	Mixed micritic/botryoidal	11.19	3.85	0.03	2560	0.34	33.71	-26.60
11	28-8-1	Micrite	10.02	3.40	0.03	2210			
12	28-8-2	Mixed micritic/botryoidal	14.83	6.12	0.03	2371			
13	28-9-1	Mixed micritic/botryoidal	18.26	6.86	0.06	2655	0.82	65.35	-25.88
14	28-9-2	Mixed micritic/botryoidal	15.21	7.37	0.03	2999			
15	28-10	Mixed micritic/botryoidal	15.61	6.82	0.02	7561			
16	28-11-1	Micrite	12.18	4.44	0.03	2122	0.27	29.43	-25.59

Table 7 con't

Lamina #	Sample No.	Lamina type	δ^{13}Ccarb (‰ vs. VPDB)	δ^{18}O (‰ vs. VPDB)	Mg/Ca	Sr (ppm)	TOC %	C/N	δ^{13}Corg (‰ vs. VPDB)
17	28-11-2	Mixed micritic/botryoidal	12.66	6.47	0.04	2088			
18	28-12	Mixed micritic/botryoidal	13.31	6.03	0.04	1750			
19	28-13	Mixed micritic/botryoidal	13.28	6.02	0.02	2701			
20	28-14	Mixed micritic/botryoidal	12.94	4.87	0.02	3659			
21	28-15	Isopachous	13.58	5.16	0.02	5096			
22	28-15-I	Isopachous	15.14	5.71	0.02	5217			
23	28-16	Mixed micritic/botryoidal	13.44	4.99	0.05	2501	0.29	-	-26.26
24	28-17	Micritic	15.37	5.13	0.02	5354			
25	28-18	Micritic	14.37	5.43	0.04	2704			
26	28-19	Botryoidal	-	-	0.03	3024			
27	28-20-1	Botryoidal	10.87	4.35	0.04	2527	1.31	-	-
28	28-20-2	Botryoidal	11.49	4.85	0.02	2565			
29	28-N-1	Not examined	13.09	4.32	0.02	2181	-	-	-
30	28-N-2	Not examined	12.36	4.64	0.02	2826	-	-	-
31	28-N-I	Not examined	12.91	4.55	0.04	2304	-	-	-

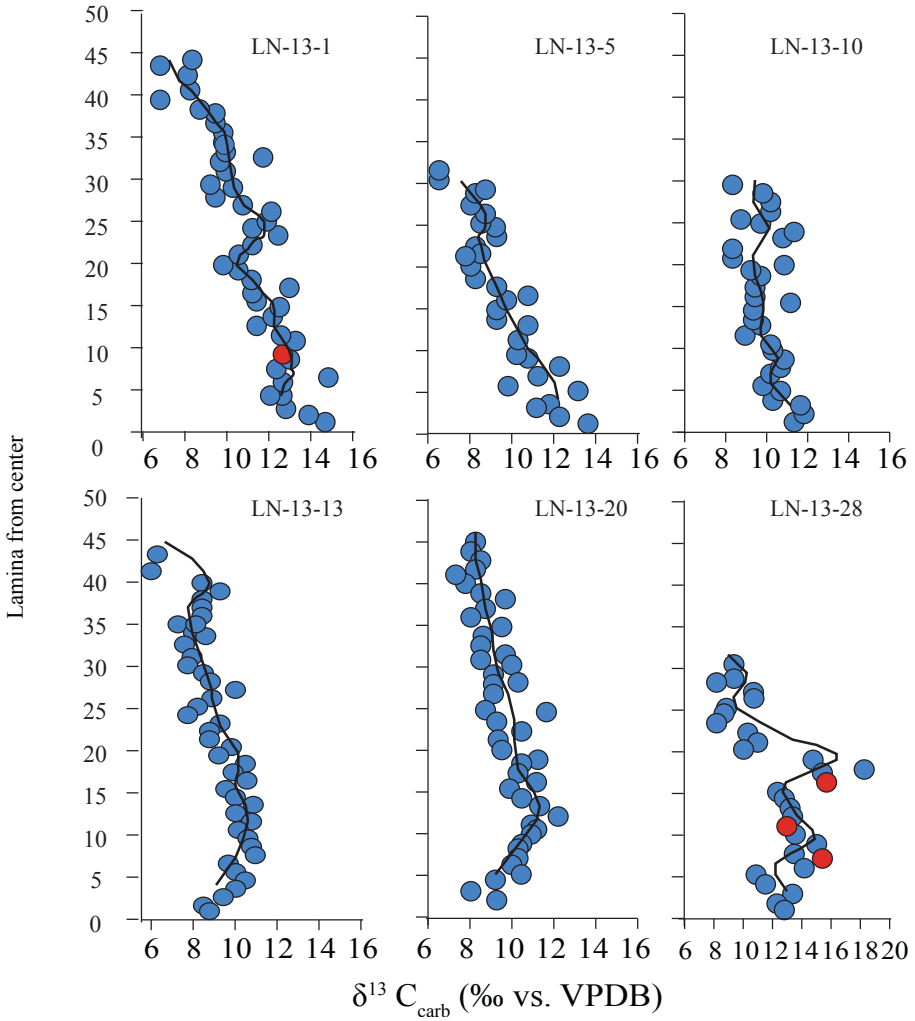

Figure 6: Time-wise carbon isotope composition of carbonate phases of Laguna Negra microbialites. Successive laminae are not correlated between samples, yet they display similar trends of lighter isotopes from the center laminae outward. Red infills indicate laminae confirmed to contain aragonite through XRD analysis.

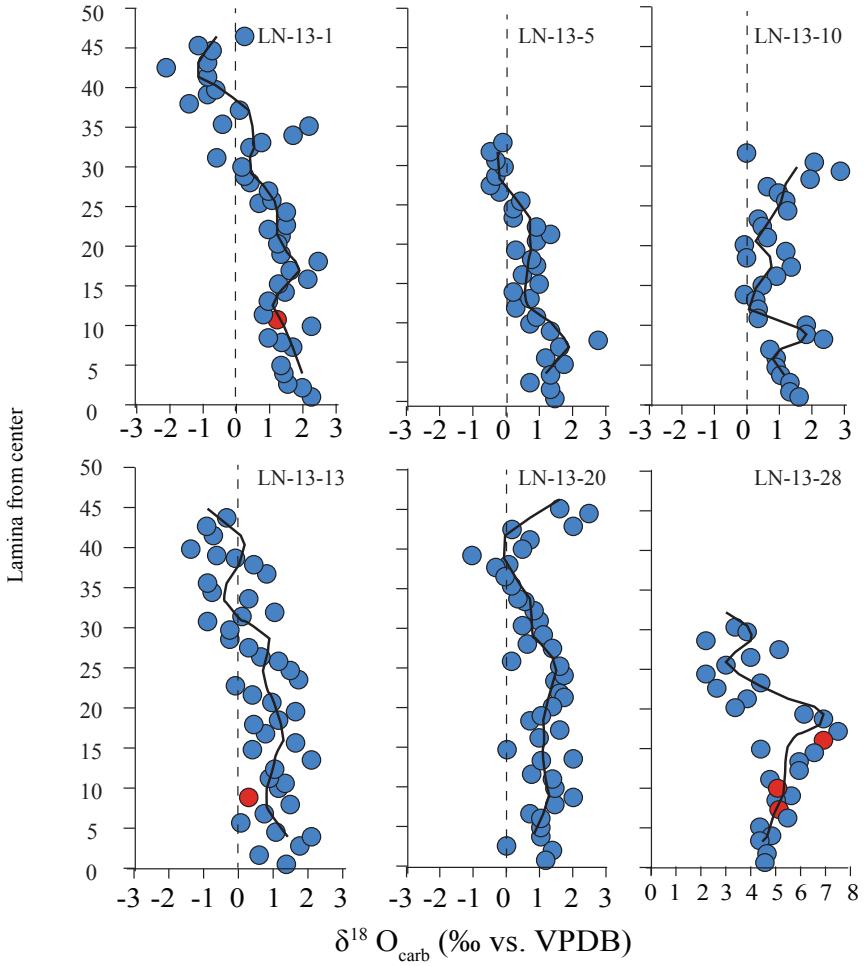

Figure 7: Time-wise oxygen isotope composition of carbonate phases of Laguna Negra microbialites. Similar to carbon isotopic trends, isotopically lighter values are observedfrom the center laminae outward is observed. Notice that the isotopically lightest values in sample LN-13-28 are among the isotopically highest in other samples. Red infills indicate laminae confirmed to contain aragonite through XRD analysis.

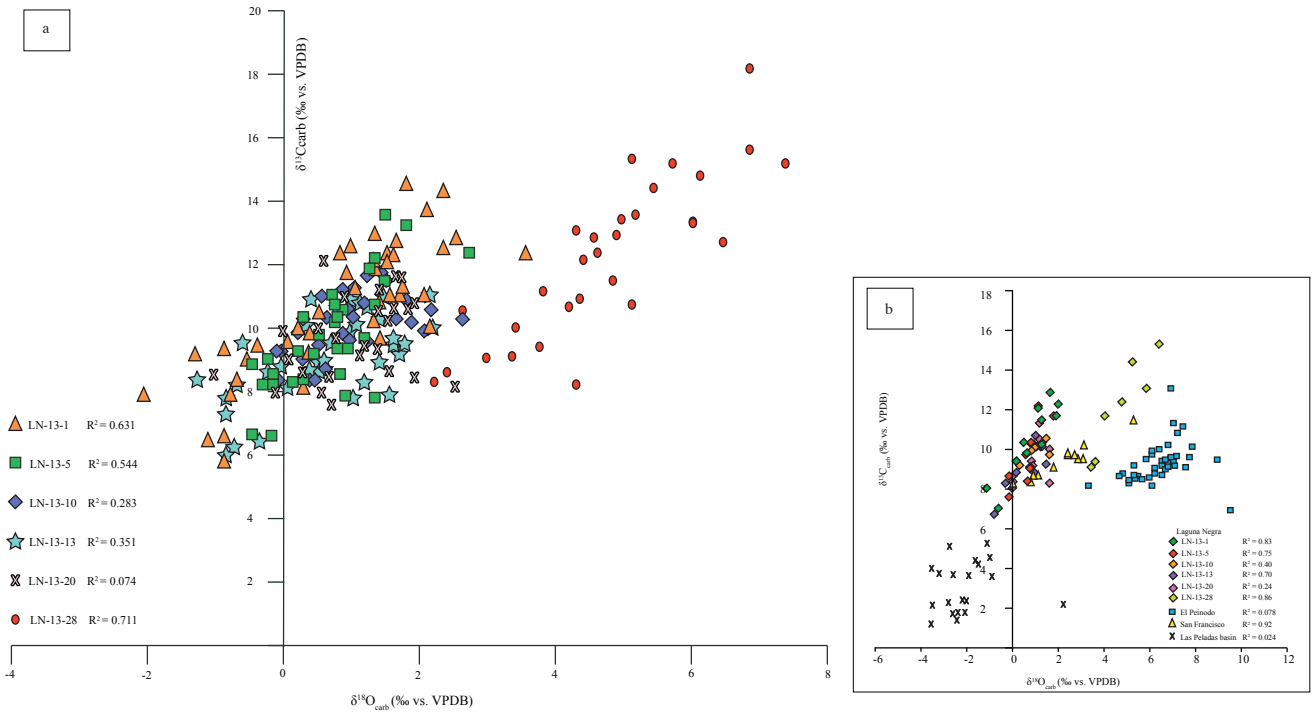

Figure 8: Isotopic covariance within carbonate phases. (a) Covariance of carbonate oxygen and carbon isotopes within individual laminae. Sample LN-13-28 is the only sample with an R^2 value characteristic of a closed-basin (Talbot, 1990). (b) 4-point running averages of microbialite laminae isotope values, which show stronger covariance, and isotopic values reported from similar saline basins within the Altiplano-Puna region (Valero-Garcés et al., 2000; Valero-Garcés et al., 2001).

.

a hydrologically less evolved basin, whereas isotopically enriched samples from El Peindo are interpreted to reflect highly evolved waters. When plotted next to data from these lakes, Laguna Negra oncolites highlight the potential for hypersaline lakes to record the spatially complexity of regional chemical signatures (Fig. 8b).

Laguna Negra is distinct from surrounding lakes in terms of both its oxygen isotopic composition and carbon isotopic composition. The average $\delta^{13}C$ values among oncolites dominated by microbial microfabrics range from +9.13 to +10.63‰ (VPDB), and the sample principally composed of isopachous laminae, LN-13-28, has a greater average $\delta^{13}C$ value of +12.22‰ (VPDB). Enriched carbon isotopic values within LN-13-28 likely arise from a combination of extensive CO_2 degassing during evaporation within Zone 3A and potentially the local photosynthetic drawdown of isotopically light inorganic carbon. Here, we report carbon isotope values up to +18.25‰, which is among the heaviest of values found in the literature (up to +16.5‰ VPDB; Stiller *et al*., 1985; Valero-Garcés *et al*., 1999). Similarity of these values to that recorded in an active travertine along the eastern margin of Laguna Negra (14.69‰; Gomez *et al*., *in press*) suggests that CO_2 degassing is the primary mechanism driving elevated $\delta^{13}C$ values. It is also critical to note that comparison of Laguna Negra data to that of other hypersaline lakes in Northwestern Argentina are based on 4-point running averages. Within Laguna Negra, these 4-point running averages show stronger covariance (R^2 = 0.83, 0.75, 0.40, 0.70, 0.24, 0.86), suggesting that, despite complexity driven by spatial variability, long-term environmental trends have been effectively recorded within Laguna Negra microbialites.

Elemental compositions

Elemental compositions of carbonate (Sr^{2+}, Mg^{2+}, Ca^{2+}) were measured as an independent assessment of the extent of evaporation in controlling the isotopic composition of Laguna Negra oncolites (Chivas *et al*., 1993; Boyle, 2001). Concentrations of Fe^{2+} and Mn^{2+} were also measured as part of standard lab protocols. Results of elemental analysis are recorded in Tables 2-7, as well as Fig. 9. Sodium concentrations (cf. Frantz *et al*., 2012) were unable to be measured because of the difficulty of sample contamination by modern lake waters. Elemental analysis shows variable trace metal incorporation. Mg^{2+} concentrations range from 1963 ppm to 23,227 ppm, and Sr^{2+} concentrations are similarly variable with a range in concentration from 1089 ppm to 7561 ppm.

Interpretation of elemental compositions

Overall, data show a generally weak correlation between Sr^{2+} and $\delta^{18}O$ (Fig. 9a; $R^2 < 0.2$ for each oncolite), although individual data points show similar patterns in Sr^{2+} and $\delta^{18}O$ variation within some samples (Fig. 9c), suggesting a potential relationship between Sr^{2+} and local evaporation. Most elevated Sr^{2+} concentrations ($Sr^{2+} > 5000$ ppm) are not uniquely correlated with ^{18}O enriched isotopic values, although they are associated with the heavier isotope compositions recorded by each sample. Although Sr^{2+} concentrations show a weak connection to oxygen isotopes, they display a strong association with mineralogy, with samples

that are aragonitic in composition averaging Sr^{2+} concentrations > 2,400 ppm. Additionally, Sr^{2+} concentrations > 5,000 ppm are associated with enriched ^{13}C (12-16‰ amongst samples). Combined, these observations suggest that precipitation of aragonite mineralogies (marked by Sr^{2+} concentrations > 5,000 ppm) are likely associated with high rates of CO_2 degassing (cf. Given & Wilkinson, 1985).

Organic compositions

Like other basins within Argentinian Puna (cf. Grosjean *et al*., 1997), total organic carbon (TOC) is low within Laguna Negra oncolites. TOC does not exceed 3.8% in any sample, and the average TOC of all samples is 1.4% (Tables 2-7). There are observed differences in TOC between oncolites that are dominated by micritic microfabrics versus the chemically precipitated sample largely composed of isopachous microfabrics. Average concentration of TOC within the chemically precipitated sample (LN-13-28) is only 0.48%, which is about half of that measured within inferred microbially mediated oncolites (TOC 1.4 % in LN-13-1, 1.0% in LN-13-5 and LN-13-10, and 1.1% in LN-13-13 and LN-13-20). Low TOC values within sample LN-13-28 are consistent with precipitation driven primarily by CO_2 outgassing during evaporation.

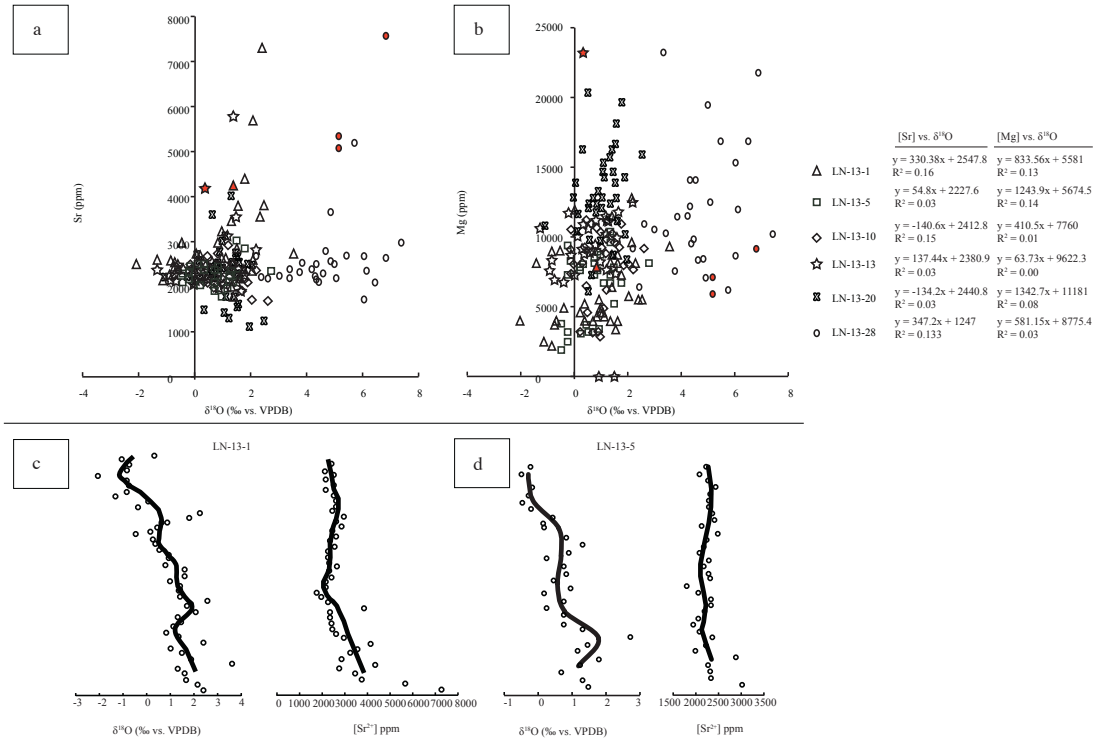

Figure 9: Comparison of trace element and isotopic data within carbonate. (a) A crossplot of oxygen isotopes and strontium concentration reveals that increases in [Sr] are not matched by increased evaporation, as recorded in oxygen isotopes, suggesting that [Sr] may not be a reliable proxy for salinity in Laguna Negra. Red infills are laminae confirmed to contain aragonite. (b) A crossplot of magnesium concentration against oxygen isotopes shows similarly low covariance. (c) Isotopic and elemental evolution within LN-13-1 display time-wise overall similarity in trends, indicating a record of basin freshening, a trend that is similarly recorded within the oxygen isotopes of LN-13-28 (d), but not within the [Sr] of this sample.

Interpretation of organic compositions

C/N ratios within extracted organic matter were converted from weight to atomic ratios by multiplying by 1.167 to reflect biological stoichiometry (Meyers & Teranes, 2001). C/N ratios range from 7.6 to 65.4 and display substantial variability both between and within microbialites (Tables 2-7). Within sedimentary organic material, carbon is, on average, an order of magnitude greater in quantity than nitrogen, and C/N ratios in lake sediments reflect, in part, the composition of OM from its production through the process of sediment formation (Wetzel, 1975). Distinct differences in C/N ratios between microbial, algal, and terrestrial OM can therefore be used to determine organic source and various end-members of OM contribution can be distinguished by characteristic C/N ratios (Wetzel, 1975; Berman, 1990; Kilham, 1990; Piovano *et al*., 2004). For example, lacustrine algae and plankton, such as green algae and cyanobacteria, have C/N ratios ranging from 6-12, whereas vascular land plants typically contain OM with C/N ratios greater than 20 (Meyers & Teranes, 2001; (Meyers & Lallier-vergés, 1999). Although there is no statistical difference between C/N ratios from different oncolites, the chemically precipitated sample LN-13-28 displays higher C/N ratios when compared to the rest of the data. With values as high as 65, the C/N ratios within LN-13-28 suggests microbial activity that is efficient in depleting nitrogen stores within available OM (Wetzel, 1975). Such elevated values place OM within this oncolite into the published range of C_3 vascular plants (Figs. 10 and 11). In the absence of C_3 vascular plants in the region (Valero-Garcés *et al*., 1996; Schwalb *et al*., 1999), however, such high values are more likely attributable to other mechanisms that affect C/N ratios.

In addition to OM provenance, C/N ratios provide insight into the degree of OM recycling, with ratios exhibit variation according to nutrient availability and OM transformation (Sterner & Elser, 2002). For instance, high degrees of microbial recycling and degradation of nitrogen-rich organic compounds leads to the selective removal of nitrogen from OM (Eglinton, 1969; Kemp, 1971; Meyers & Lallier-vergés, 1999). Proteolytic metabolisms of microorganisms, coupled with the physical transport of nitrogen by-products such as NO_3 and NH_4 have been shown to be the principle mechanisms by which OM becomes nitrogen-depleted prior to sedimentation, resulting in increased C/N values within recovered sedimentary OM (Rittenberg *et al*., 1955; Keeney, 1973).

Examination of sedimentary OM preserved within Laguna Negra microbialites reveals spatial variability, potentially related to differences in biological recycling. As stated above, the observed elevated C/N ratios within LN-13-28 likely reflects the depletion of labile OM resources associated with microbial transformation of OM prior to sedimentation, whereby denitrification, coupled with the migration of released nitrogen from pore waters, produces elevated C/N ratios. Future work focused on the detailed classification of OM within the microbialites of Laguna Negra will further elucidate the relative degrees to which microbial metabolisms impart signatures in sedimentary OM.

Carbon isotopes of bulk organic fractions from microbialites were also analyzed to further understand the nature of OM and the degree to which microbial recycling may reflect

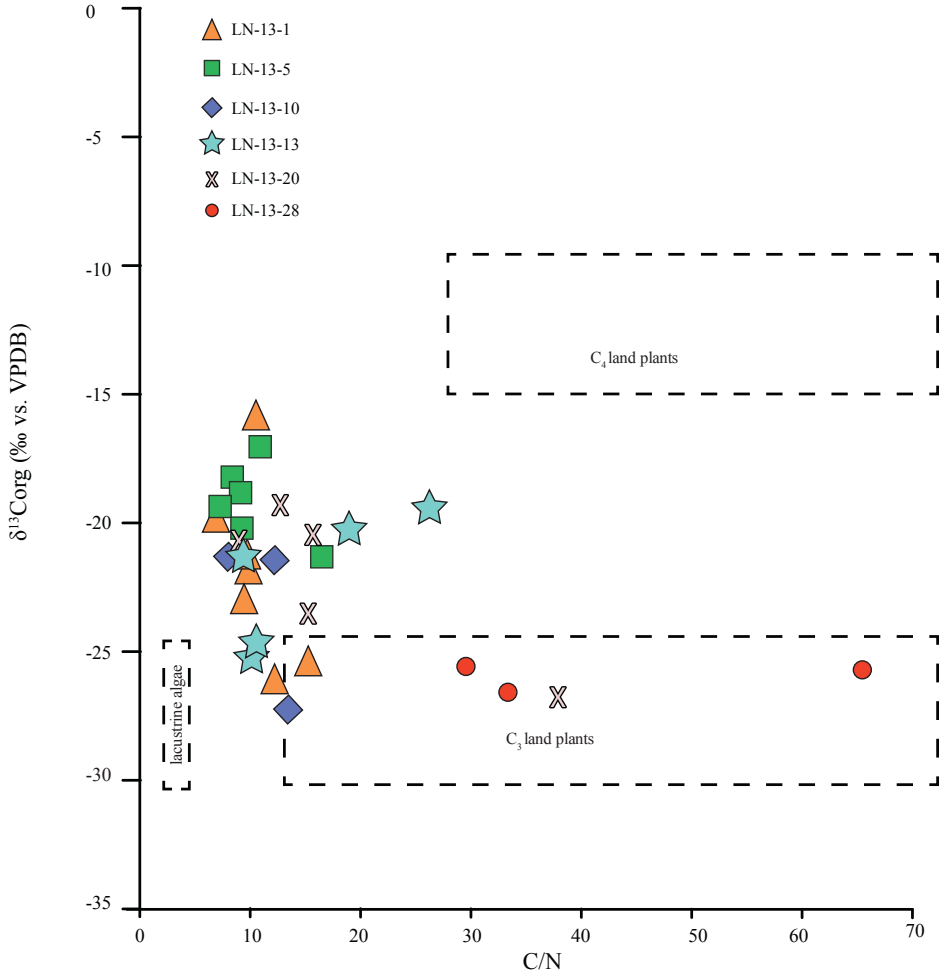

Figure 10: C/N ratios and carbon isotope compositions of organic matter within Laguna Negra bulk organic fractions. C/N values are atomic ratios. Expected values of C3, C4 plants and lacustrine phytoplankton are bounded by dashed boxes (Meyers, 1994). A large range of carbon isotopes (-15 to -26‰) suggest differential productivity across Laguna Negra (Meyers and Teranes, 2001). C/N ratios in some samples fall within the published range of C_3 plants, suggesting either high productivity, or active denitrification of organic matter (Eglinton, 1969; Kemp, 1971; Meyers and Lallier, vergés, 1999).

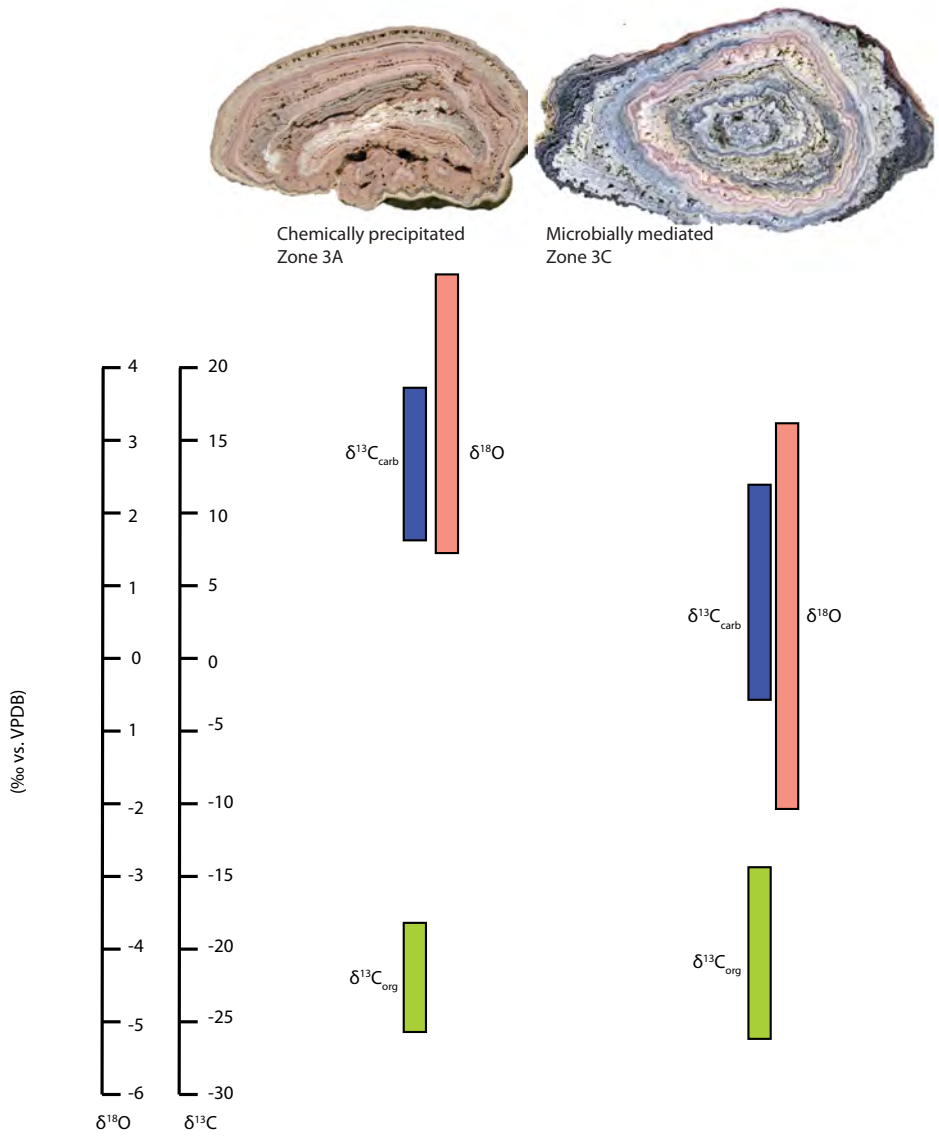

Figure 11: Range of isotopic composition according to microbialite type. Results include data from this study and that of Gomez et al. (in press). Clear isotopic separation is exhibited in oxygen isotope values between the microbially mediated oncolites from Zone 3C relative to samples from Zone 3A.

carbonate precipitation. Values of $\delta^{13}C_{org}$ range from -22 to -14‰ (vs. VPDB; Figs. 10 and 11) and are consistent with isotopic ranges reported for diatoms (-34.4 to -26.6‰) and cyanobacteria (-32.4 to -5.9‰) from a similarly hypersaline lake, Puyehue Lake, Chile (Campos *et al*., 1989; Bertrand *et al*., 2010). The average carbon isotopic composition of OM retrieved from the inferred abiotically precipitated sample (LN-13-28) is -26.1‰, which is statistically different from only one of the samples in this study (-19.4‰, LN-13-5, $p < 0.05$, $n = 4$). This data is in contrast to Gomez *et al*. (2014), which presents differences in OM carbon isotopes from oncoids collected from different zones. For instance, samples from within Zone 3A (chemically precipitated laminar crusts) have an average $\delta^{13}C_{org}$ value of ~-20‰ whereas the $\delta^{13}C_{org}$ composition of samples within Zone 3C (oncoids) is heavier, at ~-15‰. Data from Gomez *et al*. (2014) from samples collected from Zones 3A, B, and C are interpreted to reflect isotopic differences related to spatial heterogeneity of abiotic parameters within the lake, such as degree of evaporation and nutrient availability that play a formative role in biotic activity. The small sample size of each of these studies may account for inconsistent results.

Preliminary results, however, suggest differential degrees of primary and secondary productivity across zones. Studies of marine and lacustrine sedimentary deposits have shown that relative degrees of primary and secondary production can be identified through comparative examination of paired carbonate carbon and organic carbon isotopes (Gong & Hollander, 1997; Hollander & Smith, 2001; van Breugel *et al*., 2005; Guo *et al*., 2013). The isotopic fractionation between inorganic and organic compositions ($\Delta C = \delta^{13}C_{carb} - \delta^{13}C_{org}$) permits the identification of the relative roles that primary and secondary production play in the evolution of DIC. For

example, heterotrophic or secondary chemoautotrophic bacteria release CO_2 that can be several permil depleted with respect to the already isotopically light OM that is used as their carbon source (Hollander & Smith, 2001). Within oncolite LN-13-28, we speculate that increased photoautotrophy within isotopically enriched waters contributes to the average ΔC of ~40‰ in this sample. By contrast, the ΔC within the microbially mediated samples average 27 to 35‰, suggesting microbial recycling of isotopically light OM is the dominant control on carbon isotopic evolution. Identification of the potential degree to which differential biological constituents affect organic carbon isotopes within microbialites will be enhanced through ongoing research focused on determining, with greater certainty, the microbial communities and their behavior within Laguna Negra mats.

Principal Component Analysis

Statistical analysis through multivariate principal component analysis shows that fabric types (botryoidal, micritic, and isopachous) cannot be visually separated. Any observed variation between fabric types is explained by PC1, which is strontium concentration, accounting for over 99% of variation (Appendix H). The failure for fabric types to cluster in this PCA suggests that geochemistry across microfabric types is largely similar and there is no signature diagnostic of any one fabric type.

Section 6: Hydrochemical Modeling

In order to fully understand the geochemical behavior of the Laguna Negra system, and the extent to which environmental dynamics of this closed-basin lake are preserved in Laguna Negra microbialites, we employed a series of geochemical models. Specifically, we addressed questions concerning: (1) the extent to which observed lake water composition is consistent with a simple model of evaporation of surface flow; (2) the potential dependence of microbial mineralization on lake chemistry; and (3) the degree of environmental change recorded in Laguna Negra microbialites.

Evaporative concentration

To test whether lake water chemistry is consistent with a simple closed-basin model of surficial inflow and evaporative concentration, geochemical modeling was conducted with PHREEQC (Parkhurst *et al*., 1996). PHREEQC allows the prediction of dissolved chemical species in response to evaporative concentration on inlet waters. Input parameters for forward modeling are based upon *in situ* hydrochemical measurements obtained during a previous field campaign (cf. Gomez *et al*., *in press;* Table 1; Appendix A). Progressive evaporation was modeled at 25°C, with results showing concentrations of dissolved species, including salinity indicators, such as concentration of potassium, sodium, and magnesium. Saturation indices with respect to calcite and aragonite of inlet waters were produced at each step in the calculation. Most chemical constituents show an asymptotic increase with progressive evaporation, with the

exception of potassium, which displays linear behavior with an R^2 value of 1 (Fig. 12). PHREEQC-modeled concentrations are reported in molality and can be compared to measured concentrations under the assumption that density is 1 kg/L. Comparison of measured lake waters to theoretically derived ionic concentrations suggests that lake waters (based on K, Mg, Na, Cl concentrations ± 10%) represents 15-25X concentration (or 95% water loss) with respect to inlet waters (Table 8). In addition, modeled [CO_2] from 20X concentrated inlet waters (= 3162 ppm) are also in agreement with measured lake values (= 3002 ppm) obtained through end-point titration with sodium hydroxide (cf. Gomez *et al*., *in press*; Fig. 12). Notable differences occur, however, in measured concentrations of [Ca] and [SO_4]. Measured Ca concentrations (= 5776 mM) greatly exceed theoretical concentrations modeled by 25X concentration of inlet waters (= 925 mM), supporting a possible secondary source for input of calcium, such as a calcium-rich groundwater contribution (cf. Risacher, 2003; Gomez *et al*., *in press*). By contrast, measured SO_4 concentrations (1.4 mM) are substantially lower than theoretical concentrations at 25X concentration of inlet water (58 mM). Low concentrations of SO_4 are may indicate the presence of active BSR within Laguna Negra, which is consistent with the reported presence of *Bacillus* spp. (Ordoñez, 2009) which can perform dissimilatory sulfate reduction (Caspi *et al*., 2014).

An independent measure of the degree of evaporation can be modeled by comparison to measured salinity (Table 9). The conservative nature of chloride within lacustrine systems allows the concentration of chloride to be a suitable measure of salinity (Wetzel, 1975; Grosjean *et al*.,

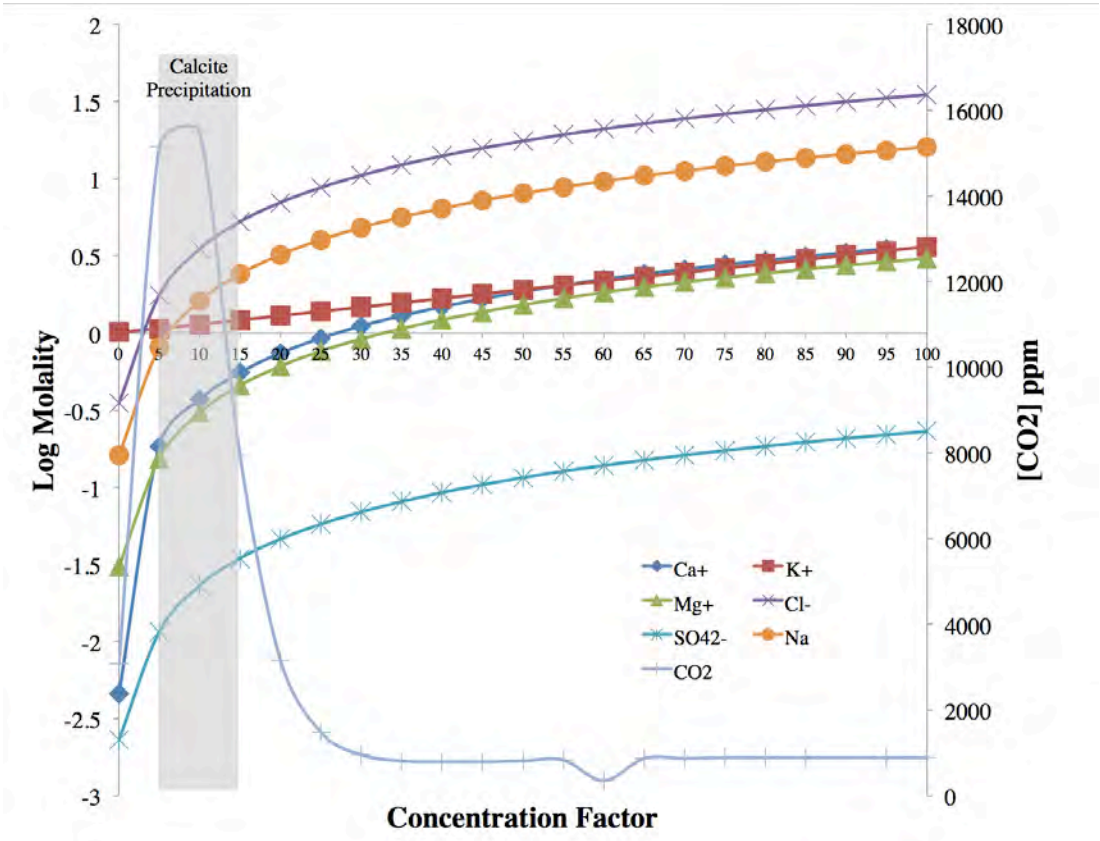

Figure 12: Ionic constituent concentrations as modeled in PHREEQC along a path of progressive evaporation of inlet waters of Laguna Negra (code in Appendix A, codes A.1 through A.19). The range of calcite precipitation was obtained through inverse modeling and shows precipitation occurs primarily in inlet waters concentrated 5 to 15X (code in Appendix A, codes A.21 through A.25).

Table 8: Summary of modeled and measured concentrations of dissolved species within Laguna Negra lake waters.

		Modeled			
Constituent	**Measured Lake Waters**	**10X Concentrated Solution**	**15X Concentrated Solution**	**20X Concentrated Solution**	**25X Concentrated Solution**
Mass of water (kg)	1	0.1001	0.06667	0.05001	0.04
Water loss (mol)	N/A	49.95	51.8	52.7	53.3
Water loss (%)	N/A	90	93.3	95	96
Ca^{+} mM	5776	369.6	554.9	739.7	924.8
K^{+} mM	204	56.04	84.15	112.2	140.2
SO_4^{2-} mM	1.414	23.03	34.58	46.1	57.6
Mg^{+} mM	392.8	304.6	457.4	609.7	762.3
Cl^{-} mM	8051	3507	5266	7019	8776
Na^{+} mM	4444	1607	2412	3216	4021
CO_2 ppm	3002	15488	7943	3162	1479

Table 9: Modeled and measured salinity of Laguna Negra lake and inlet waters. The salinity coefficient produced from chlorine representing ~66% of total dissolved solids, calculated values of salinity are in good agreement (< ~10%) with measured salinity values.

Lake Waters			
Salinity Coefficient = 1.51160			
Sample Name	**Calculated Salinity**	**Measured Salinity**	**% Difference**
	‰		
Lake Water Sample 1	324.8	324.8	8.7
Lake Water Sample 2	316.8	316.8	2.2
Lake Water Sample 10	285.6	285.6	4.8
Inlet Waters			
Salinity Coefficient = 1.51160			
Sample Name	**Calculated Salinity**	**Measured Salinity**	**% Difference**
	‰		
Inlet Water Sample 6	14.3	15.4	7.2
Inlet Water Sample 7	8.5	9.1	6.4
Inlet Water Sample 8	30.2	27.4	10.21
Inlet Water Sample 9	20.8	22.1	5.7
Inlet Water Sample 11	315	316.4	0.4
Inlet Water Sample 12	58.7	62.8	6.5

1994). Within both un-evolved inlet waters and lake waters, chloride represents ~66% of total dissolved solids, and therefore, salinity can be calculated according to:

$$\text{Salinity (‰)} = 1.55160 * Cl^{-} \text{ (mg/L)}/1000 \qquad (4) \text{ (cf. Thurman } et\ al.\text{, 2009)}$$

where 1.55160 is obtained by dividing 1 by the average the proportions of chloride represented in inlet total dissolved solids. This estimate provides agreement (within ~10%) to measured inlet waters. Assuming that lake waters of Laguna Negra represent evolved inlet waters that are concentrated 15 to 20X as suggested by comparing measured and modeled ionic concentrations, the calculated salinity is again in agreement (within ~10%) to that of measured lake waters.

Carbonate precipitation

Despite elevated ionic concentrations derived from evaporation, carbonate mineralization is restricted to the southern margin of Laguna Negra. The restriction of carbonate formation to geographical region defined by a zone of surface recharge led Gomez *et al*. (2012) to hypothesize that mixing of lake and inlet waters may be critical to microbial mineralization. PHREEQC modeling of calcite and aragonite saturation state reveals increases for both calcite and aragonite through the mixing of inlet and lake waters. Using *in situ* measurements to define inlet and lake solutions, the ratio range of mixed solutions with the highest saturation indices of calcite and aragonite is from 1:1 (50% lake water, 50% inlet water) to 1:4 (20% lake water, 80% inlet water; Table 10; Fig. 13).

Table 10: Modeled saturation indices of calcite and aragonite at 25°C during mixing of lake and inlet waters.

Ratio of LW to IW	SI Aragonite	SI Calcite	pH
100-0	0.23	0.37	5.71
95-5	0.35	0.49	5.837
90-10	0.46	0.6	5.964
85-15	0.57	0.72	6.09
80-20	0.68	0.82	6.213
75-25	0.78	0.93	6.33
70-30	0.88	1.02	6.448
65-35	0.96	1.1	6.556
60-40	1.04	1.18	6.658
55-45	1.1	1.24	6.753
50-50	1.15	1.29	6.841
45-55	1.19	1.33	6.922
40-60	1.22	1.36	6.99
35-65	1.23	1.38	7.073
30-70	1.24	1.38	7.144
25-75	1.23	1.38	7.216
20-80	1.22	1.36	7.289
15-85	1.19	1.34	7.367
10-90	1.17	1.31	7.435
5-95	1.11	1.26	7.56
0-100	1.06	1.21	7.7

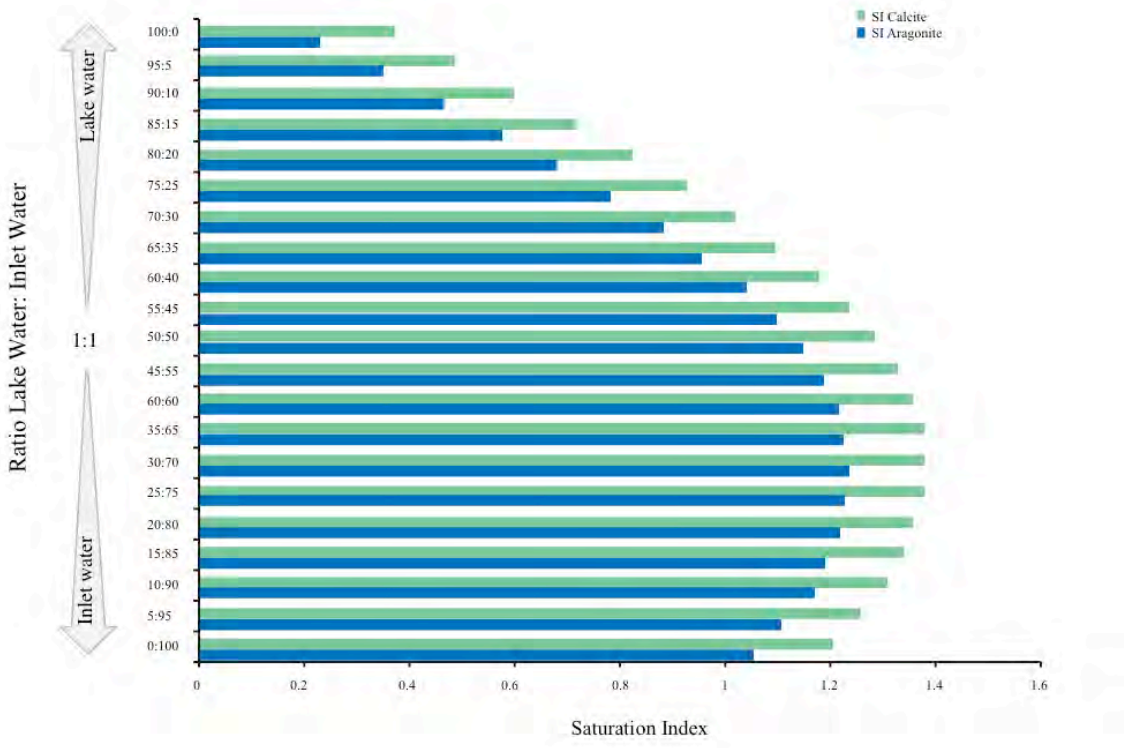

Figure 13: Modeled saturation indices of calcite and aragonite in proportions of mixed lake and inlet waters of Laguna Negra (cf. Gomez et al., in press). Values reported are from results modeled in PHREEQC at 25°C (Appendix A, code A.21 through A.25).

To better constrain the composition of the host water from which Laguna Negra microbialites precipitate, inverse modeling was conducted in PHREEQC to determine mineral precipitation along a flow path from a starting solution to an ending solution. For this modeling, it is assumed that the combined effects of evaporation, evaporite precipitation, and carbon dioxide degassing fully account for variation of all major ion concentrations within the fluid and that both starting and ending solutions are in equilibrium with atmospheric CO_2.

We conducted two end-member inverse models. The first explored mineral precipitation resulting from mixing of inlet and evolved lake waters. The mixed fluid compositions were obtained with PHREEQC mixing models using *in situ* data (Table 1) and were shown to correspond to the mixed fluid compositions with the highest modeled saturation indices for both calcite and aragonite (*see* Fig. 13). The second inverse model addressed mineral precipitation during evaporation of inlet waters by measured inlet water compositions. In both cases, calcite is produced by the model and shows that calcite is only produced within a range of concentration factors between 5 and 15X (Table 11). These results emphasize the critical role that saturation state plays in microbial mineralization and suggests that fresh water mixing is critical to the mineralization process.

Unfortunately, PHREEQC modeling is unable to directly define the potential role of microbial metabolisms in driving the mineralization process. It should be noted that the obvious presence of primary (i.e. visible sediment-binding microbial mats) and secondary (i.e. sulfurous odor emanating from muds) productivity is also restricted to this mixing zone. It is well known

Table 11: The modeled amounts of calcite precipitated as a result of inverse modeling of non-evolved inlet waters as the beginning solution and varying degrees of mixed water and concentrated inlet water as ending solutions. Results for calcite precipitation with inverse modeling of mixed fluids and evaporated fluids contains 25% and 10% uncertainty in PHREEQC, respectively. Code contained in Appendix A (A.21 through A.25).

	Beginning solution	**Ending solution**	**Calcite precipitated (moles)**
Mixing (lake water:inlet water)	Inlet water	50:50	0.0020008
	Inlet water	45:55	0.001762
	Inlet water	40:60	0.001528
	Inlet water	35:65	0.001293
	Inlet water	30:70	0.001099
	Inlet water	25:75	0.0008876
	Inlet water	20:80	0.0006898
Evaporative concentration	Inlet water	5X	0.0006811
	Inlet water	10X	0.001595
	Inlet water	15X	0.001302

that the metabolic effects of microorganisms can to some degree influence the lithification of the microbial mat system. For instance, photosynthetic drawdown of CO_2 associated with cyanobacteria and other photoautotrophs (diatoms) has been shown to result in net carbonate precipitation according to:

$$2HCO^{3-} + Ca^{2+} \rightarrow [CH_2O] + CaCO_3 + O_2 \qquad (5)\ (\text{Dupraz } \textit{et al.}, 2004)$$

wherein increases in microenvironmental pH result in elevated carbonate ion activities. Additionally, heterotrophic oxidation of organic exudates (such as EPS) of photoautotrophs provides ions that may be used in crystal growth. For example, during sulfate reduction, changes in microenvironmental alkalinity combined with OM degradation may result in net carbonate precipitation according to:

$$2[CH_2O] + SO_4^{2-} + Ca^{2+} \rightarrow CaCO_3 + CO_2 + H_2O + H_2S \qquad (6)\ (\text{Dupraz } \textit{et al.}, 2004)$$

Although models have shown that in saline environments, sulfate reduction is not effective in carbonate production (Meister, 2013), the extent to which microbial metabolisms facilitate lithification of Laguna Negra mats is still unconstrained and we hypothesize that future work focused on biomarker identification will support the idea that mineralization reflects some degree of biogeochemical influence.

Isotope modeling

PHREEQC modeling (see above) suggests that changes in saturation state associated with fresh water influx and evaporation play a primary role in carbonate formation within Laguna Negra. In order to identify the extent to which fluctuating water balance is recorded in Laguna Negra microbialites, we examined the isotopic records preserved within Laguna Negra microbialites. Although more complicated models for hydrological balance can be found in the literature, these require the definition of parameters that are not yet constrained for the Laguna Negra lacustrine system. For example, rates of evaporation and hydrological change have been modeled for Lake Titicaca (Cross, 2002) through the combined use of isotope records with empirically-based models using parameters such as mass of flux of input waters and saturation vapor pressure. Here, we address primary effects of lake recharge and evaporation with two isotopic models: First, modeling of net recharge and expansion through analysis of the degree of covariance of carbon and oxygen isotopes within carbonate phases allows first order approximation of times of fresh water influx and prolonged evaporation. Second, the ratio of precipitation to evaporation can be estimated through the use of published oxygen isotope models related to regional climate and isotope geochemistry characteristic of the basin.

Modeling episodes of basin contraction and expansion through isotopic proxy data requires understanding of the fractionation processes responsible for isotopic signals as well as sensitivity to defined parameters. Within lacustrine sediments, the $\delta^{18}O$ of carbonate phases relate directly to the host waters in which they formed. This relation can be expressed as:

$$\delta^{18}O_{water} = [(1000+ \delta^{18}O_{carbonate})/\alpha_{carbonate\text{-}water}] - 1000 \quad (7)$$ (Friedman & O'Neil, 1977)

The isotopic fractionation between water and calcite ($\alpha_{carbonate\text{-}water}$) is dependent upon both mineralogy and temperature of formation. In order to derive the oxygen isotope composition of host waters, the following empirically based equations specific to mineralogy were used:

$$1000\ln\alpha_{calcite\text{-}water} = (2.78 * 10^6/T^{-2}) - 2.89 \quad (8)$$ (Friedman & O'Neil, 1977)

$$1000\ln\alpha_{aragonite\text{-}water} = 17.88 * (1000/T) - 31.14 \quad (9)$$ (Kim *et al*., 2007)

where T is the temperature in Kelvin.

In our initial modeling, we assume that evaporation is the principle control on preserved oxygen isotope composition, rather than temperature. In order to account for extreme daily and seasonal temperature fluctuations experienced by Laguna Negra (cf. Scwalb, 1999) isotopic values were modeled across a range of temperatures from 5°C to 45°C. PHREEQC modeling of saturation indices shows that calcite remains supersaturated throughout this temperature range.

Within oncolites LN-13-1 and LN-13-5, which exhibit moderate covariation ($R^2 = 0.63$ and 0.54, respectively), there is an overall 3-5‰ variation in $\delta^{18}O_{carb}$ and ~7‰ variation in $\delta^{13}C_{carb}$. Oncolite LN-13-13 shows the highest degree of covariance, but is more variable in its

time-wise trend and presents an overall difference of 5‰ and 10‰ in $\delta^{18}O$ and $\delta^{13}C$ values, respectively. In order to test if these substantial changes in isotopic composition can be explained with degassing during evaporation, Rayleigh fractionation was modeled within waters with a starting composition of -10 (Risacher, 2003) according to:

$$R/R_0 = f^{\alpha-1} \qquad (10)\ (\text{Faure, 1986})$$

where R is the final isotopic ratio ($[^{18}O]/[^{16}O]$ or $[^{13}C]/[^{12}C]$), R_0 is the original isotopic ratio prior to evaporation, f is the fraction of the original volume of water remaining, and α is the temperature-dependent fractionation factor during phase transition. Since the Argentinian Altiplano is subjected to both seasonal and daily extremes, fractionation factors from a temperature range of 0 to 20 °C were modeled, revealing an 8 permil difference between oxygen isotopic compositions of water at 0°C (+38‰) and 20°C (+30‰) when $f = 0.01$.

Within a body of water subjected to strong evaporation, oxygen isotopic enrichment with respect to the heavier isotope is expected (Craig & Gordon, 1965). Such fractionation results from the relative ease with which the isotopically lighter isotope enters the vapor phase, thereby driving the isotopic composition of the water reservoir to be heavier. Rayleigh modeling of oxygen isotopes within vapor and liquid along a path of forward evaporation can be found in Fig. 14. In this model, we used $\alpha = 1.0102$ at 10°C (Dansgaard, 1964). Response to Rayleigh fractionation associated with evaporation suggests significant isotope enrichment, from -10 to

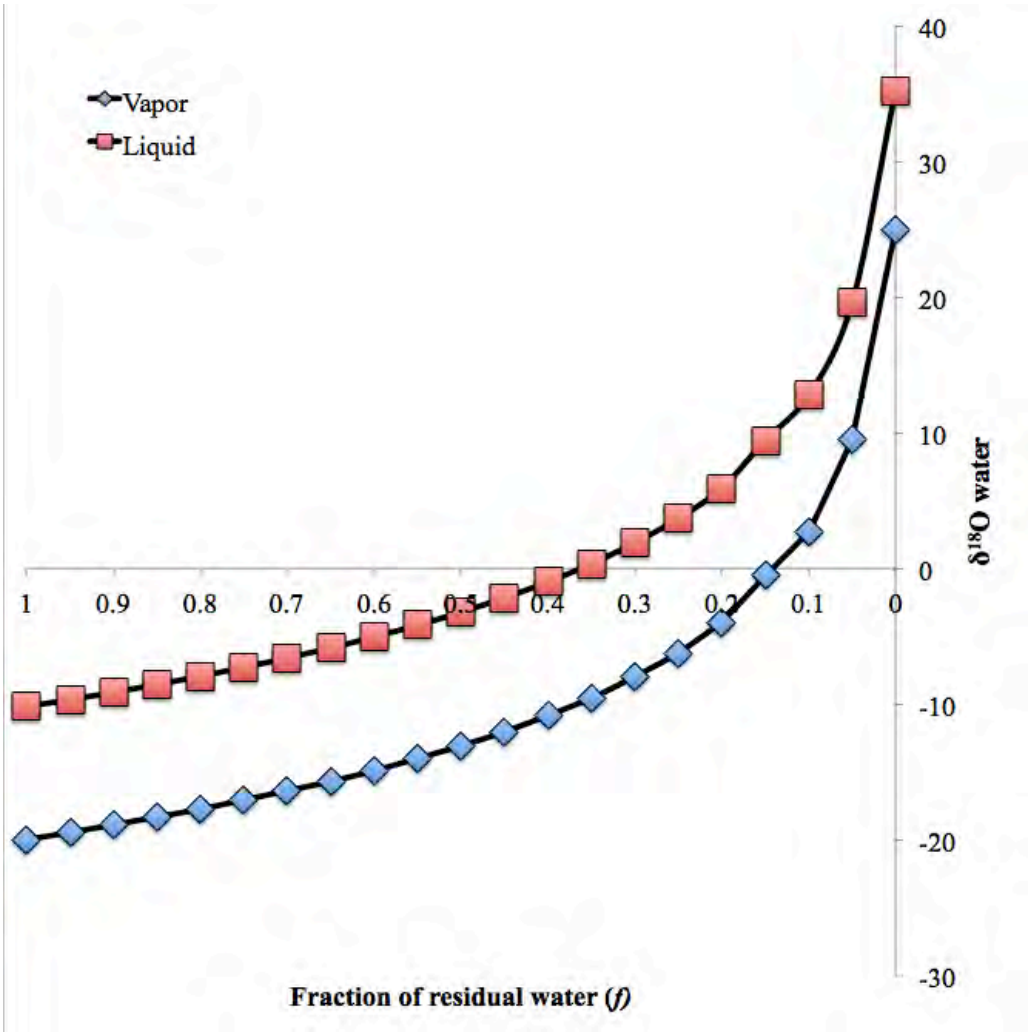

Figure 14: The response of the oxygen isotopic composition of water according to a Rayleigh fractionation model along a forward flowpath of evaporation from a starting $\delta^{18}O$ of -10 (Risacher, 2003). α = 1.0102 (Dansgaard, 1964).

35.2‰. This appreciable shift in $\delta^{18}O$ composition suggests that significant isotopic evolution within the waters of Laguna Negra can likely be attributed Rayleigh distillation.

In addition to oxygen isotopes, the application of Rayleigh fractionation to carbon isotopes is consistent with evaporation playing a key role in isotopic evolution. Rayleigh modeling of DIC with a starting composition +2, which is in isotopic equilibrium with atmospheric CO_2 (Valero-Garcés *et al*., 1999), shows that isotopic enrichment as high as +18‰ in 20% residual water (Fig. 15). The isotopically enriched values within the chemically precipitated sample of this study (from +8 to +18‰) are consistent with Rayleigh fractionation associated with degassing and removal of >80% of initial water volume. By contrast, when observed within the context of Rayleigh distillation, isotopically depleted values measured from microbially mediated samples (avg. ~+9 to +10) correspond to the removal 50 to 65% of initial water volume. These results are inconsistent with PHREEQC modeling, which suggest that calcite precipitation is only achieved after 80 to 93% water is removed. PHREEQC modeling, however, does not take into account potential biological influence during geochemical evolution. Such disparity between models therefore supports a fundamental role for biology in precipitation of oncolites that are inferred to be microbially mediated. In this scenario, calcium carbonate precipitation within "microbially mediated" oncolites within Laguna Negra without extensive evaporation may reflect locally variable DIC, potentially driven by the introduction of isotopically light DIC into the reservoir during biological remineralization. Such an interpretation of differential influences of biology on carbon

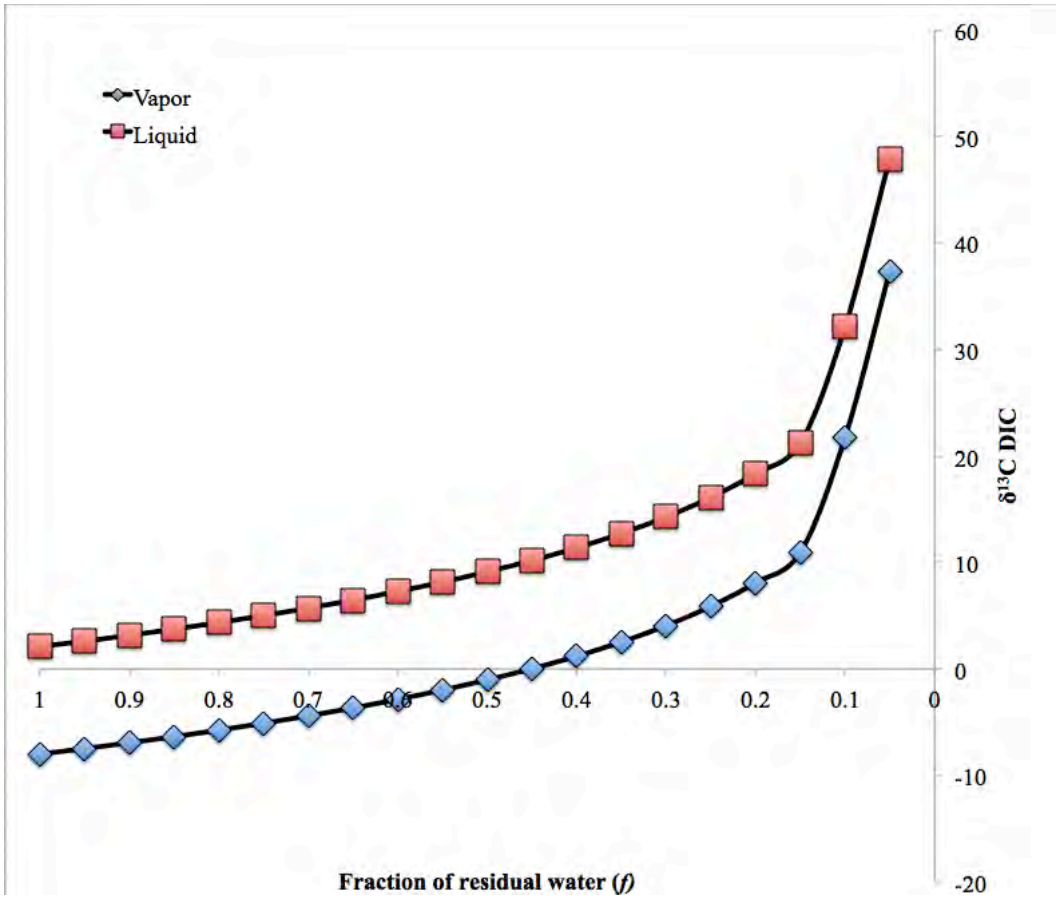

Figure 15: The response of the isotopic composition of dissolved inorganic carbon according to a Rayleigh fractionation model along a forward flowpath of evaporation from a starting $\delta^{13}C$ of +2 (Valero-Garcés et al., 1999). α = 1.01017(Emrich et at., 1970).

isotopic evolution is consistent with TOC data. Unlike the microbially mediated samples of this study, the chemically precipitated sample contains virtually no OM and has measured oxygen and carbon isotope values that are strikingly consistent with isotopic evolution via Rayleigh distillation.

The results of our modeling serve only as an approximation of the degree to which Rayleigh distillation may be responsible for isotopic signatures. Some of the underlying assumptions of a Rayleigh model of isotopic evolution, such as thermodynamic equilibrium between isotopic reservoirs with unchanging boundary conditions and a constant fractionation factor, may not be applicable throughout microbialite growth, and therefore, this modeling is only an approximation of the influence of Rayleigh processes on isotopic signals (see Gat, 1996 *for discussion*).

For more detailed modeling of hydrological balance as a function of precipitation to evaporation ratios within the basin, measured oxygen isotopes were used in concert with published models. The isotopic value of formation waters can be derived through modeling of steady state conditions according to isotopic buildup typical of lacustrine systems (Gat, 1996). Under hydrological steady state, the oxygen isotopic buildup within a lake is expressed as:

$$\Delta\delta = \delta_{\text{lake, steady state}} - \delta_{\text{in}} = (\delta_{\text{a}} - \delta_{\text{in}} + \Sigma/h)/\{1 + [(F_{\text{in}}/\text{E}) * (1 - h)/h)]\}$$

(12) (Gat, 1996)

where δ_{lake} is the oxygen isotopic composition of the lake, δ_a is $\delta^{18}O$ of atmosphere, δ_{in} is $\delta^{18}O$ of inlet waters, Σ is the evaporative enrichment factor, *h* is relative humidity, and F_{in}/E is the water balance expressed as the ratio of input to evaporation and is equal to P/E (Gat, 1995). The water balance of the lake during lamina deposition can then be derived with recorded oxygen isotope values from the lake assuming:

1. δ_a is in isotopic equilibrium with regional precipitation and inflow, $\delta_a = \delta_{in} - \Sigma$.
2. δ_{in} is equal to the reported value for input waters from Andean lakes above 4,000 m a.s.l. (-10‰ vs. SMOW), as suggested by lighter than expected oxygen isotope values recorded within carbonate (Fritz *et al*., 1981).
3. Kinetic fractionation is the driver of isotope enrichment.
4. $\alpha_{carb\text{-}vapor} = 1.0029$ (Faure, 1986). $\alpha_{calcite\text{-}water} = 1.035$ (Friedman & O'Neil, 1977). $\Sigma = 1000\ln\alpha$
5. Relative humidity (*h*) is 0.155 (Boschetti *et al*., 2007).
6. Temperature is 25°C.

Observed oxygen isotopes were examined against modeled oxygen isotopes that were produced with equation 26 along P/E ratios from 0.1 to 1 along increments of 0.01. Model sensitivity was tested for individual parameters that required definition. Both humidity and oxygen isotopic composition of inlet waters play important roles in modeled P/E values. The values of input waters (δ_{in}) and relative humidity (*h*) were selected from the published values within the region. δ_{in} was chosen from the reported value for input waters from Andean lakes above 4,000 a.s.l (-

10‰ SMOW; Risacher, 2003) and *h* was chosen as the average reported relative humidity between 27° and 28°S (Boschetti *et al*., 2007).

Isotope modeling results

Modeling revealed clear isotopic differences in lake waters between zones. Modeled values from Zone 3A (avg. = 6.8‰ vs. SMOW) are consistent with values reported for other saline lakes in the region (from 4.3 to 7.3‰; Valero-Garcés *et al*., 2001), while the average modeled values of δ_{lake} from within Zone 3C is much lighter, with average values equal to 2.7‰. Fig. 16 shows the theoretical trend of oxygen isotope response to change in the P/E ratio. By using equation 21 in concert with the aforementioned assumptions, time-wise P/E ratios were obtained. Although isotopic shifts are variable across microbialites, the data across most samples show an overall progression toward a higher water balance ratio, the result of which is either increased precipitation meltwater input or decreased rates of evaporation. The overall change in modeled P/E ratio is similar across samples (~0.04), with the exception of LN-13-1, which is calculated to reflect a change in P/E of 0.14 (Fig. 17). Surprisingly, even the chemically precipitated sample (Zone 3A) records the same degree of evaporation and basin contraction as recorded in samples from Zone 3C. Despite high frequency fluctuations that may reflect spatial differences, if we assume that the geochemical signatures within each sample is recording the same general time period, consistency in modeled P/E ratios suggests that the overall signature of basin dynamics is preserved within microbialites regardless of signal variability that is dependent upon geographic position within the lake.

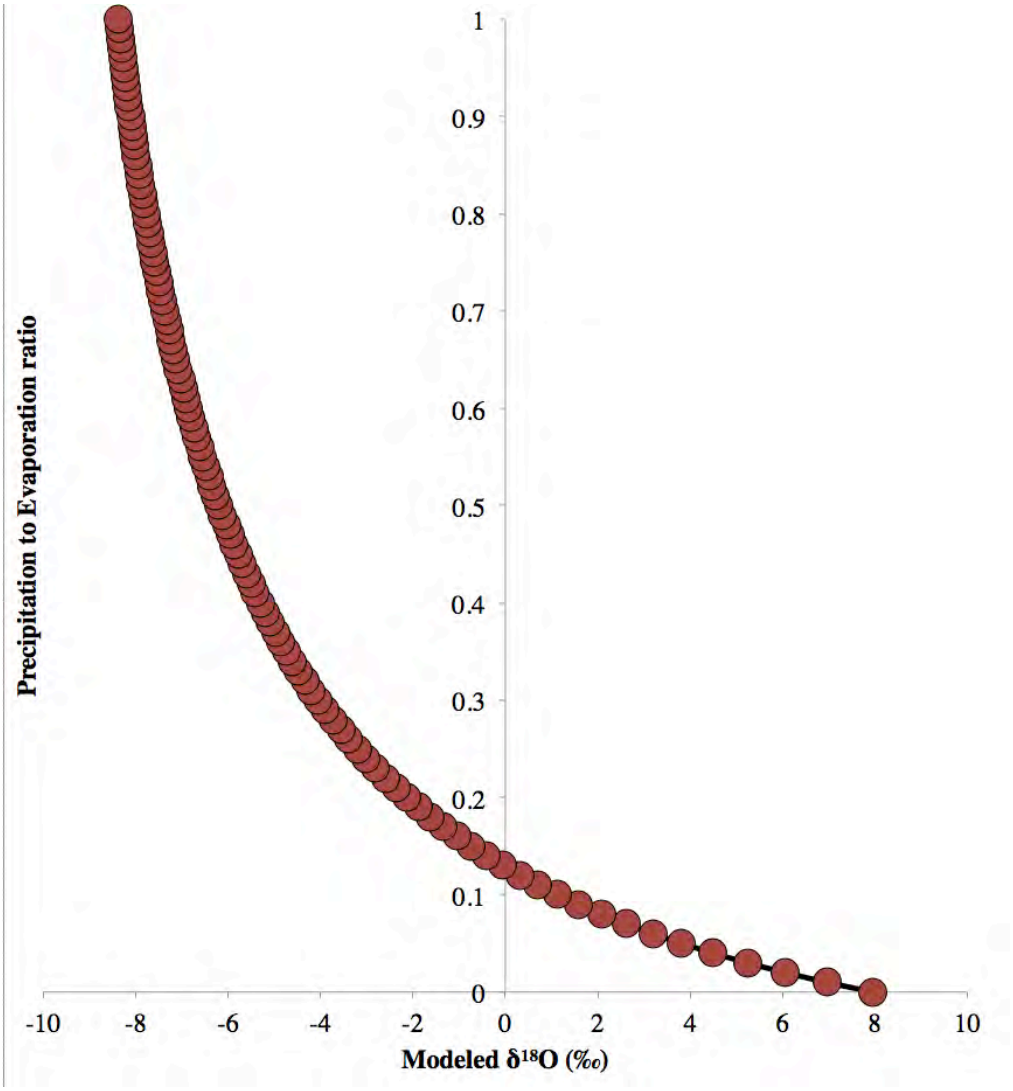

Figure 16: Modeled oxygen isotopes of calcite with increase precipitation to evaporation ratios. Light isotope enrichment displays exponential decay with decreased ratios according to the oxygen isotope buildup model from Gat (1996).

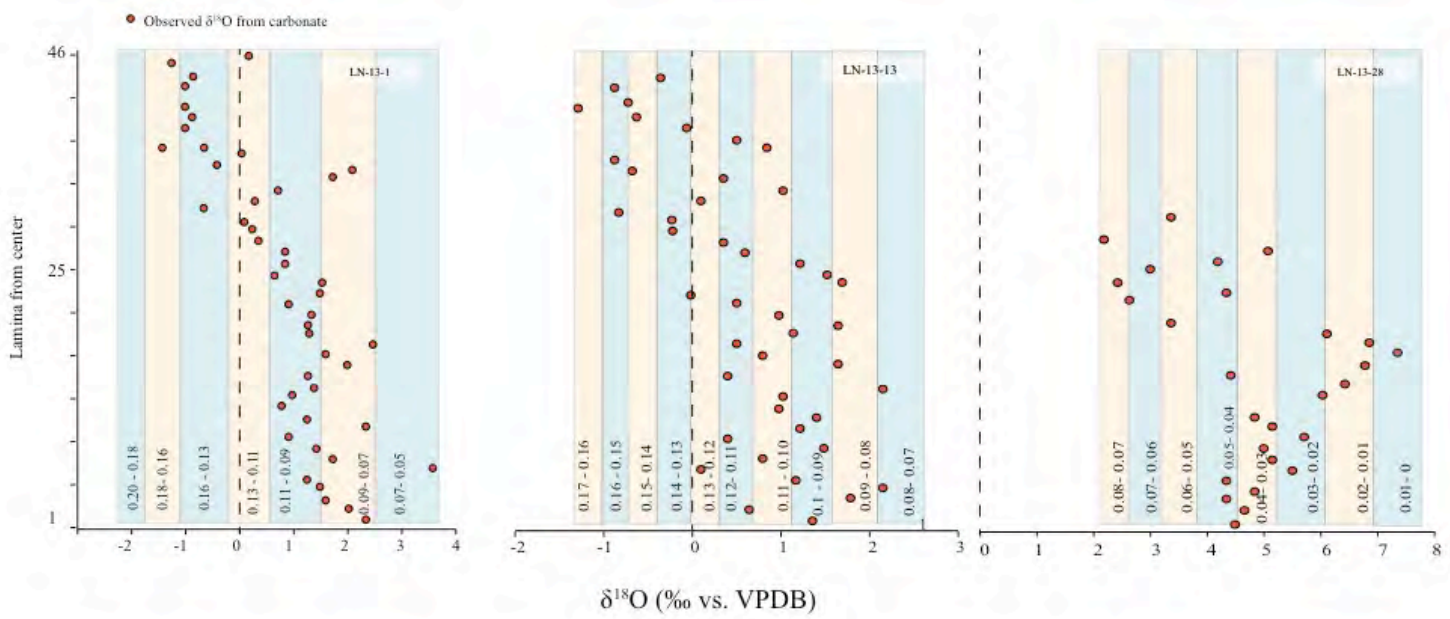

Figure 17: Observed oxygen isotopes within three microbialites. Modeling results show that a shift from the heaviest observed oxygen isotope value (3.58 ‰) to the lightest observed isotope value (-2.04 ‰), represents a change in P/E from ~0 to ~ 0.16.

Section 7: Discussion

If the microbialites of Laguna Negra represent time-series evolution of the basin from around 2,000 years ago, records of changes in effective moisture should be evident within successive laminae. Indeed, analyses of salinity proxies ([Mg] and [Sr]) (Fig. 9), coupled with models of effective moisture (see above), suggest that a systematic increase in the contribution of brackish input water is apparent throughout microbialite growth. Although high frequency changes are seen across laminae, from the center of the microbialite outward, there is an overall general trend of lightening of both $\delta^{13}C$ (Fig. 6) and $\delta^{18}O$ (Fig. 7), indicating basin-wide recharge preserved during microbialite growth and mineralization.

Data from Laguna Negra therefore suggests time-wise increases in effective moisture, which is consistent with regional lake records (Garcés *et al*., 1995; Grosjean *et al*., 1997; Schwalb *et al*., 1999). Isotope modeling of Rayleigh distillation supports the idea that the primary control on isotopic evolution may be evaporation, with mixing and biological metabolisms playing critical roles in calcite precipitation. Despite heavy carbon isotope enrichment similar to other lakes in the region (up to +18.2‰, this study), the degree of isotopic covariance commonly observed in lakes in the Altiplano is not seen in Laguna Negra. Weaker covariance appears to result from variability of local signals produced by relative spatial position within the lake and potential overprinting of abiotic signals by microbial activity.

Lacustrine systems have the potential to record distinctive biochemical signals that are imparted by primary production and microbial reworking of OM. Variability in recovered C/N ratios of sedimentary OM within Laguna Negra microbialites suggests that differential biological overprinting during biologically-mediated precipitation has likely occurred. For example, elevated C/N ratios above the published range for lake algae and plankton (6 to 10; Meyers & Teranes, 2001) suggests decomposition and remineralization of particulate and dissolved organic matter. In addition, low measured sulfate concentrations suggest the presence of microbial metabolisms, namely sulfate reducers, with the potential to influence inorganic geochemical signals.

Evidence of biological influence is also potentially recorded in organic carbon isotopes. The sedimentary $\delta^{13}C_{org}$ of bulk organic carbon, or TOC, is a function of several interconnected factors, such as heterotrophic degradation of DOM, primary production, allochthonous sources, trophic level, and the isotopic composition and concentrations of DIC (Hayes *et al*., 1989; Hinga K. R., 1994; Hayes *et al*., 1999; Kienast M., 2001; Cramer & Saltzman, 2007). Characteristic $\delta^{13}C_{org}$ ranges result from the isotopic discrimination exhibited in different photosynthetic pathways. For example, the C_3 biochemical pathway used in cyanobacterial and diatom photosynthesis selectively incorporates the lighter isotope of carbon into biomass with a discrimination of about 20‰ (O'Leary, 1988; Farquhar *et al*., 1989; Roberts *et al*., 2007), resulting in organic carbon isotopes in the range of -25 to -30‰ vs. VPDB (Meyers & Teranes, 2001). Although carbon isotope fractionation between organic and inorganic carbon within Laguna Negra sedimentary OM is consistent with the fractionation factor associated with

photosynthesis (ε = average between 29 and 40 ‰, this work), $\delta^{13}C_{org}$ may reflect microbial reworking of OM, with heavy $\delta^{13}C_{org}$ values coinciding with times of stimulated primary productivity that effectively deplete the DIC reservoir of the preferred carbon isotope, ^{12}C (Hollander & McKenzie, 1991) and negative $\delta^{13}C_{org}$ shifts arising from DIC mineralized from isotopically light OM by secondary producers (van Breugel *et al*., 2005).

In addition to the clear evidence of heterotrophic activity from organic isotopes (e.g. $\delta^{13}C_{org}$ as low as -26.9‰), interestingly, biological influence is also potentially recorded in $\delta^{13}C_{carb}$, with layers of abundant micrite relative to cement phases (microspar and botryoids) containing the lightest values of $\delta^{13}C_{carb}$. The extent to which biology overprints Rayleigh fractionation $\delta^{13}C_{carb}$ signatures is seen most clearly in the geochemistry of microbially-mediated samples, which show depleted values relative to the chemically precipitated sample.

With respect to Laguna Negra, enhanced productivity is inferred from heavy organic carbon isotope signatures. While it is difficult to assess the relative degrees of productivity between the chemical zones from our data set, when placed into the framework of previous organic carbon isotope analysis (Gomez *et al*., 2014), trends become clearer (Fig. 11). Heavier isotopic values of $\delta^{13}C_{org}$ within Zone 3C reflects higher amounts of primary productivity relative to Zone 3B, which contains no visible microbial mats. As suggested by $\delta^{13}C_{org}$ values, the physiochemical heterogeneity across the zones of Laguna Negra cause differences in either the role that biological communities play with respect to biogeochemical processes, or differences in the communities themselves. While work is currently ongoing to fully characterize the

microbiological consortia and distribution throughout the lake, fundamental differences in $\delta^{13}C_{org}$ lend to interpretations of localized differences in OM sources.

Comparison to regional records

Ongoing efforts to reconstruct past climate conditions of the Andean Altiplano have focused on changes in regional paleohydrology since the Late Glacial – Holocene transition (~19,000 BP), when abrupt moisture changes first became evident. Sedimentological analysis of paleodata from this time coupled with water budget models has allowed the identification of humid phases across the Altiplano occurring exclusively above 3500 m a.s.l (Grosjean, 1994). These phases, which have been attributed to intensification of easterly monsoonal sources within the subtropical zone (Garleff *et al*., 1993), resulted in lake level high stands within closed-basin saline lakes, such as Laguna Lejia, Chile (Grosjean, 1994; 23°30'S, 67°42'W). Lake records show that it was established during a period characterized by a wetter climate (Bobst *et al*., 2001) ~15,000 – 14,000 yr BP, and that a humid phase persisted from 13,500 to 11,300 yr BP.

A dramatic shift in moisture changes is seen with the onset of arid conditions during the Mid Holocene. This step-wise change in effective moisture has been identified within Laguna Lejia as well as additional mineralogical and authigenic carbonate geochemical proxy data from Laguna Miscanti, Chile (23°44'S, 67°46'W). The most arid phase in the Altiplano has been interpreted to have occurred from ~8,000 to 4,000 yr BP (Valero-Garcés *et al*., 1996), with current arid conditions likely being established before 8500 yr BP based upon archeological and

sediment records (Grosjean, 1994; Grosjean & Núñez, 1994). Climate proxies now reveal increasing effective moisture during the Late Holocene (4,000 – 3,000 yr BP) within the tropical and temperate regions of South America, with a systematic shift toward higher lake levels. For example, the El Peinado basin within Northwestern Argentina experienced increases lake levels during the Late Holocene (Valero-Garcés *et al*., 2000) and reconstruction of paleohydrological evolution is concordant with other multi-proxy regional records, including those from Southern Argentina (Stine, 1994), the Chilean Altiplano (Grosjean *et al*., 1997), Lake Titicaca (Mourguiart *et al*., 1992), the Pampa (Quattrocchio *et al*., 2008), and the arid Andes across 29°S (Grosjean *et al*., 1998). Currently, increased humidity within the region has been identified as two separate episodes (3,000 – 2,600 years BP and 2,200 – 1,800 years BP), which are characterized by relative humidity 15 to 20% above present levels (Boschetti, 2007). Such increased effective moisture has been attributed to strengthened extratropical winter precipitation and sources of Pacific moisture along 18°S to 27°S (Grosjean *et al*., 1997). A southern shift of tropical moisture during the Late Holocene as suggested by Garleff *et al*. (1993) and others (Grosjean *et al*., 1997) would have had a great impact on lacustrine hydrodynamics within the southern Altiplano, such as Laguna Negra, manifesting in higher lake levels and decreased salinity. Such a trend of regional increased effected moisture is consistent with Laguna Negra paleohydrological dynamics as reconstructed through observed and modeled results. Agreement between proxy data recovered from mineralized microbialites of Laguna Negra and regional records suggests that, despite the potential microbial overprinting and local effects, these deposits faithfully record general climate signals within their geochemical archives.

Section 8: Conclusion

In order to elucidate the nature and degree to which environmental fluctuations are recorded in paleodata of Laguna Negra microbialites, time-series examination of geochemical signatures within successive laminae were conducted. Multi-proxy analysis, including mineralogical, organic and inorganic geochemistry demonstrated unambiguous comprehensive trends of increase contribution from input waters or decreased evaporation within Laguna Negra throughout the Late Holocene. Geochemical modeling allowed time-wise reconstruction of phases of basin contraction and expansion as recorded through isotopic markers, the results of which were mostly in accordance with elemental data. Discrepancies in evaporation and salinity proxies ($\delta^{18}O$ and [Sr], respectively) are likely the result of discontinuous carbonate precipitation along the entire path of hydrological evolution, wherein trace metal incorporation in carbonate is only recording a small snapshot of water evolution during precipitation. PHREEQC geochemical modeling suggests that precipitation occurs only when inlet water is concentrated within the range of 5 to 15X. In addition, differential results from recoverable OM proxies within Laguna Negra microbialites suggest that microbial recycling is a critical parameter in sedimentary OM signatures. Microfabric analysis combined with bulk organic geochemistry shows that micritic microfabrics, and to a lesser degree, botryoidal fabrics, are associated with abundant microbial activity as interpreted through OM isotopes and C/N ratios. Spatial variability in geochemistry is also evident between samples from separate zones, indicating local influences on geochemistry that can be identified through inorganic geochemical proxies, and to a smaller extent, organic proxies as well.

List of References

Abbott MB, Wolfe BB, Wolfe AP, Seltzer GO, Aravena R, Mark BG, Polissar PJ, Rodbell DT, Rowe HD, Vuille M (2003) Holocene paleohydrology and glacial history of the central Andes using multiproxy lake sediment studies. *Palaeogeography, Palaeoclimatology, Palaeoecology,* **194**, 123-138.

Alonso RN, Jordan TE, Tabbutt KT, Vandervoort DS (1991) Giant evaporite belts of the Neogene central Andes. *Geology,* **19**, 401-404.

Arp G, Bielert F, Hoffmann V-E, Löffler T (2005) Palaeoenvironmental significance of lacustrine stromatolites of the Arnstadt Formation ("Steinmergelkeuper", Upper Triassic, N-Germany). *Facies,* **51**, 419-441.

Baker PA, Gieskes JM, Elderfield H (1982) Diagenesis of Carbonates in Deep-Sea Sediments--Evidence From SR/CA Ratios and Interstitial Dissolved SR2+ Data. *Journal of Sedimentary Research,* **52**.

Berman T (1990) Microbial food-webs and nutrient cycling in lakes: changing perspectives. In: *Large Lakes*. Springer, pp. 511-525.

Berner R (1975) The role of magnesium in the crystal growth of calcite and aragonite from sea water. *Geochimica et Cosmochimica Acta,* **39**, 489-504.

Bertrand S, Sterken M, Vargas-Ramirez L, De Batist M, Vyverman W, Lepoint G, Fagel N (2010) Bulk organic geochemistry of sediments from Puyehue Lake and its watershed (Chile, 40°S): Implications for paleoenvironmental reconstructions. *Palaeogeography, Palaeoclimatology, Palaeoecology,* **294**, 56-71.

Bissett A, Beer DD, Schoon R, Shiraishi F, Reimer A, Arp G (2008) Microbial Mediation of Stromatolite Formation in Karst-Water Creeks. *Limnology and Oceanography,* **53**, 1159-1168.

Bissig T, Riquelme R (2010) Andean uplift and climate evolution in the southern Atacama Desert deduced from geomorphology and supergene alunite-group minerals. *Earth and Planetary Science Letters,* **299**, 447-457.

Bobst AL, Lowenstein TK, Jordan TE, Godfrey LV, Ku T-L, Luo S (2001) A 106ka paleoclimate record from drill core of the Salar de Atacama, northern Chile. *Palaeogeography, Palaeoclimatology, Palaeoecology,* **173**, 21-42.

Bookhagen B, Haselton K, Trauth MH (2001) Hydrological modelling of a Pleistocene landslide-dammed lake in the Santa Maria Basin, NW Argentina. *Palaeogeography, Palaeoclimatology, Palaeoecology,* **169**, 113-127.

Bosak T, Knoll AH, Petroff AP (2013) The Meaning of Stromatolites. *Annual Review of Earth and Planetary Sciences,* **41**, 21-44.

Boschetti T, Cortecci G, Barbieri M, Mussi M (2007) New and past geochemical data on fresh to brine waters of the Salar de Atacama and Andean Altiplano, northern Chile. *Geofluids,* **7**, 33-50.

Boyle JF (2001) Inorganic Geochemical Methods in Palaeolimnology. In: *Tracking Environmental Change Using Lake Sediments* (eds Last W, Smol J). Springer Netherlands, pp. 83-141.

Braissant O, Decho AW, Dupraz C, Glunk C, Przekop KM, Visscher PT (2007) Exopolymeric substances of sulfate-reducing bacteria: Interactions with calcium at alkaline pH and implication for formation of carbonate minerals. *Geobiology,* **5**, 401-411.

Campos H, Steffen W, Agüero G, Parra O, Zúñiga L (1989) Estudios limnologicos en el Lago Puyehue (Chile): morfometria, factores fisicos y quimicos, plancton y productividad primaria. *Medio Ambiente,* **10**, 36-53.

Carpenter SJ, Lohmann KC (1992) SrMg ratios of modern marine calcite: Empirical indicators of ocean chemistry and precipitation rate. *Geochimica et Cosmochimica Acta,* **56**, 1837-1849.

Carrapa B, Adelmann D, Hilley GE, Mortimer E, Sobel ER, Strecker MR (2005) Oligocene range uplift and development of plateau morphology in the southern central Andes. *Tectonics,* **24**, TC4011.

Caspi Et Al. C (2014) The MetaCyc database of metabolic pathways and enzymes and the BioCyc collection of Pathway/Genome Databases. Nucleic Acids Research.

Chivas AR, De Deckker P, Cali JA, Chapman A, Kiss E, Shelley JMG (1993) Coupled stable-isotope and trace-element measurements of lacustrine carbonates as paleoclimatic indicators. *Geophysical Monograph Series,* **78**, 113-121.

Christie D, Boninsegna J, Cleaveland M, Lara A, Le Quesne C, Morales M, Mudelsee M, Stahle D, Villalba R (2011) Aridity changes in the Temperate-Mediterranean transition of the Andes since ad 1346 reconstructed from tree-rings. *Clim Dyn,* **36**, 1505-1521.

Craig H, Gordon LI (1965) Deuterium and oxygen 18 variations in the ocean and the marine atmosphere.

Cramer BD, Saltzman MR (2007) Early Silurian paired δ13Ccarb and δ13Corg analyses from the Midcontinent of North America: Implications for paleoceanography and paleoclimate. *Palaeogeography, Palaeoclimatology, Palaeoecology,* **256**, 195-203.

Cross S, Baker, P., Seltzer, G., Fritz, S., Dunbar, R. (2002) Late Quaternary climate and hydrology of tropical South America inferred from an isotopic and chemical model of Lake Titicaca, Bolivia and Peru. *Quaternary Research,* **56**, 1 - 9.

Dansgaard W (1964) Stable isotopes in precipitation. *Tellus,* **16**, 436-468.

Dupraz C, Fowler A, Tobias C, Visscher PT (2013) Stromatolitic knobs in Storr's Lake (San Salvador, Bahamas): a model system for formation and alteration of laminae. *Geobiology,* **11**, 527-548.

Dupraz C, Reid RP, Braissant O, Decho AW, Norman RS, Visscher PT (2009) Processes of carbonate precipitation in modern microbial mats. *Earth-Science Reviews,* **96**, 141-162.

Dupraz C, Visscher PT (2005) Microbial lithification in marine stromatolites and hypersaline mats. *Trends in Microbiology,* **13**, 429-438.

Dupraz C, Visscher PT, Baumgartner LK, Reid RP (2004) Microbe–mineral interactions: early carbonate precipitation in a hypersaline lake (Eleuthera Island, Bahamas). *Sedimentology,* **51**, 745-765.

Eglinton G (1969) Organic Geochemistry The Organic Chemist's Approach. In: *Organic Geochemistry* (eds Eglinton G, Murphy MJ). Springer Berlin Heidelberg, pp. 20-73.

Ehrlich HL (1998) Geomicrobiology: its significance for geology. *Earth-Science Reviews,* **45**, 45-60.

Farquhar GD, Ehleringer JR, Hubick KT (1989) Carbon isotope discrimination and photosynthesis. *Annual review of plant biology,* **40**, 503-537.

Faure G (1986) *Principles of isotope geology,* Wiley New York.

Frantz CM, Petryshyn VA, Corsetti FA, Berelson WM, Pedro J, Tripati A (2012) Local environmental change durin gthe early eocene climatic optiumum detected using chemical analyses of a Green River Formation (lacustrine) stromatolite. In: *2012 GSA Annual Meeting in Charlotte*.

Fritz P, Suzuki O, Silva C, Salati E (1981) Isotope hydrology of groundwaters in the Pampa del Tamarugal, Chile. *Journal of Hydrology,* **53**, 161-184.

Füchtbauer H, Hardie L (1976) Experimentally determined homogeneous distribution coefficients for precipitated magnesian calcites: application to marine carbonate cements. In: *Geological Society of America Abstracts with Programs,* pp. 877.

Gallagher K, Dupraz C, Braissant O, Norman R, Decho A, Visscher PT (2010) Mineralization of sedimentary biofilms: modern mechanistic insights. *Biofilm: Formation, Development and Properties. Nova Science Publishers*.

Garcés BLV, Kelts K, Ito E (1995) Oxygen and carbon isotope trends and sedimentological evolution of a meromictic and saline lacustrine system: the Holocene Medicine Lake basin, North American Great Plains, USA. *Palaeogeography, Palaeoclimatology, Palaeoecology,* **117**, 253-278.

Garleff K, Stingl H, Veit H (1993) New dates on the Late Quaternary history of landscape and climate in the Bolsón of Fiambalá, Argentina (Province Catamarca). *Zbl. Geol. Paläont,* **1**, 333-341.

Garreaud RD, Vuille M, Compagnucci R, Marengo J (2009) Present-day South American climate. *Palaeogeography, Palaeoclimatology, Palaeoecology,* **281**, 180-195.

Garrels RMC, Christ. M. (1965) Solutions, Minerals, and Equilibria.

Gat J (1995) Stable isotopes of fresh and saline lakes. In: *Physics and chemistry of lakes*. Springer*,* pp. 139-165.

Gat JR (1996) Oxygen and hydrogen isotopes in the hydrologic cycle. *Annual Review of Earth and Planetary Sciences,* **24**, 225-262.

Ghinassi M, D'oriano F, Benvenuti M, Awramik S, Bartolini C, Fedi M, Ferrari G, Papini M, Sagri M, Talbot M (2012) Shoreline fluctuations of Lake Hayk (northern Ethiopia) during the last 3500 years: Geomorphological, sedimentary, and isotope records. *Palaeogeography, Palaeoclimatology, Palaeoecology,* **365–366**, 209-226.

Given RK, Wilkinson BH (1985) Kinetic control of morphology, composition, and mineralogy of abiotic sedimentary carbonates. *Journal of Sedimentary Research,* **55,** 109-119.

Golubic S, Focke JW (1978) Phormidium hendersonii Howe: identity and significance of a modern stromatolite building microorganism. *Journal of Sedimentary Research,* **48**, 751-764.

Gomez F, Fike, D., Buongiorno, J., Kah, L., Mlewski, C., Boidi, F. (2014) Sulphur-carbon cycling recorded in microbial carbonates in high-altitude hypersaline lakes of Catamarca, Argentina. *Joint meeting of the Nordic Network of Astrobiology and the Centre of Geobiology*, 76-77.

Gomez FJ, Kah LC, Bartley JK, Astini RA, Anonymous (2012) Microbialites in a high-altitude Andean lake as a natural analogue for Proterozoic stromatolite fabrics. *Abstracts with Programs - Geological Society of America,* **44**, 211.

Gong C, Hollander DJ (1997) Differential contribution of bacteria to sedimentary organic matter in oxic and anoxic environments, Santa Monica Basin, California. *Organic Geochemistry,* **26**, 545-563.

Gouramanis C, De Deckker P (2010) Alkalinity control on the partition coefficients in lacustrine ostracodes from Australia. *Geology,* **38**, 359-362.

Grosjean M (1994) Paleohydrology of the Laguna Lejia (north Chilean Altiplano) and climatic implications for late-glacial times. *Palaeogeography, Palaeoclimatology, Palaeoecology,* **109**, 89-100.

Grosjean M (2001) Mid-Holocene Climate in the South-Central Andes: Humid or Dry? *Science,* **292**, 2391.

Grosjean M, Cartajena I, Geyh MA, Nuñez L (2003) From proxy data to paleoclimate interpretation: the mid-Holocene paradox of the Atacama Desert, northern Chile. *Palaeogeography, Palaeoclimatology, Palaeoecology,* **194**, 247-258.

Grosjean M, Geyh M, Messerli B, Schreier H, Veit H (1998) A late-Holocene (< 2600 BP) glacial advance in the south-central Andes (29 S), northern Chile. *The Holocene,* **8**, 473-479.

Grosjean M, Núñez AL (1994) Lateglacial, early and middle Holocene environments, human occupation, and resource use in the Atacama (northern Chile). *Geoarchaeology,* **9**, 271-286.

Grosjean M, Valero-Garcés BL, Geyh MA, Messerli B, Schotterer U, Schreier H, Kelts K (1997) Mid- and late-Holocene limnogeology of Laguna del Negro Francisco, northern Chile, and its palaeoclimatic implications. *The Holocene,* **7**, 151-159.

Grotzinger JP, Knoll AH (1999) STROMATOLITES IN PRECAMBRIAN CARBONATES: Evolutionary Mileposts or Environmental Dipsticks? *Annual Review of Earth and Planetary Sciences,* **27**, 313-358.

Guo H, Du Y, Kah LC, Huang J, Hu C, Huang H, Yu W (2013) Isotopic composition of organic and inorganic carbon from the Mesoproterozoic Jixian Group, North China: Implications for biological and oceanic evolution. *Precambrian Research,* **224**, 169-183.

Hammer Ø, Harper DaT, Ryan PD (2001) Past: Paleontological Statistics Software Package for education and data analysis. Paleontología Electrónica 4: 1-9. *URL:*< http://palaeo-electronica. *org/2001_1/past/issue1_01. html*.

Hayes J, Popp BN, Takigiku R, Johnson MW (1989) An isotopic study of biogeochemical relationships between carbonates and organic carbon in the Greenhorn Formation. *Geochimica et Cosmochimica Acta,* **53**, 2961-2972.

Hayes JM, Strauss H, Kaufman AJ (1999) The abundance of 13C in marine organic matter and isotopic fractionation in the global biogeochemical cycle of carbon during the past 800 Ma. *Chemical Geology,* **161**, 103-125.

Hinga K. R. AMA, Pilson M. E. Q., and Whitaker D., 1994 (1994) Carbon isotope fractionation by marine phytoplankton in culture: The effects of CO2 concentration, pH, temperature, and species. *Global Biogeochem. Cycles,* **8**, 91-102.

Holland H (1966) The coprecipitation of metallic ions with calcium carbonate. *Final Report, US AEC Contract No. AT (30-1),* **2266**.

Holland H, Borcsik M, Munoz J, Oxburgh U (1963) The coprecipitation of Sr< sup>+ 2</sup> with aragonite and of Ca< sup>+ 2</sup> with strontianite between 90° and 100° C. *Geochimica et Cosmochimica Acta,* **27**, 957-977.

Holland H, Holland H, Munoz J (1964) The coprecipitation of cations with CaCO< sub> 3</sub>—II. The coprecipitation of Sr^{+2} with calcite between 90° and 100° C. *Geochimica et Cosmochimica Acta,* **28**, 1287-1301.

Hollander DJ, Mckenzie JA (1991) CO2 control on carbon-isotope fractionation during aqueous photosynthesis: A paleo-pCO2 barometer. *Geology,* **19**, 929-932.

Hollander DJ, Smith MA (2001) Microbially mediated carbon cycling as a control on the δ^{13}C of sedimentary carbon in eutrophic Lake Mendota (USA): new models for interpreting isotopic excursions in the sedimentary record. *Geochimica et Cosmochimica Acta,* **65**, 4321-4337.

Katz A (1973) The interaction of magnesium with calcite during crystal growth at 25–90 C and one atmosphere. *Geochimica et Cosmochimica Acta,* **37**, 1563-1586.

Katz A, Sass E, Starinsky A, Holland H (1972) Strontium behavior in the aragonite-calcite transformation: An experimental study at 40–98 C. *Geochimica et Cosmochimica Acta,* **36**, 481-496.

Kaźmierczak J, Kempe S, Kremer B, López-García P, Moreira D, Tavera R (2011) Hydrochemistry and microbialites of the alkaline crater lake Alchichica, Mexico. *Facies,* **57**, 543-570.

Keeney DR (1973) The nitrogen cycle in sediment-water systems. *Journal of Environmental Quality,* **2**, 15-29.

Kemp ALW (1971) Organic carbon and nitrogen in the surface sediments of Lakes Ontario, Erie and Huron. *Journal of Sedimentary Research,* **41**, 537 - 548.

Kienast M. CS, Pelejero C., Grimalt J. (2001) A critical review of marine sedimentary delta 13 C org-pco2 estimates: New palaeorecords from South China Sea and a revisit of other low-latitude delta 13c org-pco2 records. *Global Biogeochem. Cycles,* **15**, 113-127.

Kilham SS (1990) Relationship of phytoplankton and nutrients to stoichiometric measures. In: *Large Lakes*. Springer, pp. 403-413.

Kim S-T, O'neil JR, Hillaire-Marcel C, Mucci A (2007) Oxygen isotope fractionation between synthetic aragonite and water: Influence of temperature and Mg^{2+}concentration. *Geochimica et Cosmochimica Acta,* **71**, 4704-4715.

Kinsman DJ, Holland H (1969) The co-precipitation of cations with CaCO< sub> 3</sub>—IV. The co-precipitation of Sr< sup> 2+</sup> with aragonite between 16° and 96° C. *Geochimica et Cosmochimica Acta,* **33**, 1-17.

Konhauser KO, Phoenix VR, Bottrell SH, Adams DG, Head IM (2001) Microbial–silica interactions in Icelandic hot spring sinter: possible analogues for some Precambrian siliceous stromatolites. *Sedimentology,* **48**, 415-433.

Last FM, Last WM, Halden NM (2010) Carbonate microbialites and hardgrounds from Manito Lake, an alkaline, hypersaline lake in the northern Great Plains of Canada. *Sedimentary Geology,* **225**, 34-49.

Li HC, Ku TL (1997) δ^{13}C– δ^{18}C covariance as a paleohydrological indicator for closed-basin lakes. *Palaeogeography, Palaeoclimatology, Palaeoecology,* **133**, 69-80.

Lorens RB (1981) Sr, Cd, Mn and Co distribution coefficients in calcite as a function of calcite precipitation rate. *Geochimica et Cosmochimica Acta,* **45**, 553-561.

Mastandrea A, Guido A, Demasi F, Ruffolo SA, Russo F (2011) The characterisation of sedimentary organic matter in carbonates with Fourier-Transform Infrared (FTIR) spectroscopy. In: *Advances in Stromatolite Geobiology*. Springer, pp. 331-342.

Meister P (2013) Two opposing effects of sulfate reduction on carbonate precipitation in normal marine, hypersaline, and alkaline environments. *Geology,* **41**, 499-502.

Meyers P, Lallier-Vergés E (1999) Lacustrine Sedimentary Organic Matter Records of Late Quaternary Paleoclimates. *Journal of Paleolimnology,* **21**, 345-372.

Meyers PA, Horie S (1993) An organic carbon isotopic record of glacial-postglacial change in atmospheric pCO2 in the sediments of Lake Biwa, Japan. *Palaeogeography, Palaeoclimatology, Palaeoecology,* **105**, 171-178.

Mitchell AC, Ferris FG (2005) The coprecipitation of Sr into calcite precipitates induced by bacterial ureolysis in artificial groundwater: Temperature and kinetic dependence. *Geochimica et Cosmochimica Acta,* **69**, 4199-4210.

Mlewski E, Boidi, F., Gerard, E., Gomez, F. (2014) Calcification processes in cyanobacteria-dominated pustular microbial mats in a high-altitude Andean lake (Catamarca, Argentina). *Joint meeting of the Nordic Network of Astrobiology and the Centre of Geobiology*, 127-128.

Mourguiart P, Wirmann D, Fournier M, Servant M (1992) Reconstruction quantitative des niveaux du petit lac Titicaca au cours de l'Holocene. *Comptes rendus de l'Académie des sciences. Série 2, Mécanique, Physique, Chimie, Sciences de l'univers, Sciences de la Terre,* **315**, 875-880.

Mucci A (1986) Growth kinetics and composition of magnesian calcite overgrowths precipitated from seawater: Quantitative influence of orthophosphate ions. *Geochimica et Cosmochimica Acta,* **50**, 2255-2265.

Mucci A, Morse JW (1983) The incorporation of Mg< sup> 2+</sup> and Sr< sup> 2+</sup> into calcite overgrowths: influences of growth rate and solution composition. *Geochimica et Cosmochimica Acta,* **47**, 217-233.

Müller MN, Lebrato M, Riebesell U, Barcelos E Ramos J, Schulz K, Blanco Ameijeiras S, Sett S, Eisenhauer A, Stoll H (2014) Influence of temperature and CO 2 on the strontium and magnesium composition of coccolithophore calcite. *Biogeosciences,* **11**, 1065-1075.

O'leary MH (1988) Carbon isotopes in photosynthesis. *Bioscience*, 328-336.

Ohde SK, Y. (1984) Coprecipitation of strontium with marine Mg-Ca carbonates. *Geochem. J.,* **18**, 143 - 146.

Oomori T, Kaneshima H, Maezato Y, Kitano Y (1987) Distribution coefficient of Mg< sup> 2+</sup> ions between calcite and solution at 10–50° C. *Marine Chemistry,* **20**, 327-336.

Ordoñez OF, Flores M. R., Dib J. R. (2009) Extremophile culture collection from Andean lakes: Extreme pristine environments that host a wide diversity of microorganisms with tolerance to UV radation. *Microbial Ecology,* **58**, 461-473.

Paquette J, Reeder RJ (1995) Relationship between surface structure, growth mechanism, and trace element incorporation in calcite. *Geochimica et Cosmochimica Acta,* **59**, 735-749.

Parkhurst DLaA, C. A. J. (1999) User's guide to PHREEQC-a computer program for speciation, batch-reaction, one-dimentional transport, and inverse geochemical calculations. *U.S. Geological Survey Water Resources Investigation*, 99 - 4259.

Pentecost A, Riding R (1986) Calcification in cyanobacteria. *Biomineralization in lower plants and animals,* **30**, 73-90.

Petryshyn VA, Corsetti FA, Berelson WM, Beaumont W, Lund SP (2012) Stromatolite lamination frequency, Walker Lake, Nevada: Implications for stromatolites as biosignatures. *Geology,* **40**, 499-502.

Pingitore and Eastman MP (1986) The coprecipitation of Sr^{2+} with calcite at 25° C and 1 atm. *Geochimica et Cosmochimica Acta,* **50**, 2195-2203.

Piovano EL, Ariztegui D, Bernasconi SM, Mckenzie JA (2004) Stable isotopic record of hydrological changes in subtropical Laguna Mar Chiquita (Argentina) over the last 230 years. *The Holocene,* **14**, 525-535.

Proteau P, Gerwick W, Garcia-Pichel F, Castenholz R (1993) The structure of scytonemin, an ultraviolet sunscreen pigment from the sheaths of cyanobacteria. *Experientia,* **49**, 825-829.

Pueyo JJ, Sáez A, Giralt S, Valero-Garcés BL, Moreno A, Bao R, Schwalb A, Herrera C, Klosowska B, Taberner C (2011) Carbonate and organic matter sedimentation and isotopic signatures in Lake Chungará, Chilean Altiplano, during the last 12.3 kyr. *Palaeogeography, Palaeoclimatology, Palaeoecology,* **307**, 339-355.

Quattrocchio ME, Borromei AM, Deschamps CM, Grill SC, Zavala CA (2008) Landscape evolution and climate changes in the Late Pleistocene–Holocene, southern Pampa (Argentina): evidence from palynology, mammals and sedimentology. *Quaternary International,* **181**, 123-138.

Reid P, Dupraz CD, Visscher PT, Sumner DY (2003) Microbial processes forming marine stromatolites. In: *Fossil and Recent Biofilms*. Springer, pp. 103-118.

Reid RP, Visscher PT, Decho AW, Stolz JF, Bebout BM, Dupraz C, Macintyre IG, Paerl HW, Pinckney JL, Prufert-Bebout L, Steppe TF, Desmarais DJ (2000) The role of microbes in accretion, lamination and early lithification of modern marine stromatolites. *Nature,* **406**, 989.

Riding R (2000) Microbial carbonates: the geological record of calcified bacterial–algal mats and biofilms. *Sedimentology,* **47**, 179-214.

Riding R (2011) The nature of stromatolites: 3,500 million years of history and a century of research. In: *Advances in Stromatolite Geobiology*. Springer, pp. 29-74.

Risacher F, Alonso H, Salazar C (1999) Geoquímica de aguas en cuencas cerradas: I, II y III regiones-Chile. *Ministerio de Obras Públicas,* **1**, 209.

Risacher F, Alonso H, Salazar C (2003) The origin of brines and salts in Chilean salars: a hydrochemical review. *Earth-Science Reviews,* **63**, 249-293.

Rittenberg S, Emery KO, Orr WL (1955) Regeneration of nutrients in sediments of marine basins. *Deep Sea Research (1953),* **3**, 23-45.

Roberts K, Granum E, Leegood RC, Raven JA (2007) C3 and C4 pathways of photosynthetic carbon assimilation in marine diatoms are under genetic, not environmental, control. *Plant physiology,* **145**, 230-235.

Schwalb A, Burns SJ, Kelts K (1999) Holocene environments from stable isotope stratigraphy of ostracods and authigenic carbonate in Chilean Altiplano Lakes. *Palaeogeography, Palaeoclimatology, Palaeoecology,* **148**, 153-168.

Sterner RW, Elser JJ (2002) *Ecological stoichiometry: the biology of elements from molecules to the biosphere,* Princeton University Press.

Stiller M, Rounick J, Shasha S (1985) Extreme carbon-isotope enrichments in evaporating brines. *Nature*, **316**, 434-435.

Stine S (1994) Extreme and persistent drought in California and Patagonia during mediaeval time. *Nature,* **369**, 546-549.

Strecker MR, Alonso RN, Bookhagen B, Carrapa B, Hilley GE, Sobel ER, Trauth MH (2007) Tectonics and Climate of the Southern Central Andes. *Annual Review of Earth and Planetary Sciences,* **35**, 747-787.

Strecker MR, Cerveny P, Bloom AL, Malizia D (1989) Late Cenozoic tectonism and landscape development in the foreland of the Andes: Northern Sierras Pampeanas (26°–28°S), Argentina. *Tectonics,* **8**, 517-534.

Tang J, Dietzel M, Böhm F, Köhler SJ, Eisenhauer A (2008) Sr2+/Ca2+ and 44Ca/40Ca fractionation during inorganic calcite formation: II. Ca isotopes. *Geochimica et Cosmochimica Acta,* **72**, 3733-3745.

Thompson LG, Mosley-Thompson E, Henderson KA (2000) Ice-core palaeoclimate records in tropical South America since the Last Glacial Maximum. *Journal of Quaternary Science,* **15**, 377-394.

Thurman HV, Trujillo AP, Abel DC, Mcconnell R (1999) *Essentials of oceanography,* Prentice Hall.

Valero-Garcés B, Delgado-Huertas A, Ratto N, Navas A, Edwards L (2000) Paleohydrology of Andean saline lakes from sedimentological and isotopic records, Northwestern Argentina. *Journal of Paleolimnology,* **24**, 343-359.

Valero-Garcés B, Grosjean M, Schwalb A, Geyh M, Messerli B, Kelts K (1996) Limnogeology of Laguna Miscanti: evidence for mid to late Holocene moisture changes in the Atacama Altiplano (Northern Chile). *Journal of Paleolimnology,* **16**, 1-21.

Valero-Garcés BL, Arenas C, Delgado-Huertas A (2001) Depositional environments of Quaternary lacustrine travertines and stromatolites from high-altitude Andean lakes, northwestern Argentina. *Canadian Journal of Earth Sciences,* **38**, 1263-1283.

Valero-Garcés BL, Delgado-Huertas A, Ratto N, Navas A (1999) Large 13C enrichment in primary carbonates from Andean Altiplano lakes, northwest Argentina. *Earth and Planetary Science Letters,* **171**, 253-266.

Van Breugel Y, Schouten S, Paetzel M, Nordeide R, Sinninghe Damsté JS (2005) The impact of recycling of organic carbon on the stable carbon isotopic composition of dissolved inorganic carbon in a stratified marine system (Kyllaren fjord, Norway). *Organic geochemistry,* **36**, 1163-1173.

Visscher PT, Reid RP, Bebout BM (2000) Microscale observations of sulfate reduction: Correlation of microbial activity with lithified micritic laminae in modern marine stromatolites. *Geology,* **28**, 919-922.

Visscher PT, Reid RP, Bebout BM, Hoeft SE, Macintyre IG, Thompson JA (1998) Formation of lithified micritic laminae in modern marine stromatolites (Bahamas): the role of sulfur cycling. *American Mineralogist,* **83**, 1482-1493.

Vuille M, Ammann C (1997) REGIONAL SNOWFALL PATTERNS IN THE HIGH, ARID ANDES. *Climatic Change,* **36**, 413-423.

Wetzel RG (1975) Limnology: Philadelphia. *WB Saunders Company,* **3**.

Wilkinson BH, Given RK (1986) Secular variation in abiotic marine carbonates: constraints on Phanerozoic atmospheric carbon dioxide contents and oceanic Mg/Ca ratios. *The Journal of Geology*, **94**, 321-333.

Appendices

Appendix A: PHREEQC CODE

Geochemical modeling in this work was, in part, conducted through the free USGS software program for speciation, batch-reaction, and inverse geochemical calculations called PHREEQC-Interactive (Parkhurst and Appelo, 1999). The reader can find more detailed information about modeling capabilities, databases, and iterative methods within the third version of the manual online at http://pubs.usgs.gov/tm/06/a43/pdf/tm6-A43.pdf.

Forward evaporative modeling

Since carbonate formation accompanies evaporative evolution of lake waters, we wanted to model ionic concentration of dissolved constituents resulting from the removal of water from the hydrochemical system. In PHREEQC-I, evaporation was modeled in inlet water evolution through the removal of an irreversible reactant with a negative reaction coefficient. Forward modeling reactions are accomplished by inputing the amount of moles of water to be removed from the initial inlet waters to form a new solution defined by a desired concentration factor. For example, the concentration of inlet waters by a factor of 10 requires the removal of 49.95 moles of water, or 90% of water, leaving only 0.1 kg of water.

In the code below, anything following "#" is not read by the program and instead serves as annotations for clarity.

A.1 TITLE Evaporation of inlet water 10X
SOLUTION 1 Inlet water average values # these values come from *in situ* measurements of inflow waters of Laguna Negra

Units mg/L

pH 7.7

pe 4 # electron activity; value is default in program

temp 25.0

Ca 1455

Mg 727.5

Na 3628.25

K 215.25

Cl 12212.5

C 273.54

S 217.3

-water 1

REACTION 1

H2O -1.0 #coefficient multiplied to amount of moles h2o added

49.95 moles #since 1kg water contains ~ 55.5 moles, removal of 90% water, or concentration factor of 10, calls for 49.95 moles h20 removed. (55.5*0.9)

SAVE solution 2

END

A.2 TITLE Evaporation of inlet water 15X

SOLUTION 1 Inlet water average values

Units	mg/L
pH	7.7
pe	4
temp	25.0
Ca	1455
Mg	727.5
Na	3628.25
K	215.25
Cl	12212.5
C	273.54
S	217.3

-water 1

REACTION 1

H2O -1.0

51.8056 moles

SAVE solution 2

END

A.3 TITLE Evaporation of inlet water 20X

SOLUTION 1 Inlet water average values

Units	mg/L
pH	7.7
pe	4
temp	25.0
Ca	1455
Mg	727.5
Na	3628.25
K	215.25
Cl	12212.5
C	273.54
S	217.3

-water 1

REACTION 1

H2O -1.0

52.73 moles

SAVE solution 2

END

TITLE Example 4b.--Factor of 20 more solution

```
MIX
    2       20.
SAVE solution 3
END
```

A. 4 TITLE Evaporation of inlet water 25X

SOLUTION 1 Inlet water average values

Units	mg/L
pH	7.7
pe	4
temp	25.0
Ca	1455
Mg	727.5
Na	3628.25
K	215.25
Cl	12212.5
C	273.54
S	217.3

-water 1

```
REACTION 1
        H2O     -1.0
        53.28576  moles
SAVE solution 2
END
```

A.5 TITLE Evaporation of inlet water 30X

```
SOLUTION 1 Inlet water average values
Units           mg/L
pH              7.7
pe              4
temp        25.0
Ca              1455
Mg              727.5
Na              3628.25
K               215.25
Cl              12212.5
C               273.54
S               217.3
 -water 1
```

REACTION 1

H2O -1.0

53.6558 moles

SAVE solution 2

END

A.6 TITLE Evaporation of inlet water 35X

SOLUTION 1 Inlet water average values

Units	mg/L
pH	7.7
pe	4
temp	25.0
Ca	1455
Mg	727.5
Na	3628.25
K	215.25
Cl	12212.5
C	273.54
S	217.3

-water 1

```
REACTION 1
        H2O     -1.0
        53.92011429  moles
SAVE solution 2
END
```

A.7 TITLE Evaporation of inlet water 40X

```
SOLUTION 1 Inlet water average values
Units           mg/L
pH              7.7
pe              4
temp        25.0
Ca              1455
Mg              727.5
Na              3628.25
K               215.25
Cl              12212.5
C               273.54
S               217.3
 -water 1
```

```
REACTION 1
     H2O     -1.0
     54.11835  moles
SAVE solution 2
END
```

A.8 TITLE Evaporation of inlet water 45X

```
SOLUTION 1 Inlet water average values
Units           mg/L
pH              7.7
pe              4
temp       25.0
Ca              1455
Mg              727.5
Na              3628.25
K               215.25
Cl              12212.5
C               273.54
S               217.3
```

-water 1

REACTION 1

H2O -1.0

54.2725333 moles

SAVE solution 2

END

A.9 TITLE Evaporation of inlet water 50X

SOLUTION 1 Inlet water average values

Units	mg/L
pH	7.7
pe	4
temp	25.0
Ca	1455
Mg	727.5
Na	3628.25
K	215.25
Cl	12212.5
C	273.54

S 217.3

-water 1

REACTION 1

H2O -1.0

54.39588 moles

SAVE solution 2

END

A.10 TITLE Evaporation of inlet water 55X

SOLUTION 1 Inlet water average values

Units mg/L

pH 7.7

pe 4

temp 25.0

Ca 1455

Mg 727.5

Na 3628.25

K 215.25

Cl 12212.5

C 273.54

S 217.3

-water 1

REACTION 1

H2O -1.0

54.4968 moles

SAVE solution 2

END

A.11 TITLE Evaporation of inlet water 60X

SOLUTION 1 Inlet water average values

Units mg/L

pH 7.7

pe 4

temp 25.0

Ca 1455

Mg 727.5

Na 3628.25

K 215.25

Cl 12212.5

C 273.54

S 217.3

-water 1

REACTION 1

H2O -1.0

54.5809 moles

SAVE solution 2

END

A.12 TITLE Evaporation of inlet water 65X

SOLUTION 1 Inlet water average values

Units mg/L

pH 7.7

pe 4

temp 25.0

Ca 1455

Mg 727.5

Na 3628.25

K 215.25

Cl 12212.5

C 273.54

S 217.3

-water 1

REACTION 1

H2O -1.0

54.65206154 moles

SAVE solution 2

END

A.13 TITLE Evaporation of inlet water 70X

SOLUTION 1 Inlet water average values

Units mg/L

pH 7.7

pe 4

temp 25.0

Ca 1455

Mg 727.5

Na 3628.25

K 215.25

Cl 12212.5

C 273.54

S 217.3

-water 1

REACTION 1

H2O -1.0

54.71305714 moles

SAVE solution 2

END

A.14 TITLE Evaporation of inlet water 75X

SOLUTION 1 Inlet water average values

Units mg/L

pH 7.7

pe 4

temp 25.0

Ca 1455

Mg 727.5

Na 3628.25

K 215.25

Cl 12212.5

C 273.54

S 217.3

-water 1

REACTION 1

H2O -1.0

54.76592 moles

SAVE solution 2

END

A.15 TITLE Evaporation of inlet water 80X

SOLUTION 1 Inlet water average values

Units mg/L

pH 7.7

pe 4

temp 25.0

Ca 1455

Mg 727.5

Na 3628.25

K 215.25

Cl 12212.5

C 273.54

S 217.3

-water 1

REACTION 1

H2O -1.0

54.812175 moles

SAVE solution 2

END

A.16 TITLE Evaporation of inlet water 85X

SOLUTION 1 Inlet water average values

Units mg/L

pH 7.7

pe 4

temp 25.0

Ca 1455

Mg 727.5

Na 3628.25

K 215.25

Cl 12212.5

C 273.54

S 217.3

-water 1

REACTION 1

H2O -1.0

54.85298824 moles

SAVE solution 2

END

A.17 TITLE Evaporation of inlet water 90X

SOLUTION 1 Inlet water average values

Units mg/L

pH 7.7

pe 4

temp 25.0

Ca 1455

Mg 727.5

Na 3628.25

K 215.25

Cl 12212.5

C 273.54

S 217.3

-water 1

REACTION 1

H2O -1.0

54.88926667 moles

SAVE solution 2

END

A.18 TITLE Evaporation of inlet water 95X

SOLUTION 1 Inlet water average values

Units mg/L

pH 7.7

pe 4

temp 25.0

Ca 1455

Mg 727.5

Na 3628.25

K 215.25

Cl 12212.5

C 273.54

S 217.3

-water 1

REACTION 1

H2O -1.0

54.92172632 moles

SAVE solution 2

END

A.19 TITLE Evaporation of inlet water 100X

SOLUTION 1 Inlet water average values

Units mg/L

```
pH              7.7
pe              4
temp        25.0
Ca              1455
Mg              727.5
Na              3628.25
K               215.25
Cl              12212.5
C               273.54
S               217.3
 -water 1


REACTION 1
      H2O     -1.0
      54.95094  moles
SAVE solution 2
END
```

Mixing

Within the mixing zone of Laguna Negra, large degrees of spatial variability in hydrochemistry have been measured (Gomez *et al*., *in press*). Modeled saturation indices and chemical constituents are given with various mixing proportions according to the input codes below, which have solution 1 and 2 defined by measured values of Laguna Negra Lake and Inlet waters, respectively.

A.20 Title Laguna Negra Mixing

Solution 1 Lake water

Units	mg/L
pH	5.71
Ca	16193.3
Mg	6680
Na	71468.3
K	5579.33
Cl	199666.6
Alkalinity	833.3 as HCO3
S	95

END

Title Laguna Negra Mixing

Solution 2	Inlet water
Units	mg/L
pH	7.7
Ca	1455
Mg	727.5
Na	3628.25
K	215.25
Cl	12212.5
Alkalinity	270 as HCO3
S	217.3

END

Title Mixing 95% Lake water, 5% Inlet water

Mix 1 # this tells the program to mix 95% of solution 1 (lake water) with 5% of solution 2 (inlet waters)

1	0.95
2	0.05

SAVE solution 3 # the program saves the mixture as a new solution if the user decides to do iterative equilibrium modeling within the same run

END

```
Title Mixing 90% Lake water, 10% Inlet water
Mix 1
        1       0.9
        2       0.1
SAVE solution 4
END

Title Mixing 85% Lake water, 15% Inlet water
Mix 1
        1       0.85
        2       0.15
SAVE solution 5
END

Title Mixing 80% Lake water, 20% Inlet water
Mix 1
        1       0.8
        2       0.2
SAVE solution 6
END
```

```
Title Mixing 75% Lake water, 25% Inlet water
Mix 1
        1       0.75
        2       0.25
SAVE solution 7
END

Title Mixing 70% Lake water, 30% Inlet water
Mix 1
        1       0.7
        2       0.3
SAVE solution 8
END

Title Mixing 65% Lake water, 35% Inlet water
Mix 1
        1       0.65
        2       0.35
SAVE solution 9
END

Title Mixing 60% Lake water, 40% Inlet water
```

```
Mix 1
        1       0.6
        2       0.4
SAVE solution 10
END

Title Mixing 55% Lake water, 45% Inlet water
Mix 1
        1       0.55
        2       0.45
SAVE solution 11
END

Title Mixing 50% Lake water, 50% Inlet water
Mix 1
        1       0.5
        2       0.5
SAVE solution 12
END

Title Mixing 45% Lake water, 55% Inlet water
Mix 1
```

```
        1       0.45
        2       0.55
SAVE solution 13
END

Title Mixing 40% Lake water, 60% Inlet water
Mix 1
        1       0.4
        2       0.6
SAVE solution 14
END

Title Mixing 35% Lake water, 65% Inlet water
Mix 1
        1       0.35
        2       0.65
SAVE solution 15
END

Title Mixing 30% Lake water, 70% Inlet water
Mix 1
        1       0.3
```

```
        2       0.7
SAVE solution 16
END

Title Mixing 25% Lake water, 75% Inlet water
Mix 1
        1       0.25
        2       0.75
SAVE solution 17
END

Title Mixing 20% Lake water, 80% Inlet water
Mix 1
        1       0.2
        2       0.8
SAVE solution 18
END

Title Mixing 15% Lake water, 85% Inlet water
Mix 1
        1       0.15
        2       0.85
```

```
SAVE solution 19
END

Title Mixing 10% Lake water, 90% Inlet water
Mix 1
        1       0.1
        2       0.8
SAVE solution 20
END

Title Mixing 5% Lake water, 95% Inlet water
Mix 1
        1       0.05
        2       0.95
SAVE solution 21
END
```

Inverse modeling

Calculations of inverse modeling can be used to identify the various geochemical reactions that occur along a flow path of water composition. In this type of model, two solutions are defined with chemical compositions and mole-balances, or a set of mole transfers of reactants, are produced that should account for the chemical changes that occur in the evolution of solution 1 to solution 2. The inverse modeling for this work was conducted on inlet water, which is assumed to have experienced no evaporation and/or mixing (Table 1), and chemical definitions of evaporated water at various concentrations. Models were no longer produced in PHREEQC along flow paths from fresh inlet waters to waters concentrated past 30X. In the following codes, all chemical species definitions and density were provided by PHREEQC in distribution of species and are equivalent to measured ppm values. Uncertainty values were chosen by trial and error to produce at least one model.

A.21 TITLE Inverse modeling of 5X concentrated water evolution from inlet water

SOLUTION 1 Inlet water

Units mol/kgs #moles / kilogram solution

pH 7.7 #measured pH

density 1.0165

Ca 0.037

Mg 0.03049

Na 0.1608

K 0.00561

Cl 0.351

S 0.002305

C 1 CO2(g) -3.65 #logPCO2 at 4.1 km elevation

SOLUTION 2 5X concentrated inlet water

units mol/kgs

density 1.06136

pH 7.397

Ca 0.185

K 0.028065

Mg 0.1525

Cl 1.755

S 0.001153

Na 0.8042

C 1 CO2(g) -3.65

INVERSE_MODELING

-solution 1 2

-uncertainties 0.1 #uncertainty in flow path models produced in evolution from solution 1 to solution 2

-range

-balances

K

Mg

-phases #phases to be the potential reactants during flow path

H2O(g) pre

Calcite pre

CO2(g) pre

Halite pre

Gypsum pre

END

A.22 TITLE Inverse modeling of 10X concentrated water evolution from inlet water

SOLUTION 1 Inlet water

Units	mol/kgs
pH	7.7
density	1.0165
Ca	0.037
Mg	0.03049

```
Na              0.1608
K               0.00561
Cl              0.351
S               0.002305
C 1 CO2(g) -3.65

SOLUTION 2 10X concentrated inlet water
units    mol/kgs
density         1.11862
pH              6.922
Ca              0.3696
K               0.05604
Mg              0.3046
Cl              3.507
S               0.02303
Na              1.607
C 1 CO2(g) -3.65
INVERSE_MODELING
        -solution 1 2
        -uncertainties 0.25
        -range
        -balances
```

K

Mg

-phases

H2O(g) pre

Calcite pre

CO2(g) pre

Halite pre

Gypsum pre

END

A.23 TITLE Inverse modeling of 15X concentrated water evolution from inlet water

SOLUTION 1 Inlet water

Units mol/kgs

pH 7.7

density 1.0165

Ca 0.037

Mg 0.03049

Na 0.1608

K 0.00561

Cl 0.351

```
S               0.002305
C 1 CO2(g) -3.65

SOLUTION 2 15X concentrated inlet water
 units   mol/kgs
density         1.17046
pH              7.359
Ca              0.5549
K               0.08415
Mg              0.4574
Cl              5.266
S               0.03458
Na              2.412
C 1 CO2(g) -3.65
INVERSE_MODELING
        -solution 1 2
        -uncertainties 0.1
        -range
        -balances
        K
        Mg
        -phases
```

H2O(g) pre

Calcite pre

CO2(g) pre

Halite pre

Gypsum pre

END

A. 24 TITLE Inverse modeling of 20X concentrated water evolution from inlet water

SOLUTION 1 Inlet water

Units	mol/kgs
pH	7.7
density	1.0165
Ca	0.037
Mg	0.03049
Na	0.1608
K	0.00561
Cl	0.351
S	0.002305

C 1 CO2(g) -3.65

```
SOLUTION 2 20X concentrated inlet water
units   mol/kgs
density         1.21711
pH      7.469
Ca      0.09134
K       0.1122
Mg      0.6097
Cl      7.019
S       0.04609
Na      3.216
C 1 CO2(g) -3.65
INVERSE_MODELING
        -solution 1 2
        -uncertainties 0.25
        -range
        -balances
        K
        Mg
        -phases
                H2O(g) pre
                Calcite pre
```

CO2(g) pre

Halite pre

Gypsum pre

END

A. 25 TITLE Inverse modeling of 30X concentrated water evolution from inlet water

SOLUTION 1 Inlet water

Units	mol/kgs
pH	7.7
density	1.0165
Ca	0.037
Mg	0.03049
Na	0.1608
K	0.00561
Cl	0.351
S	0.002305

C 1 CO2(g) -3.65

SOLUTION 2 30X concentrated inlet water

units	mol/kgs
density	1.29726

```
pH              7.364
Ca              0.1683
K               0.1683
Mg              0.9148
Cl              10.53
S               0.06915
Na              4.825
 C 1 CO2(g) -3.65
INVERSE_MODELING
        -solution 1 2
        -uncertainties 0.25
        -range
        -balances
        K
        Mg
        -phases
                H2O(g) pre
                Calcite pre
                CO2(g) pre
                Halite pre
                Gypsum pre
END
```

Appendix B: Supplemental Field and Sample Photos

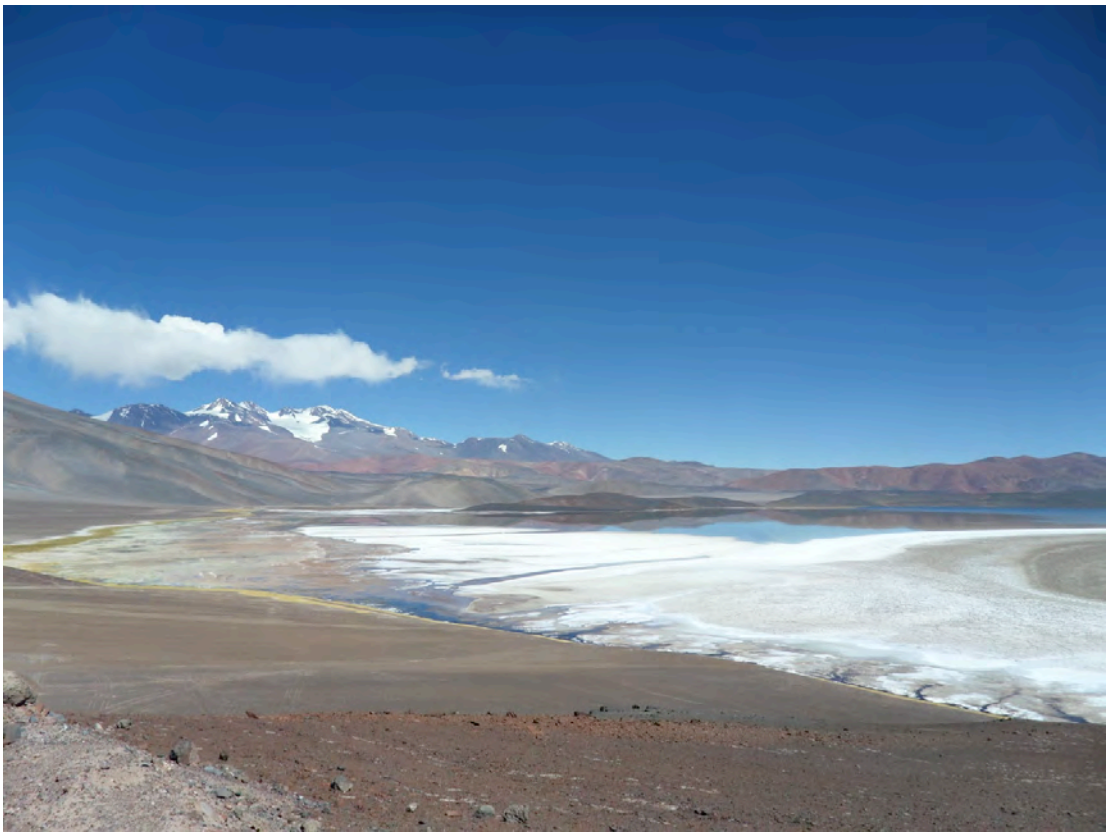

Figure 18: The southern margin of Laguna Negra where microbialites are found.

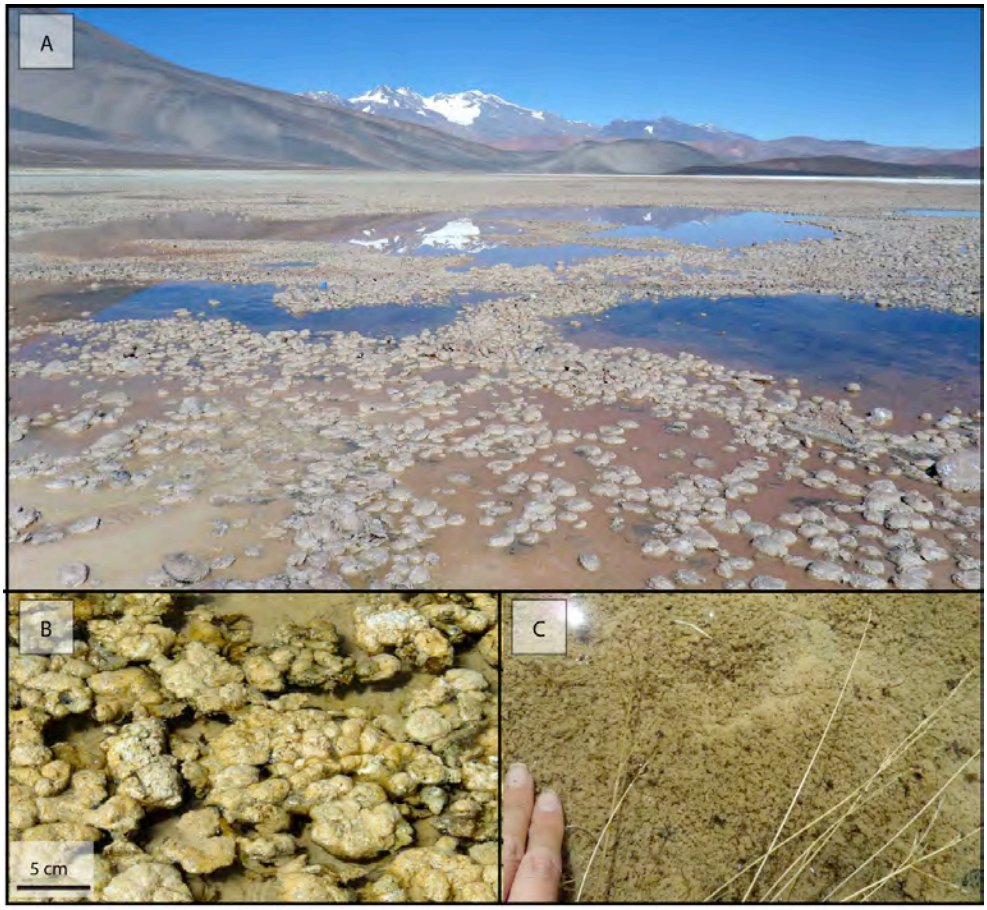

Figure 19: Microbial mats of Laguna Negra. (A) Location within mixing zone where microbial mats can be found. Mats vary in color and morphology (B and C).

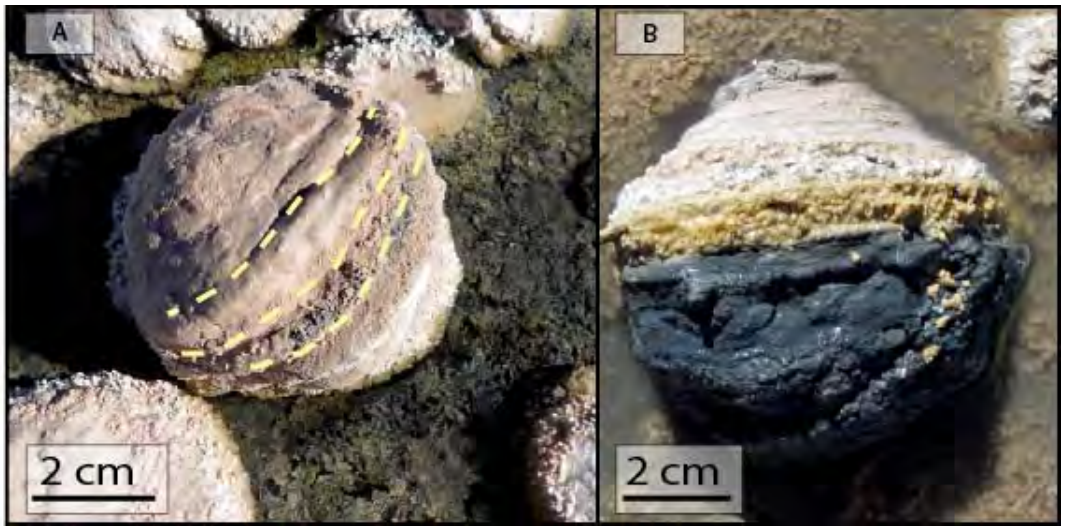

Figure 20: Typical external morphology of microbialites. (A) Ridges skirting microbialite surface mark the sediment-water interface. (B) External coloration potentially from microbial pigments. The black layers are buried in the sediment, while orange layers are aerially exposed.

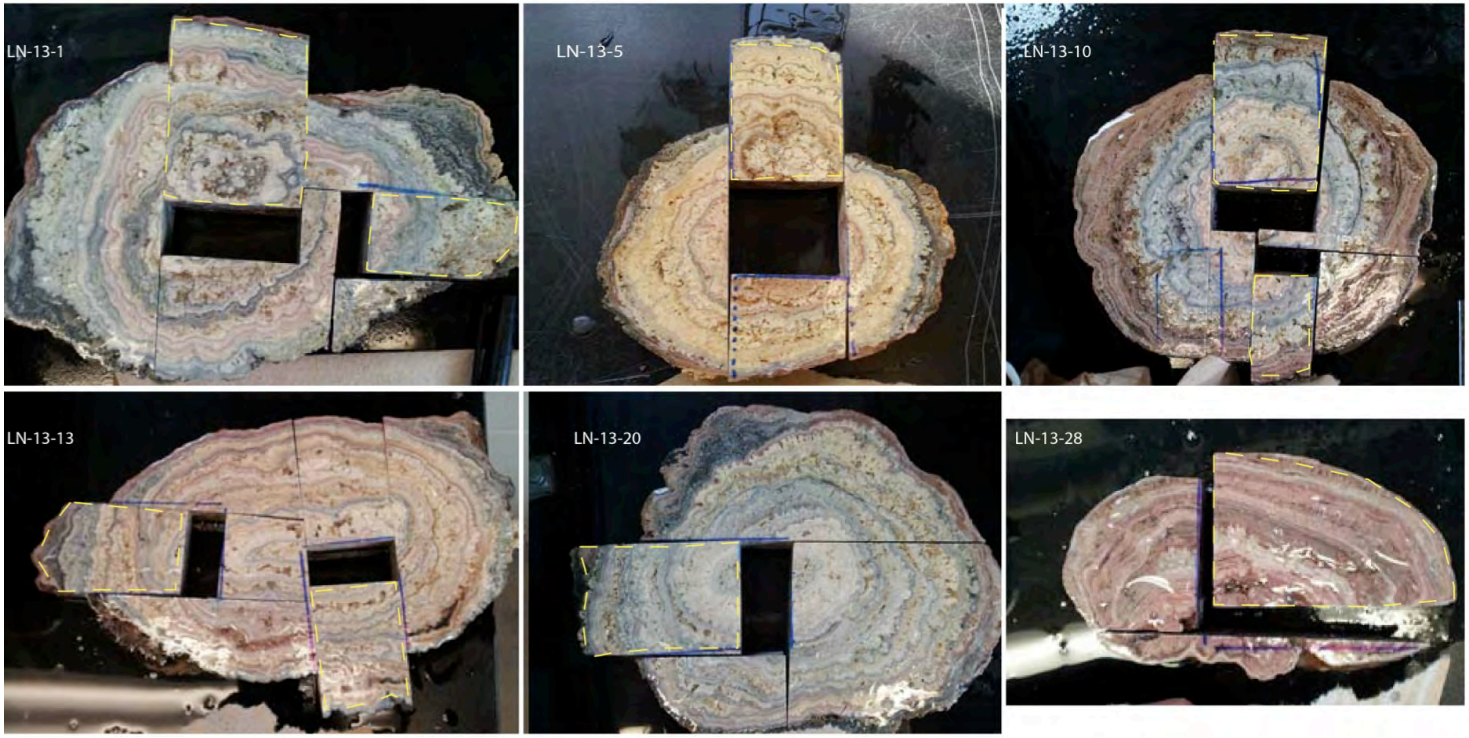

Figure 21: Thin section preparation. Dashed lines indicate sections that were examined petrographically.

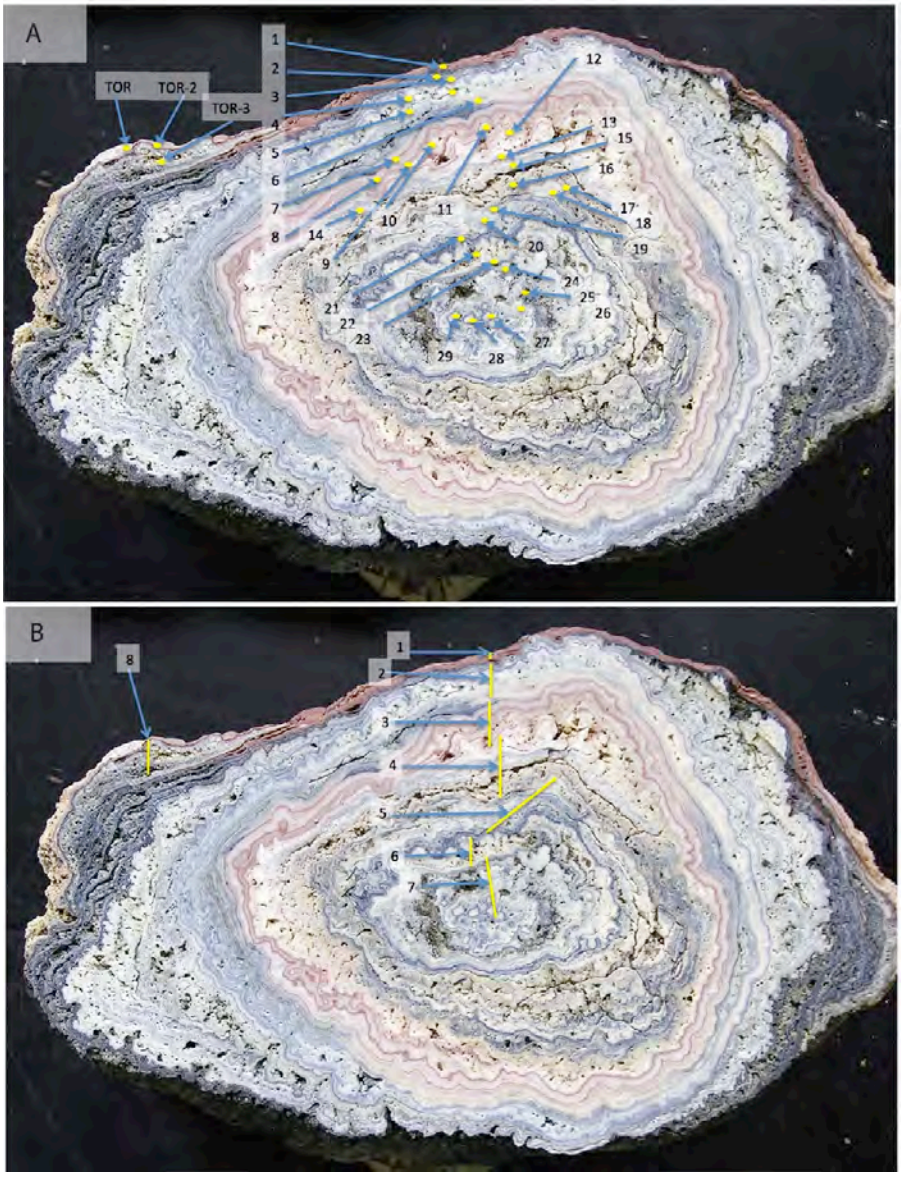

Figure 22: Laminae labels for microbialite LN-13-1. (A) Laminae used in inorganic isotope and elemental measurement. (B) Laminae combined for organic analyses.

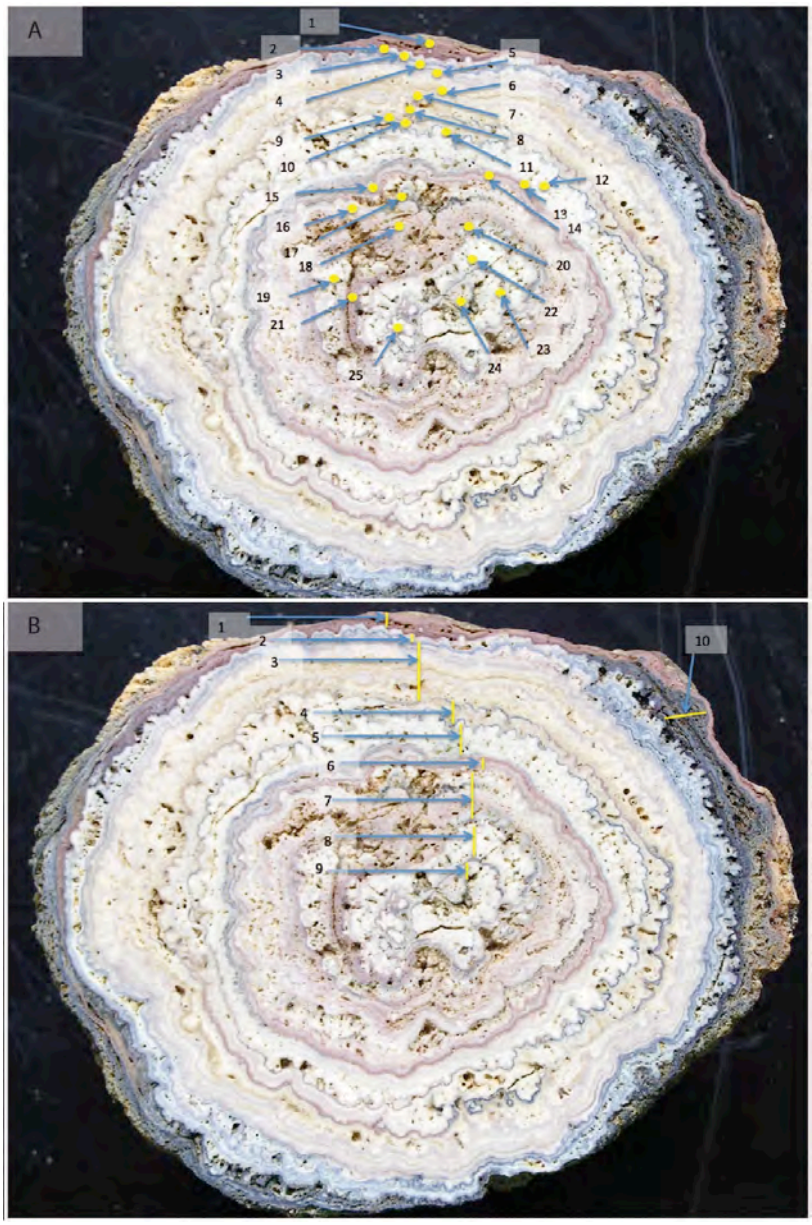

Figure 23: Laminae labels for microbialite LN-13-5. (A) Laminae used in inorganic isotope and elemental measurement. (B) Laminae combined for organic analyses.

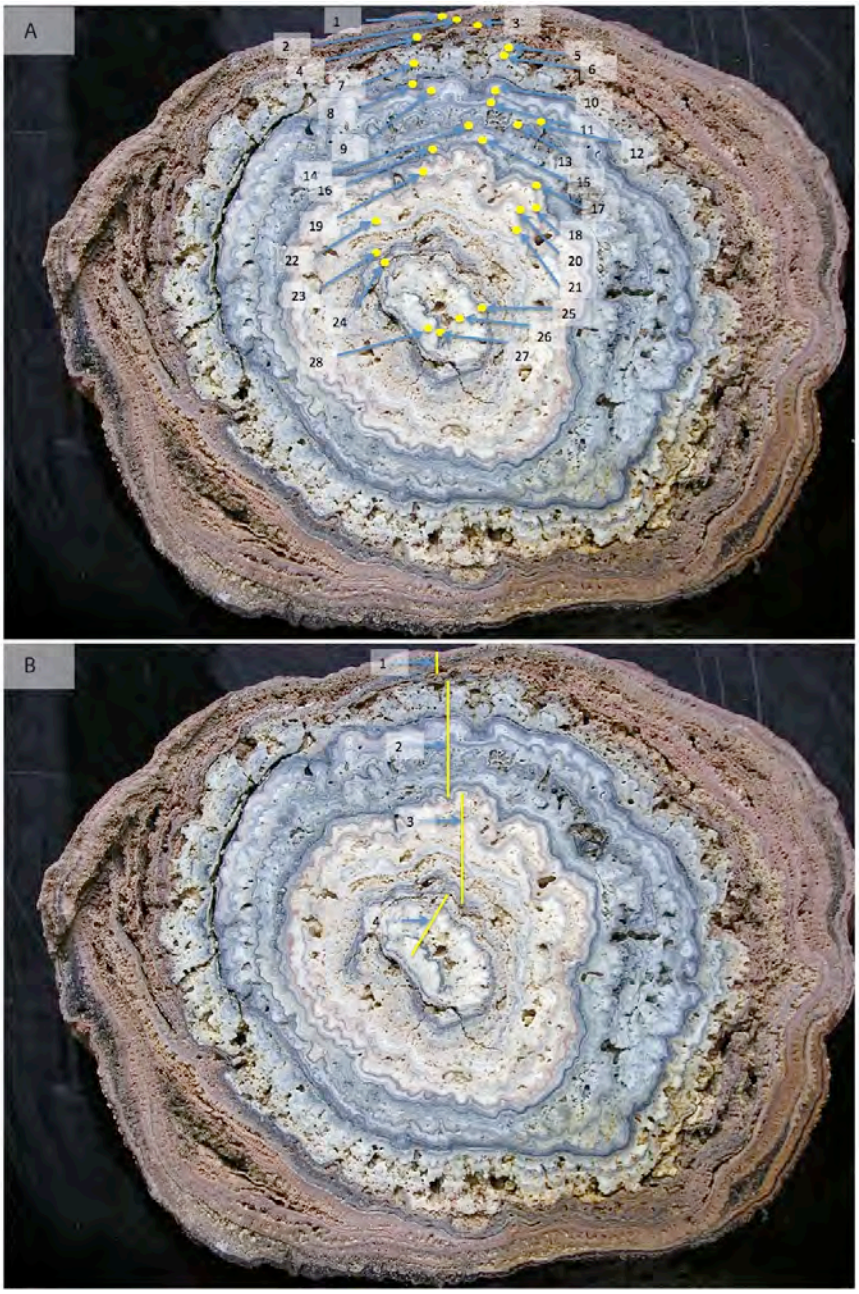

Figure 24: Laminae labels for microbialite LN-13-10. (A) Laminae used in inorganic isotope and elemental measurement. (B) Laminae combined for organic analyses.

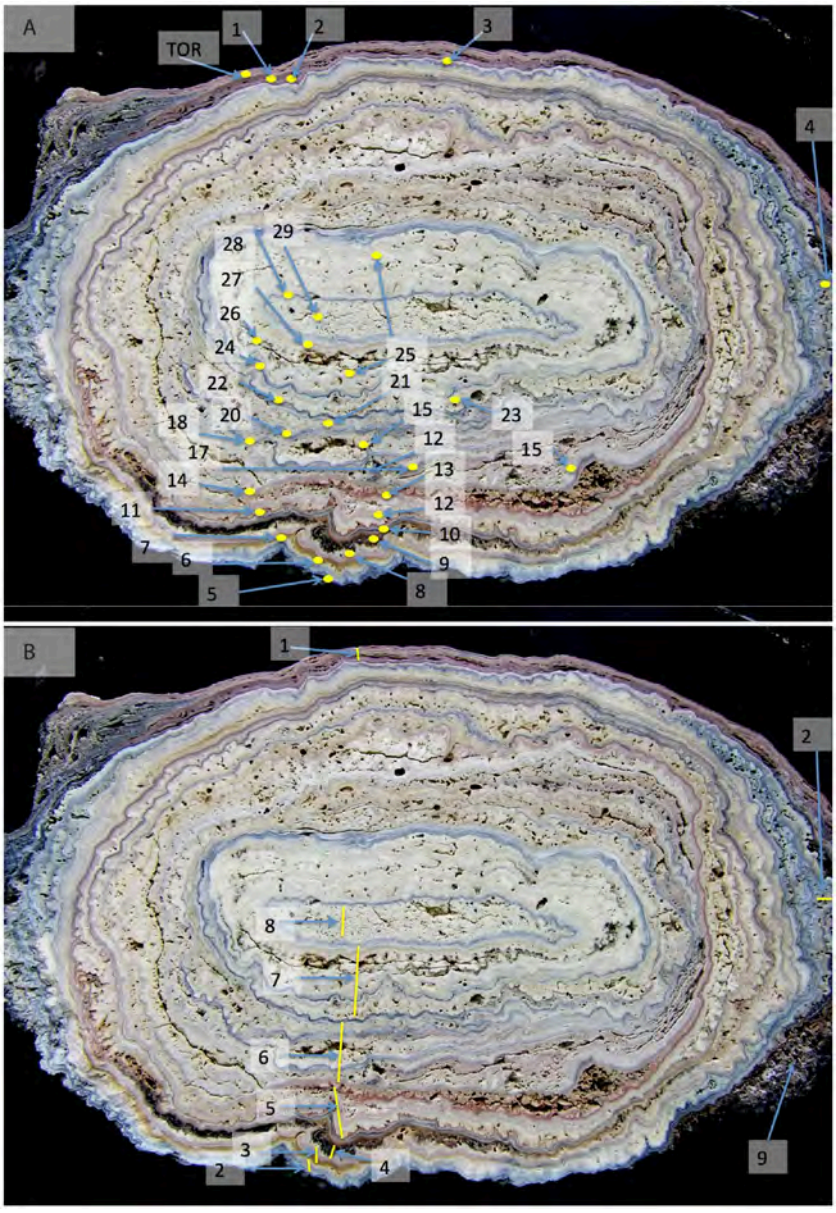

Figure 25: Laminae labels for microbialite LN-13-13. (A) Laminae used in inorganic isotope and elemental measurement. (B) Laminae combined for organic analyses.

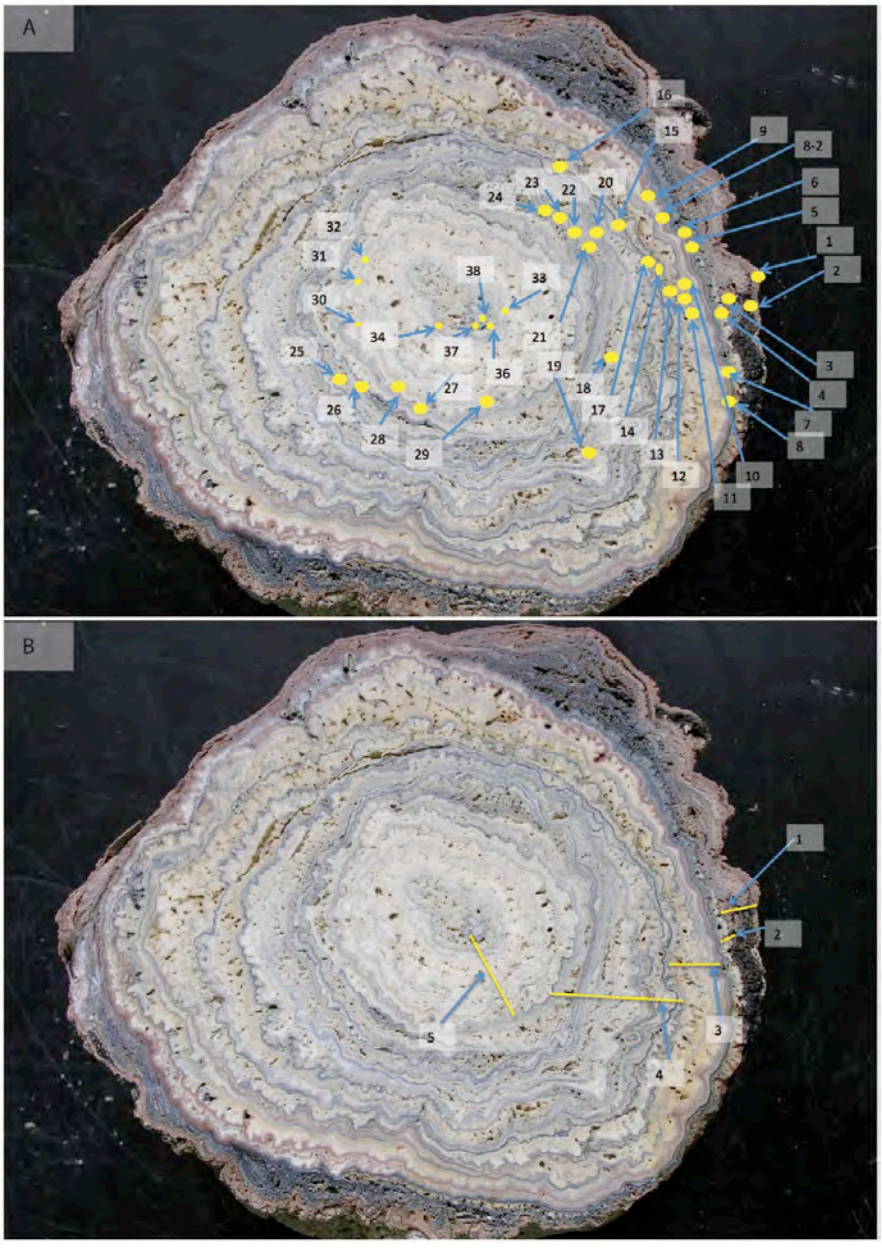

Figure 26: Laminae labels for microbialite LN-13-20. (A) Laminae used in inorganic isotope and elemental measurement. (B) Laminae combined for organic analyses.

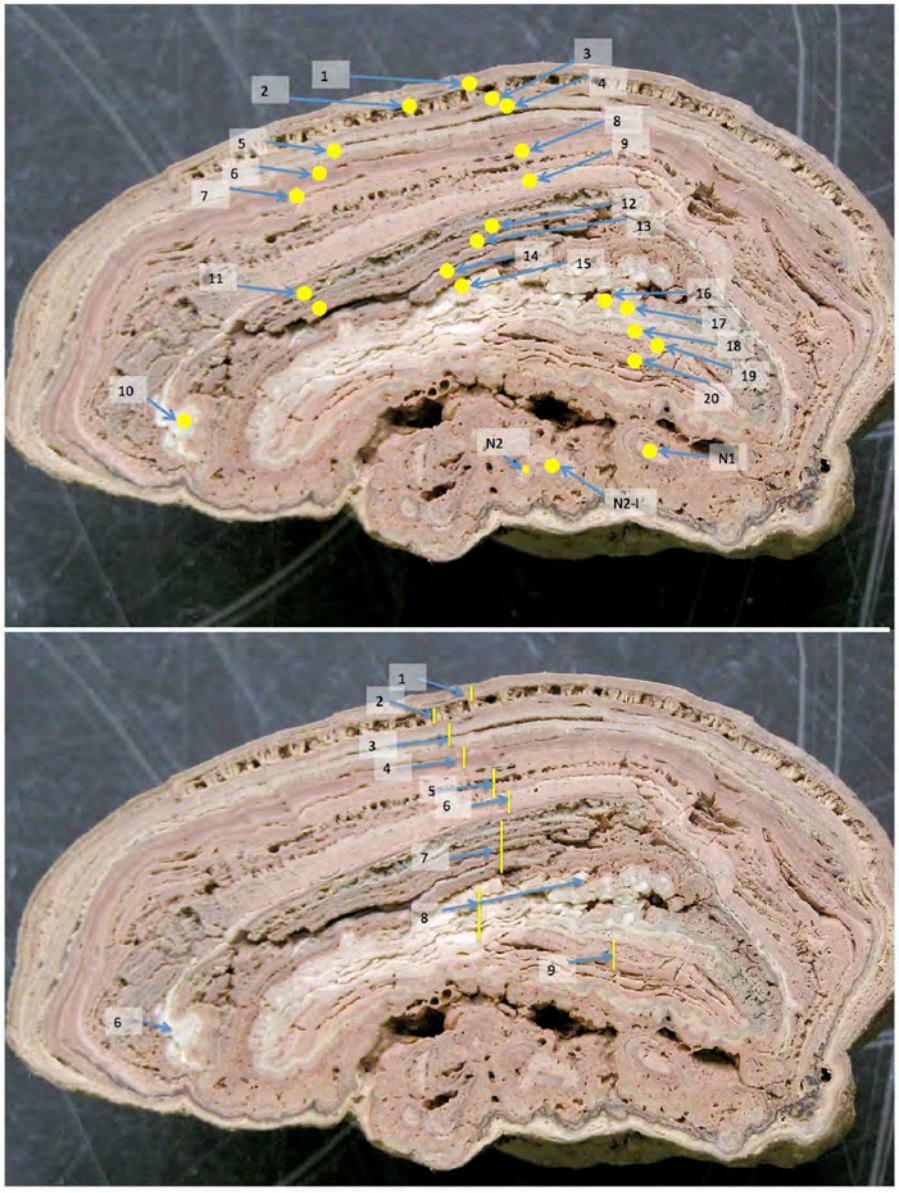

Figure 27: Laminae labels for microbialite LN-13-28. (A) Laminae used in inorganic isotope and elemental measurement. (B) Laminae combined for organic analyses.

Appendix C: Supplementary Photomicrographs

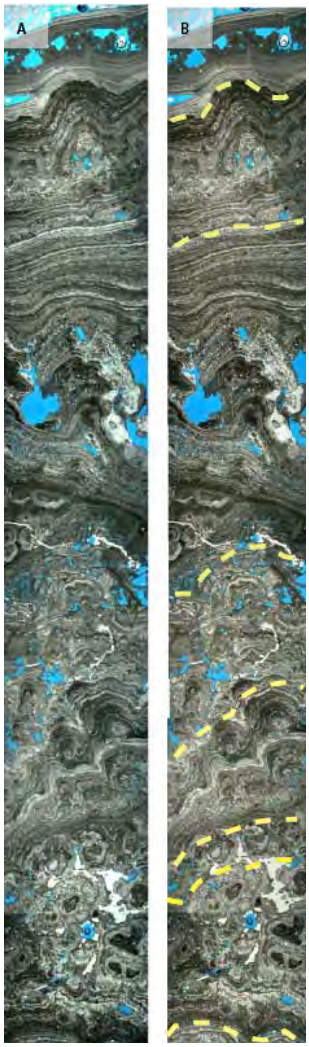

Figure 28: Photomosaic of microbialite LN-13-1 in PPL (A) and XPL (B). Short dimension is 8 mm.

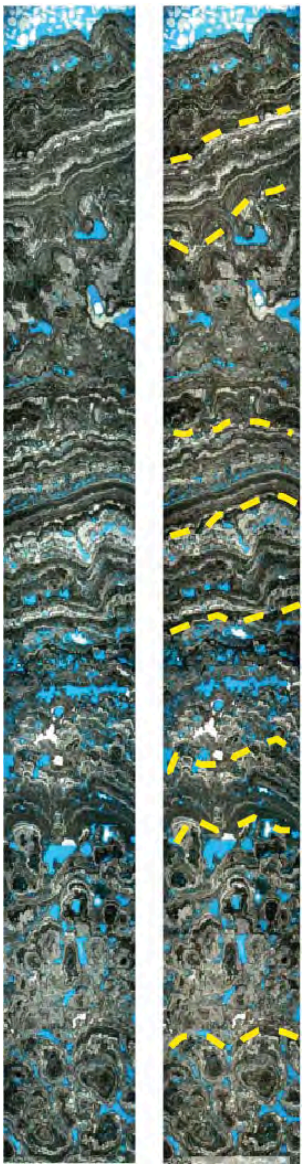

Figure 29: Photomosaic of microbialite LN-13-5 in PPL (A) and XPL (B). Short dimension is 8 mm.

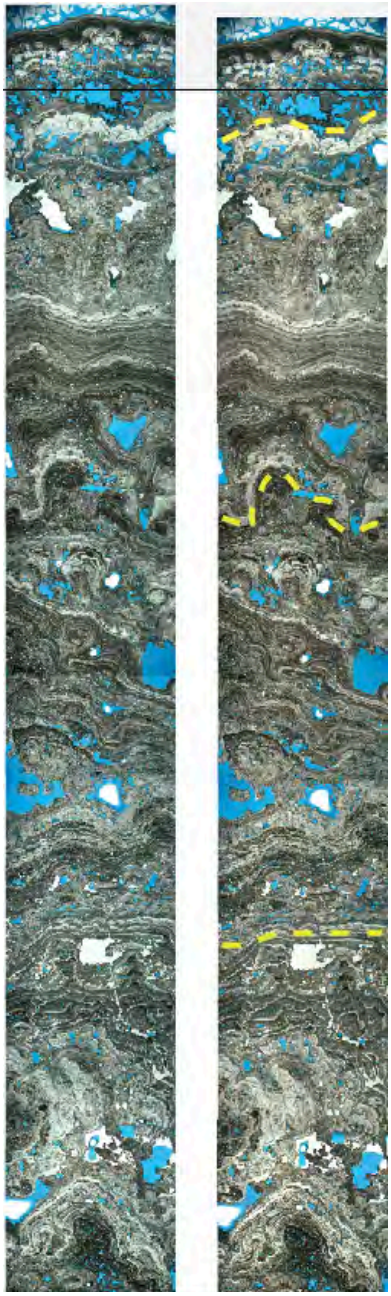

Figure 30: Photomosaic of microbialite LN-13-10 in PPL (A) and XPL (B). Short dimension is 8 mm.

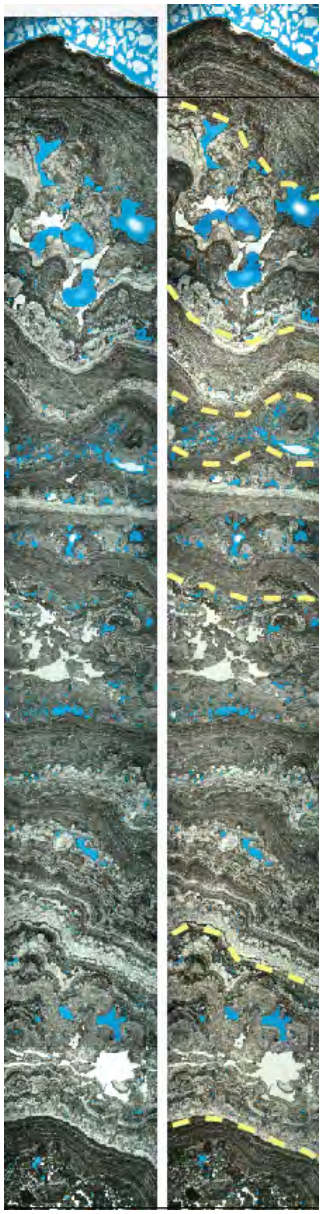

Figure 31: Photomosaic of microbialite LN-13-13 in PPL (A) and XPL (B). Short dimension is 8 mm.

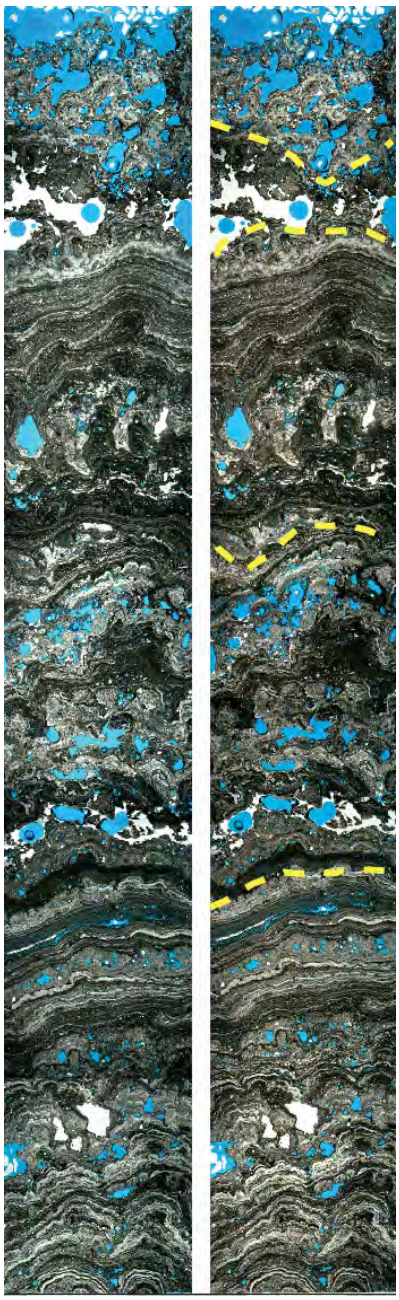

Figure 32: Photomosaic of microbialite LN-13-20 in PPL (A) and XPL (B). Short dimension is 8 mm.

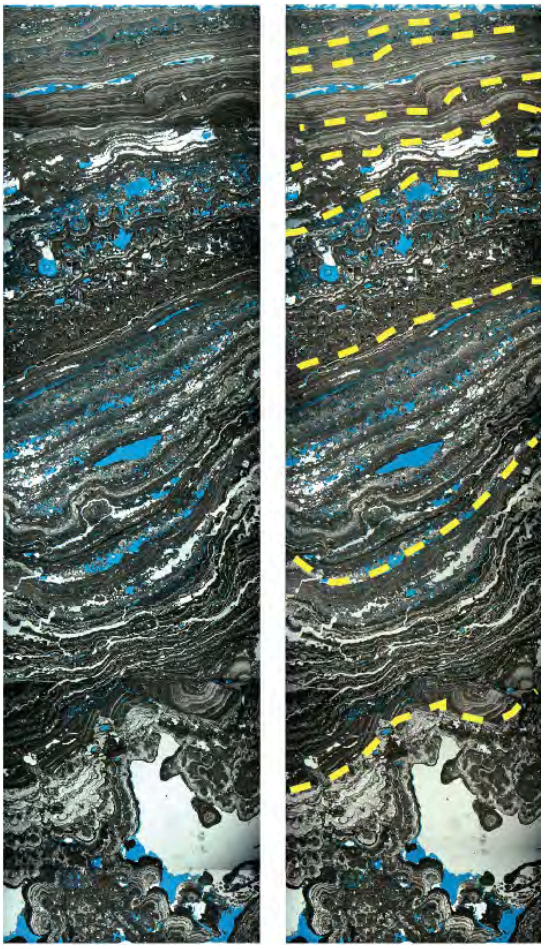

Figure 33: Photomosaic of microbialite LN-13-28 in PPL (A) and XPL (B). Short dimension is 8 mm.

Appendix D: Additional Hydrochemical Modeling

Coprecipitation of trace metals (Sr^{2+}, Mg^{2+})

The quantification of trace metal substitution within the calcium carbonate crystal lattice is a tool often used in paleoenvironmental reconstruction of climate, temperature, and other hydrochemical conditions (Lorens, 1981; Wilkinson & Given, 1986; Chivas et al., 1993; Mitchell & Ferris, 2005; Gouramanis & De Deckker, 2010). Assuming the calcium carbonate formed in thermodynamic equilibrium with the waters of formation (Katz *et al*., 1972), coprecipitation of trace metals in the carbonate lattice is defined by the partition, or distribution, coefficient (D_x) between the molar ratio of the trace metal to calcium of the water:

$$\frac{m_X^C}{m_{Ca^{2+}}^C} = D_X^C \frac{m_X^L}{m_{Ca^{2+}}^L} \qquad (1) \qquad \text{(Katz } et\ al\text{., 1972)}$$

where m is the molar ratio, X is the trace metal being examined (Sr^{2+}, $Mg,^{2+}$ or any other divalent cation), C is calcium carbonate, and L is the liquid.

Geochemical modeling of Sr/Ca water composition was performed to reconstruct water evolution in response to fluctuating chemical conditions. Since D_{Sr} is dependent upon kinetics and mechanism of crystal growth (Kinsman & Holland, 1969), in order to build a robust model and produce a D_{Sr} that simultaneously accounts for the Mg/Ca ratio of the water, while being both rate-dependent and temperature specific, the distribution coefficient of strontium (D_{Sr}) in calcite was found through the integration of published models and assumptions (Table 12). Since the relationship between the molar Mg/Ca ratio of the host waters is such that precipitation is

Table 12: Assumptions in Sr/Ca model for host waters based upon calcite formation.

Parameter	**Description**	**Equation/Source**	**Reference**
D_{Sr}	Homogeneous distribution coefficient	$D_{Sr} = \frac{Sr}{Ca_{liquid}} / \frac{Sr}{Ca_{rock}}$	Katz et al., 1972
Steady-state solution composition	Homogenous precipitation process	$Ca(HCO_3)_2 + MgCl_2 \rightarrow CaCO_3$	Mucci and Morse, 1983; (Oomori et al., 1987)
Rock/water interaction	Equilibrium at 25°C		
logK	Rate constant	$\log K = -0.2727(Mg/Ca_{sol'n}) - 5.007$	Mucci and Morse, 1983; equation obtained from plotting Table IV
$Mg/Ca_{sol'n}$	Molar concentration of Mg/Ca in solution	Average value from modeled and measured Mg/Ca ratios within the mixing zone	This work
logR	Precipitation rate of calcite	$\log R = \log K + n\log(\Omega - 1)$	Mucci and Morse, 1983
n	Empirical reaction order	$n = 3.07$	Mucci and Morse, 1983; $Mg/Ca_{sol'n} = 1$
Ω	7.47 @ 25°C	Average *in situ* mixing zone value from PHREEQC-I. $\Omega = \frac{Ion\ Activity\ Product}{K_{sp}}$ $K_{sp} = 10^{-8.48}$	(Parkhurst, 1999)

slowed through kinetic inhibition, the D_{Sr} of calcite may be obtained through the integration of published models:

$$\log K = -0.2727\ (Mg/Ca_{L}) + (-5.007) \qquad (2)$$ (Mucci and Morse, 1983)

where K is the rate constant and Mg/Ca is the measured molar ratio within the liquid. With average $Mg/Ca_{L} \sim 0.831$ (from averaging the Mg/Ca molar concentrations provided by PHREEQC with *in situ* mixing zone samples 3 and 4; Table 13):

$$\log K = -0.2727\ (0.831459) + (-5.007) \qquad (2b)$$

$$\log K = -5.233738869 \qquad (2c)$$

From a known rate constant, the next step in determining D_{Sr} in the case of calcite is to find a suitable precipitation rate, such that at 25°C:

$$\log D_{Sr} = (0.214 \pm 0.026)*\log R - 1.67 \pm 0.09 \qquad (3)$$ (Tang *et al*., 2008)

where R is the precipitation rate expressed in micromoles/hr*m^2. Quantification of precipitation rate, while difficult to constrain, is essential to coprecipitation models that are based upon calcite precipitation rate (Lorens, 1981; Mucci, 1986; Carpenter & Lohmann, 1992; Tang *et al*., 2008). Obtaining probable precipitation rates is made possible through extrapolation from saturation

Table 13: Average measured and modeled molar concentrations of Mg^{2+} and Ca^{2+} within the mixing zone of Laguna Negra.

Sample	Description	Mg^{2+}	Ca^{2+}	Mg/Ca
		Molar		
1	Modeled 50% Lake, 50% Inlet	0.24	0.34	0.69
2	Modeled 45% Lake, 55% Inlet	0.22	0.31	0.69
3	Modeled 40% Lake, 60% Inlet	0.19	0.28	0.70
4	Modeled 35% Lake, 65% Inlet	0.17	0.25	0.70
5	Modeled 30% Lake, 70% Inlet	0.15	0.21	0.70
6	Modeled 25% Lake, 75% Inlet	0.13	0.18	0.71
7	Modeled 20% Lake, 80% Inlet	0.11	0.15	0.71
8	*Measured in situ* Mixing Zones sample 3	0.02	0.01	1.9
9	Measured in situ Mixing Zones sample 4	0.09	0.15	0.58
Avg		0.15	0.21	0.83

state. Modeled saturation states were garnered through PHREEQC geochemical modeling (Parkhurst, 1999) of *in situ* mixing zone water chemistry and iterative modeling of lake to inlet water mixtures of 50:50 to 20:80. Saturation state (Ω) of the modeled solutions with respect to the solid phase of calcite is expressed as a ratio of the ion activity product (IAP) reported in PHREEQC to the solubility constant:

$$\Omega = \frac{IAP}{Ksp} \Omega = \frac{\text{IAP}}{\text{Ksp}} \quad (4)$$

where *Ksp* is the equilibrium stoichiometric solubility constant for calcite at 5°C, 25°C, 40°C (Garrels, 1965).

With the average mixing zone saturation state of calcite of 7.47, logR was obtained according to:

$$\log R = \log K + n * \log(\Omega - 1) \quad \text{(Mucci, 1986)} \quad (5)$$

where rate is expressed as moles/hr*m^2 and n is the empirical reaction order. The modeled average saturation state given in PHREEQC from mixing zone water samples produces Ω = 7.47. With a liquid molar Mg/Ca ratio of 0.831 (Table 13), n = 3.07 (Mucci and Morse, 1983) and the rate constant from equation 2c:

$$\log R = -5.233738869 + 3.07 * \log(7.47 - 1) \quad (5b)$$

$$\log R = -2.744 \quad (5c)$$

After converting precipitation rate from moles/hr*m^2 to micromoles/hr*m^2, logR from equation 2c can be used in equation 5 to produce the D_{Sr} of calcite, and in turn, the Sr/Ca composition of host waters, under the assumption of constant temperature:

$$D_{Sr}^{Calcite} = 0.106 \pm 0.001 \quad (6)$$

This value falls within the range of published values for calcite of 0.02 – 0.4 (Katz et al., 1972; Berner, 1975; Lorens, 1981; Mucci, 1986). Sensitivity testing shows that both temperature and saturation state play a role in the modeled Sr/Ca composition of the water, with greater variability seen in at low temperature (Fig. 34). Theoretical high, medium, and low saturation states were scaled according to temperature and corresponding K_{sp} (Garrels, 1965). At 5°C, we see a very large spread in modeled Sr/Ca water ratios across saturation states (7.2). Such large deviations suggest that Mg/Ca, and in turn, precipitation rates, play critical role in modeled values. Similarly, the Sr/Ca molar rock ratios also show nearly identical behavior to the modeled Sr/Ca ratios of water with the lowest saturation state of calcite (2.8) at 40°C. The Sr/Ca composition of the waters of calcite formation can be constrained though this model of rate-dependent, temperature specific D_{Sr} for calcite if a constant temperature is assumed. Sensitivity of this model to saturation state and defined reaction order was also tested. Although the saturation state of calcite affects modeled log R values, the modeled results of D_{Sr} still fall between 0.04 and 0.1 with Log R ranging from -4.5 to -2.5.

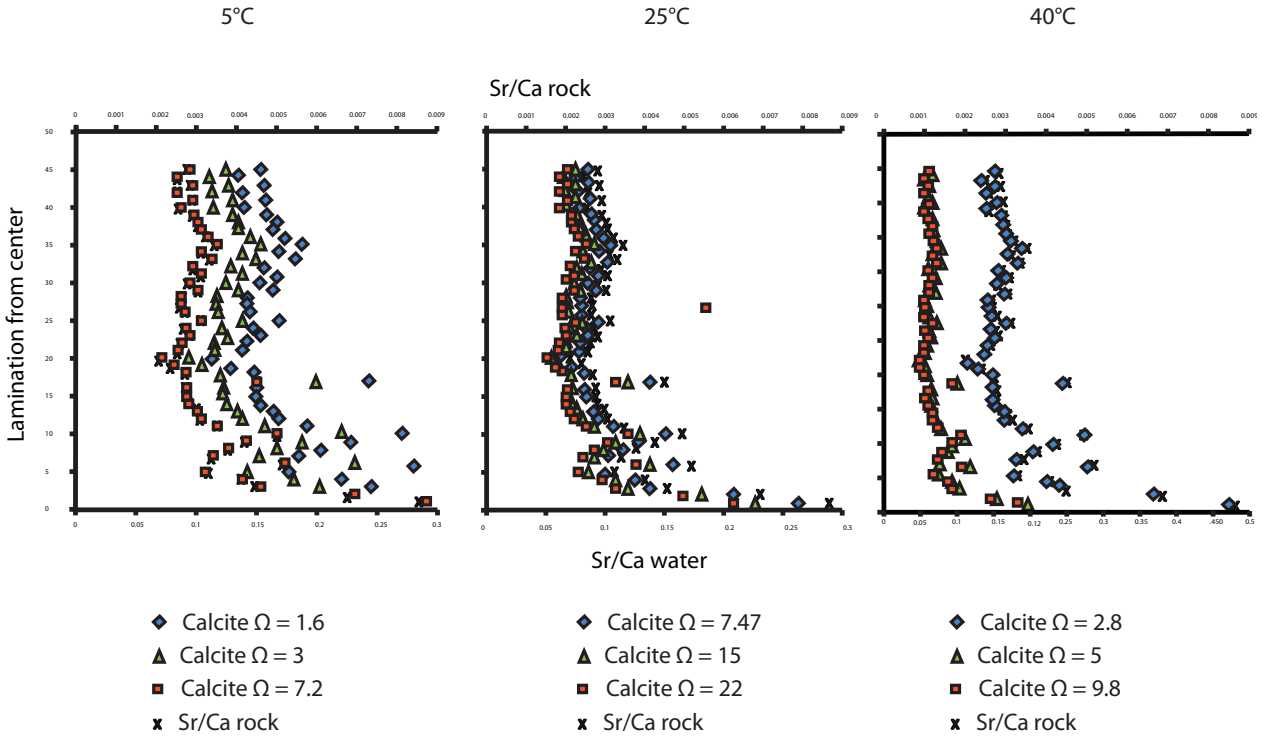

Figure 34: Modeled molar Sr/Ca of waters of formation. Trace metal abundance data used from microbialite LN-13-1. Rate determined according to Mucci, 1986. Saturation state of calcite found by using modeled ion activity product and Ksp values according to temperature (Garrels and Christ, 1965). Water composition plays a significant role in trace metal incorporation, with increased temperature causing precipitate rate increases.

The relationship between measured Sr^{2+} (ppm), modeled D_{Sr}, and mole percent $MgCO_3$ is displayed in Fig. 35. With outliers removed after microfabric and geochemical evidence suggestive of aragonitic content, it is clear that the amount of Sr^{2+} incorporated into the lattice structure, and in turn, the D_{Sr}, is influenced to some degree by the amount of $MgCO_3$ within the lattice. This trend has been reported as directly proportional by other workers (Holland, 1966; Katz et al., 1972; Carpenter & Lohmann, 1992) and can be related to microstructural defects induced by magnesium incorporation that facilitate coprecipitation of Sr^{2+} through the addition of kinks into which the large Sr^{2+} ion can fit (Paquette & Reeder, 1995). Indeed, throughout the literature, both abiotic and biogenic carbonate display systematic covariance between Sr^{2+} and Mg^{2+} (Mucci & Morse, 1983; Ohde, 1984; Carpenter & Lohmann, 1992). However, our data do not show a relationship as strong as published empirical findings (Fig. 36). One striking difference between the strong covariant relationships found in previous works and this study is that the concentrations of both Sr^{2+} and Mg^{2+} are extremely elevated, with average Sr^{2+} values around 2800 ppm and Mg^{2+} averages between 6284 and 11477 ppm. Such extraordinarily high values suggest extremely rapid precipitation rates, which have been suggested to significantly increase D_{Sr} (Lorens, 1981; Baker *et al*., 1982; Mucci, 1986; Pingitore and Eastman, 1986; Carpenter & Lohmann, 1992).

Increases in temperature, saturation state, and precipitation rates all act to increase the D_{Sr} between calcite and host waters. By contrast, increases in CO_3^{2-}, or alkalinity, decrease D_{Sr}. Interpreting trends in our data, therefore, requires attention to the chemical pathway whereby stable carbonates are formed and the bulk chemistry of their host waters. Increased degassing of

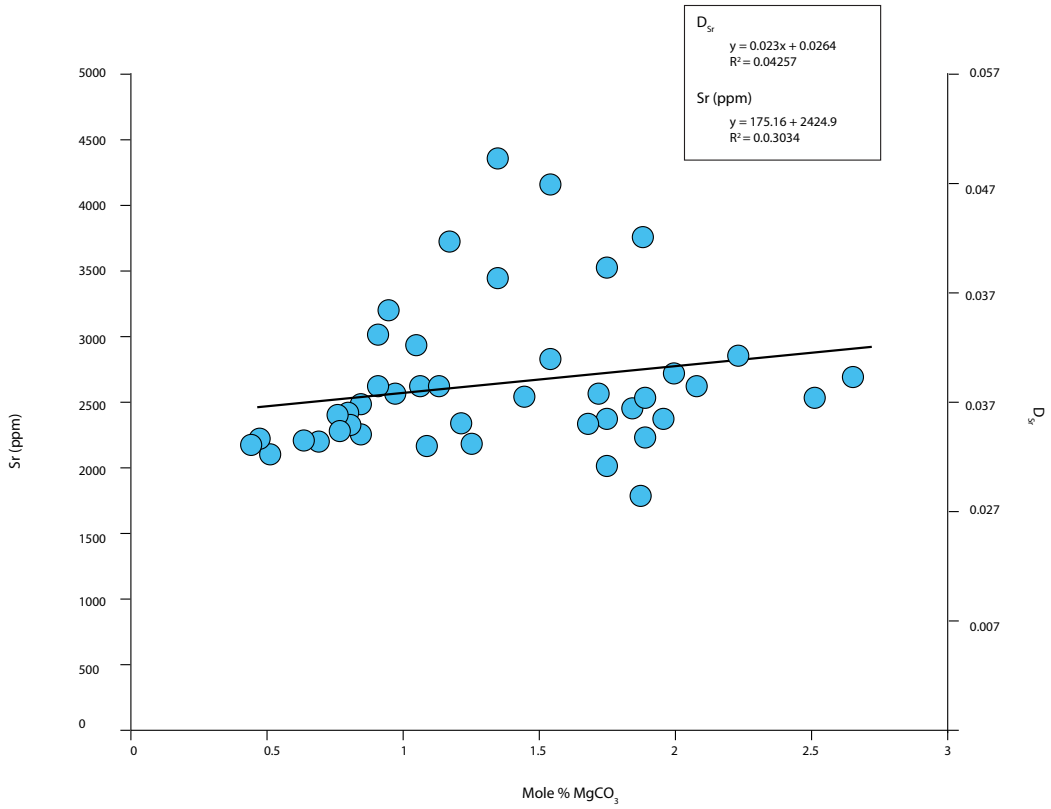

Figure 35: The modeled distribution coefficient of strontium (D_{Sr}) as a function of the amount of MgCO3 within calcite of LN-13-1. Outliers removed (laminae 1-28 and 1-29) which show botryoidal microfabric, elevated strontium concentrations (5669 ppm and 7285, respectively), and high modeled D_{Sr} values close to 1, all characteristic of aragonite.

CO_2 with evaporation causes both increases in $\delta^{18}O$ and pH, the effect of which is a depressed D_{Sr}, which explains the initially low values of Sr. However, prolonged evaporation within the basin causes an overall increase in D_{Sr} resulting from the increase in Sr/Ca within waters that are likely progressively enhancing with respect to calcite saturation state that is coinciding with increased temperatures in a shallower water body. In addition, should the precipitation of LMC and/or discharge of saline groundwater remained tightly coupled to and keep pace with evaporative concentration, both the salinity and Mg/Ca of the waters of formation increase. This, in turn, causes the stable phase of calcium carbonate to be aragonite, the D_{Sr} of which is much larger than that of calcite (Kinsman & Holland, 1969; Visscher *et al*., 1998). The result of a larger D_{Sr} is higher amount of Sr^{2+} in the carbonate. Mineralogical investigation of Laguna Negra microbialites show that, while it is not uniformly true, the laminations found to contain both highly enriched $\delta^{18}O$ values and high Sr^{2+} concentrations contain aragonite.

Time-wise trends of elemental salinity indicators (Mg/Ca and Sr/Ca) within carbonate are variable across samples; however, the laminations most recently deposited show considerably depressed values. Decreased values reflect decreased salinity within the basin, which is also mirrored by light values of oxygen and carbon isotopes within carbonate. High fluctuation in ratios between laminations of an individual sample can be tied to spatial position in the lake with relation to the lake's source of input waters, with samples nearest to the shore displaying heightened sensitivity to inflow (LN-13-5; LN-13-13).

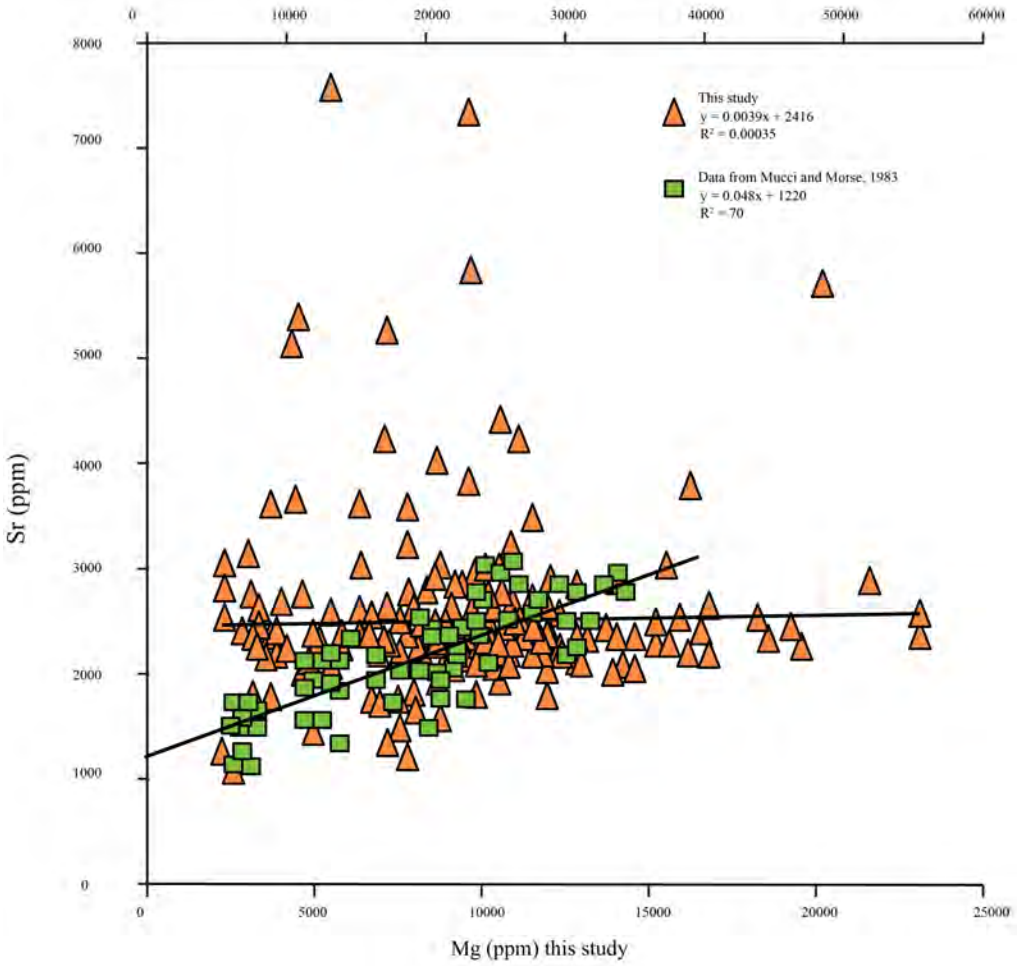

Figure 36: Strontium and magnesium covariance within calcium carbonates. Orange triangles are data from this study, which illustrate no covariance. Several samples with extreme Sr^{+} enrichment contain aragonite. Green rectangles are data from Mucci and Morse, 1983, which show strong covariance. For their study, strontium and magnesium concentrations were obtained from calcites grown at 25 degrees C within solutions with Mg/Ca ratios from 1 to 10.3. Note secondary X-axis.

Since laminae of microbialites contain aragonite as well as calcite, the distribution coefficient for strontium in aragonite needs to be addressed. Predicated on the work of Holland *et al*. (1963) and Holland *et al*. (1964), Kinsman and Holland (1969) found that the D_{Sr} between aragonite and dissolved bicarbonate decreased linearly with increasing temperature and has a value of 1.17 ± 0.004 at 16°C, 1.13 ± 0.03, at 25°C, and 1.15 ± 0.05 at 30°C. Modeling of water Sr/Ca composition using these values differs by about an order of magnitude when compared to values obtained with $D_{Sr\text{-}calcite}$ (Table 14). In laminations that had the presence of aragonite confirmed through XRD, the modeled Sr/Ca ratios within host water are not statistically different from layers containing only calcite ($p = 0.0796$ at 15°C and $p = 0.0737$ at 30°C). However, in order to make any inference as to the validity of modeled water composition beyond preliminary findings, greater resolution of mineralogical analysis should be conducted for better recognition of the influence that aragonite imparts on trace metal incorporation and its subsequent affect on paleosalinity proxy data.

As with coprecipitaiton of strontium in calcium carbonate, the degree to which magnesium is incorporated in a growing lattice depends upon the distribution coefficient of magnesium (D_{Mg}). In calcite forming from waters with molar Mg/Ca ratios between 0.04 and 2, the role that solution Mg/Ca ratio plays in D_{Mg} is nominal (Oomori *et al*., 1987). Instead, the value of D_{Mg} is highly temperature dependent:

f

Table 14: Sr/Ca of water derived through D_{sr} for aragonite at 15, 25, and 30°C.

	Sr/Ca water		
	Temperature °C		
Microbialite	15	25	30
D_{Sr}*	1.17	1.13	1.15
LN-13-1	0.002850865	0.00295178	0.002893707
LN-13-5	0.00228431	0.002518636	0.002324037
LN-13-10	0.002313253	0.002395138	0.002353484
LN-13-13	0.002495526	0.002583863	0.002538926
LN-13-20	0.002330418	0.002412911	0.002370947
LN-13-28	0.002967363	0.003072402	0.003018969

*D_{Sr} between aragonite and dissolved bicarbonate (Kinsman and Holland, 1969).

$D_{Mg} = 0.000898 * °C + 0.0348$ (Katz, 1973) (7)

$D_{Mg} = 0.00066 * °C + 0.0042$ (Oomori *et al*., 1987) (8)

Unfortunately, reliable derivation of temperature fluctuations throughout microbialite growth requires comprehensive and constrainable time-series records of the water Mg/Ca composition. Even with measured Mg/Ca ratios of the carbonate, such heightened sensitivity to temperature that is characteristic of D_{Mg} precludes extrapolation of water Mg/Ca ratios from our current data. However, if we assume that Mg/Ca ratio of the waters of formation have remained stable throughout lamination accretion, a Mg/Ca water ratio of 0.8314, then the average theoretical D_{Mg} is between 0.032 and 0.065 (Table 15), which is congruent with published results of empirical studies at 25°C (Füchtbauer & Hardie, 1976). Relatively depressed modeled D_{Mg} values in samples LN-13-1 (0.032) and LN-13-5 (0.033) could be linked to photosynthetic activity. Experiments focused on the relationship between trace metal partitioning and biochemical pathways identified a direct negative relationship between chlorophyll *a* production and D_{Mg}, which suggests that biomolecular pathways have considerable influence on the ability of free ions to be utilized in a calcium carbonate lattice (Müller *et al*., 2014).

Table 15: Average theoretical D_{Mg} values for microbialite samples. Values were derived by dividing molar rock Mg/Ca ratios by solution Mg/Ca ratio.

	$[Mg]/[Ca]_{rock}$	**Avg. D_{Mg}**
Rock	Average	*Mg/Ca solution = 0.8314*
LN-13-1	0.016	0.032 ± 0.01
LN-13-5	0.017	0.034 ± 0.01
LN-13-10	0.019	0.042 ± 0.01
LN-13-13	0.005	0.052 ± 0.01
LN-13-20	0.006	0.066 ± 0.02
LN-13-28	0.021	0.060 ± 0.02

Appendix E: Supplementary Tables

Table 16: Running average concentrations of Mg^{2+} and Ca^{2+}, ratios, and Mole % of $MgCO_3$ within carbonate. Laminae are ordered with 1 referring to the outer rim of the microbialite.

Microbialite LN-13-1				
Lamina	Mg (ppm)	Ca (ppm)	Mg/Ca	Mole % $MgCO_3$
1	3979.188	389714	0.010251	0.854236
2	4739.836	389378.4	0.012216	1.018004
3	8643.732	385457.9	0.022481	1.873376
4	7449.662	387557.1	0.019241	1.603433
5	3774.683	391582.7	0.00964	0.803365
6	5147.32	389415.1	0.013243	1.103567
7	7632.42	385598.8	0.019811	1.650917
8	4683.582	390671.7	0.011994	0.999484
9	6802.623	387767.9	0.017617	1.468072
10	7246.499	387426.4	0.018738	1.561463
11	9208.721	384233.3	0.024026	2.002154

Microbialite LN-13-5				
Lamina	Mg (ppm)	Ca (ppm)	Mg/Ca	Mole % $MgCO_3$
1	4990.957	389413.1	0.012863	1.071898
2	5043.54	389770.6	0.012993	1.082738
3	7715.396	386079.2	0.019988	1.665636
4	7371.307	385706.7	0.019111	1.592596
5	4600.351	388688.2	0.011871	0.989263
6	6998.307	386925.3	0.01813	1.510813
7	7771.428	385356.9	0.020167	1.680592
8	7858.071	386431	0.020347	1.69558

Microbialite LN-13-10				
Lamina	Mg (ppm)	Ca (ppm)	Mg/Ca	Mole % $MgCO_3$
1	8241.31	382159.8	0.021574	1.797806
2	8810.074	384984.1	0.022947	1.912275

Table 16 con't

Lamina	Mg (ppm)	Ca (ppm)	Mg/Ca	Mole % $MgCO_3$
3	8969.697	385281.8	0.023342	1.945162
4	7738.614	385871.9	0.020113	1.676062
5	8321.133	385086.7	0.021614	1.801151
6	7881.092	385818.6	0.020495	1.707897
7	6608.095	386874.1	0.017183	1.431926

Microbialite LN-13-13				
Lamina	Mg (ppm)	Ca (ppm)	Mg/Ca	Mole % $MgCO_3$
1	7960.749	385303.6	0.020679	1.723284
2	10949.32	382798.8	0.028608	2.384003
3	8838.405	382017.1	0.02313	1.927484
4	9535.993	382863.5	0.024915	2.076245
5	8758.45	383115.4	0.022858	1.9048
6	9211.217	381975.4	0.024115	2.009564
7	10454.17	382042.2	0.027374	2.28118
8	9304.049	384446.1	0.024204	2.017029
9	14603.81	387190.7	0.029338	3.259784
10	10918.22	393183.1	0.021376	2.375126
11	11510.17	381797.4	0.03015	2.512493

Microbialite LN-13-20				
Lamina	Mg (ppm)	Ca (ppm)	Mg/Ca	Mole % $MgCO_3$
1	12545.09	377506.7	0.033306	2.775541
2	9505.555	383166.3	0.024875	2.072955
3	11562.09	380564.3	0.030443	2.53689
4	14133.19	377575.9	0.037534	3.127827

Table 17: Microbialite microfabrics by lamination and abundance fabric components by layers used in carbon coulometry.

Microbialite LN-13-1		
Lamina	Fabric type	Abundance of components
1-TOR-1 1-TOR-2 1-TOR-3 1-1-1 1-1-2	Isopachous Isopachous Isopachous Micritic Mixed micritic/microsparitic	70% micrite, 30% cement
1-2 1-3-W 1-3-1 1-3-2 1-3-3 1-4-1 1-4-2 1-5 1-6-1 1-6-2	Mixed micritic/microsparitic Isopachous Isopachous Isopachous Botryoidal Isopachous Isopachous Mixed micritic/botryoidal Mixed botryoidal/micrite Mixed micrite/Microspariticitic	80% micrite, 20% cement
1-7 1-8-1 1-8-2 1-9 1-10-1 1-10-2 1-11	Micritic Micritic Mixed micritic/botryoidal Micritic Mixed micritic/ microsparitic Mixed micritic/ microsparitic Mixed micritic/ microsparitic	80% micrite, 20% cement
1-12 1-13 1-14 1-15 1-16 1-17	Mixed micritic/microsparitic Mixed micritic/ microsparitic Mixed micritic/ microsparitic Mixed micritic/ microsparitic Mixed micritic/microsparitic Mixed micritic/microsparitic	10% micrite, 90% cement

Table 17 con't

Lamina	Fabric type	Abundance of components
1-18	Mixed micritic/microsparitic	50% micrite, 50% cement
1-19-1	Mixed micritic/microsparitic	
1-19-2	Mixed micritic/microsparitic	
1-20-1	Mixed micritic/microsparitic	
1-20-2	Mixed micritic/microsparitic	
1-21-1	Mixed micritic/microsparitic	
1-21-2	Mixed micritic/microsparitic	
1-22-1	Mixed micritic/microsparitic	40% micrite, 60% cement
1-22-2	Mixed micritic/botryoidal	
1-23-1	Mixed micritic/botryoidal	30% micrite, 70% cement
1-23-2	Mixed micritic/botryoidal	
1-24	Mixed micritic/botryoidal	
1-25	Mixed micritic/botryoidal	
1-26-1	Mixed micritic/microsparitic	
1-26-2	Mixed micritic/microsparitic	
1-27	Micritic	
1-28	Mixed micritic/botryoidal	
1-29	Mixed micritic/botryoidal	

Table 17 con't

Microbialite LN-13-5		
Lamina	Fabric type	Abundance of components
5-1 5-2	Mixed micritic/microsparitic Mixed micritic/microsparitic	85% Micrite, 15% cement
5-3-1 5-3-2	Mixed micritic/botryoidal Mixed micrite/botryoidal	80% micrite, 20% cement
5-4 5-5-1 5-5-2 5-6 5-7-1 5-7-2 5-8-1 5-8-2	Micrite Mixed micritic/botryoidal Micritic Mixed micritic/botryoidal Mixed micritic/microsparitic Botryoidal Micritic Micritic	80% Micrite, 20% cement
5-9 5-10-1 5-10-2 5-11	Mixed micritic/microsparitic Mixed micritic/microsparitic Isopachous Isopachous	70% micrite, 30% cement
Lamina	Fabric type	Abundance of components
5-12	Mixed micritic/botryoidal	60% micrite, 40% cement
5-13 5-14-1 5-14-2 5-15-1	Mixed micritic/botryoidal Mixed micritic/botryoidal Mixed micritic/botryoidal Mixed micritic/botryoidal	85% Micrite, 15% cement
5-15-2 5-16 5-17 5-18-1 5-18-2	Mixed micritic/microsparitic Mixed micritic/microsparitic Isopachous Isopachous Mixed micritic/microsparitic	80% micrite, 20% cement
5-19 5-20 5-21 5-22	Mixed micritic/microsparitic Mixed micritic/microsparitic Mixed micritic/microsparitic Mixed micritic/microsparitic	20% micrite, 80% cement
5-23 5-24 5-25-1 5-25-2	Mixed micritic/microsparitic Mixed micritic/botryoidal Mixed micritic/botryoidal Mixed micritic/botryoidal	40% micrite, 60% cement

Table 17 con't

Microbialite LN-13-10		
Lamina	Fabric type	Abundance of components
10-1 10-2 10-3	Isopachous Mixed micrite/botryoidal Micritic	90% micrite, 10% cement
10-4 10-5 10-6 10-7-1 10-7-2 10-8 10-9 10-10 10-11 10-12 10-13 10-14 10-15 10-16-1 10-16-2 10-17	Botryoidal Mixed micrite/botryoidal Mixed micrite/botryoidal Mixed micrite/microsparitic Mixed micrite/microsparitic Mixed micrite/microsparitic Botryoidal Isopachous Isopachous Isopachous Micritic Micritic Micritic Mixed micrite/microsparitic Mixed micrite/microsparitic Botryoidal	70% micrite, 30% cement
10-18 10-19 10-20 10-21 10-22 10-23-1 10-23-2	Micritic Mixed micritic/botryoidal Botryoidal Mixed micritic/botryoidal Micritic Mixed micritic/botryoidal Mixed micritic/botryoidal	65% micrite, 35% cement
10-24 10-25 10-26 10-27 10-28	Mixed micritic/botryoidal Micritic Mixed micritic/botryoidal Mixed micritic/botryoidal Micritic	15% micrite, 85% cement

Table 17 con't

Microbialite LN-13-13		
Lamina	Fabric type	Abundance of components
13-TOR	Micritic	80% micrite, 20% cement
13-1	Micritic	
13-2	Micritic	
13-3	Botryoidal	
13-4	Mixed micrite/botryoidal	
13-5-1	Micritic	70% micrite, 30% cement
13-5-2	Mixed micrite/botryoidal	
13-6	Botryoidal	
13-7	Isopachous	
13-8-1	Botryoidal	65% micrite, 35% cement
13-8-2	Isopachous	
13-9	Mixed micritic/botryoidal	70% micrite, 30% cement
13-10-1	Micritic	
13-10-2	Micritic	
13-11-1	Botryoidal	
13-11-2	Isopachous	
13-12-1	Mixed micritic/botryoidal	50% micrite, 50% cement
13-12-2	Mixed micritic/botryoidal	
13-12-3	Mixed micritic/botryoidal	
13-13-1	Mixed micritic/microsparitic	
13-13-2	Mixed micritic/microsparitic	
13-14	Micritic	
13-15	Mixed micrite/botryoidal	
13-16	Micritic	
13-17-1	Micritic	
13-17-2	Mixed micritic/microsparitic	
13-18	Botryoidal	
13-19-1	Micritic	50% micrite, 50% cement
13-19-2	Mixed micrite/botryoidal	
13-20	Micritic	
13-21	Mixed micrite/microsparitic	
13-22-1	Mixed micrite/microsparitic	
13-22-2	Micritic	
13-22-3	Botryoidal	

Table 17 con't

Lamina	Fabric type	Abundance of components
13-23-1	Micritic	
13-23-2	Mixed micrite/botryoidal	
13-23-3	Mixed micrite/botryoidal	
13-24	Botryoidal	
13-25-1	Mixed micrite/microsparitic	20% micrite, 80% cement
13-25-2	Mixed micrite/microsparitic	
13-26	Botryoidal	
13-27	Botryoidal	
13-28	Mixed micrite/botryoidal	
13-29	Mixed micrite/botryoidal	98% micrite, 2% cement

Microbialite LN-13-20		
Lamina	Fabric type	Abundance of components
20-1	Botryoidal	
20-2	Botryoidal	10% micrite, 90% cement
20-3	Botryoidal	
20-4	Micritic	98% micrite, 2% cement
20-5	Mixed micritic/botryoidal	
20-6	Micritic	
20-7-1	Micritic	
20-7-2	Mixed micritic/botryoidal	
20-7-3	Mixed micritic/botryoidal	
20-8-1	Micritic	
20-8-2	Mixed micritic/botryoidal	90% micrite, 10% cement
20-8-3	Mixed micritic/botryoidal	
20-9	Micritic	
20-10	Mixed micritic/microsparitic	
20-11	Mixed micritic/microsparitic	
20-12	Micritic	
20-13	Mixed micritic/microsparitic	

Table 17 con't

Lamina	Fabric type	Abundance of components
20-14	Micritic	85% micrite, 15% cement
20-15	Mixed micritic/microsparitic	
20-16	Botryoidal	
20-17	Micritic	
20-18	Mixed micritic/microsparitic	
20-19-1	Micritic	
20-19-2	Botryoidal	
20-20-1	Micritic	
20-20-2	Mixed micritic/botryoidal	
20-21	Mixed micritic/microsparitic	
20-22	Mixed micritic/microsparitic	
20-23	Micritic	
20-24	Mixed micritic/microsparitic	
20-25	Mixed micritic/microsparitic	
20-26-1	Mixed micritic/botryoidal	
20-26-2	Micritic	
20-26-3	Mixed micritic/microsparitic	
20-27	Micritic	
20-28	Botryoidal	50% micrite, 50% cement
20-29	Micritic	
20-30	Mixed micritic/botryoidal	
20-31	Mixed micritic/botryoidal	
20-32-1	Micritic	
20-32-2	Mixed micritic/botryoidal	
20-33	Mixed micritic/botryoidal	
20-34	Mixed micritic/botryoidal	
20-35	Mixed micritic/botryoidal	
20-36	Mixed micritic/botryoidal	
20-37	Mixed micritic/microsparitic	
20-38	Mixed micritic/microsparitic	

Table 17 con't

Microbialite LN-13-28		
Lamina	Fabric type	Abundance of components
28-1-1 28-1-2	Isopachous Isopachous	50% micrite, 50% cement
28-2	Micritic	90% micrite, 10% cement
28-3 28-4 28-5	Isopachous Isopachous Isopachous	70% micrite, 30% cement
28-6-1 28-6-2 28-7 28-7-R	Micritic Mixed micritic/botryoidal Mixed micritic/botryoidal Mixed micritic/botryoidal	70% micrite, 30% cement
28-8-1 28-8-2	Micritic Mixed micritic/botryoidal	95% micrite, 5% cement
28-9-1 28-9-2 28-10	Mixed micritic/botryoidal Mixed micritic/botryoidal Mixed micritic/botryoidal	95% micrite, 5% cement
28-11-1 28-11-2 28-12 28-13 28-14	Micritic Mixed micritic/botryoidal Mixed micritic/botryoidal Mixed micritic/botryoidal Mixed micritic/botryoidal	95% micrite, 5% cement
28-15 28-15-I 28-16 28-17 28-18	Isopachous Isopachous Mixed micritic/botryoidal Micritic Micritic	60% micrite, 40% cement
28-19 28-20-1 28-20-2	Botryoidal Botryoidal Botryoidal	30% micrite, 70% cement

Table 18: Total carbon, total inorganic carbon, and total organic carbon measurements for each microbialite. The layers comprise laminae that have similar isotopic composition and coloration.

Microbialite LN-13-1							
Layer from center	Sample	Laminae included	Total Inorganic carbon (TIC)		Total carbon (TC)		% Total organic carbon (TC-TIC)
			wt (mg)	% C	wt (mg)	% C	
8	C-1-8	1-TOR-1 1-TOR-2 1-TOR-3	8.1	9.5659	6.5	10.6904	1.1245
7	C-1-1	1-1-1 1-1-2	6.2	9.6418	6	10.0373	0.3955
6	C-1-2	1-2 1-3-1 1-3-2 1-3-3 1-3-W 1-4-1 1-4-2 1-5 1-6-1 1-6-2	4.4	10.1304	6.1	11.3134	1.183
5	C-1-3	1-7 1-8-1 1-8-2 1-9 1-10-1 1-10-2 1-11	5.7	10.0092	4.9	11.2292	1.22
4	C-1-4	1-12 1-13 1-14 1-15 1-16 1-17	5.1	9.6283	7.5	11.4397	1.8114
3	C-1-5	1-18 1-19-1 1-19-2 1-20-1 1-20-2	7.3	9.8631	6.9	10.8237	0.9606

Table 18 con't

Layer from center	Sample	Laminae included	Total Inorganic Carbon (TIC)	Total Carbon (TC)	Total carbon (TC)		% Total organic carbon (TC-TIC)
			wt (mg)	% C	wt (mg)	% C	
		1-21-1 1-21-2					
2	C-1-6	1-22-1 1-22-2	5.2	10.1072	5.7	13.9814	3.8742
1	C-1-7	1-23-1 1-23-2 1-24 1-25 1-26-1 1-26-2 1-27 1-28 1-29	4.5	10.0018	4.7	10.9231	0.9213
							Avg. TOC = 1.48085714

Table 18 con't

Microbialite LN-13-5							
Layer from Center	Sample	Laminations included	Total Inorganic Carbon (TIC)		Total Carbon (TC)		% Total Organic Carbon (TC-TIC)
			wt (mg)	% C	wt (mg)	% C	
10	C-5-1	5-1 5-2	6.4	9.9843	6.5	10.3511	0.3668
9	C-5-2	5-3-1 5-3-2	6	9.6018	6.5	11.0743	1.4725
8	C-5-3	5-4 5-5-1 5-5-2 5-6 5-7-1 5-8-1 5-8-2	6.4	9.9216	5.6	11.6764	1.7548
7	C-5-4	5-9 5-10-1 5-10-2 5-11	6.4	9.9752	5.8	11.5793	1.6041
6	C-5-5	5-12	7.1	10.0108	6	11.302	1.2912
5	C-5-6	5-13 5-14-1 5-14-2 5-15-1	7.5	9.984	6.9	11.6274	1.6434
4	C-5-7	5-16 5-17 5-18-1 5-18-2	4.7	9.8856	6.9	10.773	0.8874
3	C-5-8	5-19 5-20 5-21 5-22	5.1	10.1343	6.5	6.3	0
2	C-5-9	5-23 5-24	5.1	10.3085	5.6	11.0528	0.7443
1	C-5-10	-	5.4	10.699	9.7	11.0968	0.3978
							Avg.TOC = 1.01623

Table 18 con't

Microbialite LN-13-10							
Layer from center	Sample	Laminations included	Total Inorganic Carbon (TIC)		Total Carbon (TC)		% Total Organic Carbon (TC-TIC)
			wt (mg)	% C	wt (mg)	% C	
4	C-10-1	10-1 10-2 10-3	6	9.6896	6.5	11.071	1.3814
3	C-10-2	10-4 10-5 10-6 10-7-1 10-7-2 10-8 10-9 10-10 10-11 10-12 10-13 10-14 10-15 10-16-1 10-16-2 10-17	7.1	10.2041	7.1	11.244	1.0399
2	C-10-3	10-18 10-19 10-20 10-21 10-22 10-23-1 10-23-2	7	10.0571	5.2	10.7194	0.6623
1	C-10-4	10-24 10-25 10-26 10-27 10-28	6.6	10.2762	6.2	11.5359	1.2597
							Avg. TOC = 1.085825

Table 18 con't

Microbialite LN-13-13							
Layer from center	Sample	Laminations included	Total Inorganic Carbon (TIC)		Total Carbon (TC)		% Total Organic Carbon (TC-TIC)
			wt (mg)	% C	wt (mg)	%C	
1	C-13-9	-	5	10.0153	32.3	10.6651	0.6498
9	C-13-1	13-TOR 13-1 13-2	5.8	9.7723	6.8	10.3481	0.5758
8	C-13-2	13-3 13-4 13-5-1 14-5-2 13-6	6.5	10.3139	6.2	11.0589	0.745
7	C-13-3	13-7 13-8-1 13-8-2	6.2	10.565	6.1	11.6677	1.1027
6	C-13-4	13-9	7.5	10.2087	5.8	11.1941	0.9854
5	C-13-5	13-10-1 13-10-2 13-11-1 13-11-2 13-12-1 13-12-2 13-13-1 13-13-2	5.4	10.1451	6.1	11.0599	0.9148
4	C-13-6	13-13-3 13-14 13-15 13-16 13-17-1 13-17-2 13-18 13-19-1 13-19-2 13-20 13-21 13-22-1 13-22-2 13-22-3	4.7	9.7373	9.4	10.6197	0.8824

Table 18 con't

Layer from center	Sample	Laminations included	Total Inorganic Carbon (TIC)		Total Carbon (TC)		% Total Organic Carbon (TC-TIC)
			wt (mg)	% C	wt (mg)	%C	
3	C-13-7	13-23-1 13-23-2 13-23-3 13-24 13-25-1 13-25-2 13-26 13-27 13-28	5.7	9.2353	5.2	11.5671	2.3318
2	C-13-8	13-29	8.3	10.3158	6.2	11.9929	1.6771
							Avg. TOC = 1.09608889

Microbialite LN-13-20							
Layer from center	Sample	Laminations included	Total Inorganic Carbon (TIC)		Total Carbon (TC)		%Total Organic Carbon (TC-TIC)
			wt (mg)	% C	wt (mg)	% C	
5	C-20-1	20-1 20-2 20-3	7.2	9.6014	6.4	10.6347	1.0333
4	C-20-2	20-4	4.8	9.9976	5.3	10.7704	0.7728
3	C-20-3	20-5 20-6 20-7-1 20-7-2 20-7-3 20-8-1 20-8-2 20-8-3 20-9 20-10 20-11	6.5	10.351	8.6	10.7785	0.4275

Table 18 con't

Layer from center	Sample	Laminations included	Total Inorganic Carbon (TIC)		Total Carbon (TC)		%Total Organic Carbon (TC-TIC)
			wt (mg)	% C	wt (mg)	% C	
		20-12 20-13					
2	C-20-4	20-14 20-15 20-16 20-17 20-18 20-19-1 20-19-2 20-20-1 20-20-2 20-21 20-23 10-24 20-25 20-26-1 20-26-2 20-27	6.2	9.6859	6.6	11.4381	1.7522
1	C-20-5	20-28 20-29 20-30 20-31 20-32-1 20-32-2 20-33 20-34 20-35 20-36 20-38 20-37	5.4	9.9985	7	11.2052	1.2067
							Avg. TOC = 1.0385

Table 18 con't

Microbialite LN-13-28							
Layer from center	Sample	Laminations included	Total Inorganic Carbon (TIC)		Total Carbon (TC)		% Total Organic Carbon (TC-TIC)
			wt (mg)	% C	wt (mg)	% C	
9	C-28-1	28-1-1 28-1-2	6.6	9.5442	6.6	10.2061	0.6619
8	C-28-2	28-2	7.6	8.1251	7.1	8.3717	0.2466
7	C-28-3	28-3 28-4 28-5	7.8	9.9487	7.7	9.6876	0
6	C-28-4	28-6-1 28-6-2 28-7	5.4	9.854	7.1	10.553	0.699
5	C-28-5	28-7-R 28-8-1 28-8-2	8.4	9.4105	6.7	9.7527	0.3422
4	C-28-6	28-9-1 28-9-2 28-10	8.2	9.3767	5.4	10.1961	0.8194
3	C-28-7	28-11-1 28-11-2 28-12 28-13 28-14	7.8	9.3881	7.1	9.6558	0.2677
2	C-28-8	28-15 28-15-I 28-16 28-17 28-18	6.6	10.3526	4.8	10.6431	0.2905
1	C-28-9	28-20-1 28-20-2	6	9.3294	4.8	10.6431	1.3137
							Avg. TOC = 0.51566667

Table 19: Results of sedimentary organic matter analyses, including isotopic weight percent composition of organic carbon. Dashes indicate either insufficient sample powders or amounts below detection limits. C/N ratios were converted to atomic values to reflect biological stoichiometry.

Microbialite LN-13-1						
Layer from center	Sample	Laminae included	$\delta^{13}C_{org}$	C	N	C/N
			‰ vs. VPDB	Weight percent		
8	C-1-8	1-TOR-1 1-TOR-2 1-TOR-3	-16.1	5.02	0.57	10.3
7	C-1-1	1-1-1 1-1-2	-23.2	4.18	0.25	9.7
6	C-1-2	1-2 1-3-1 1-3-2 1-3-3 1-3-W 1-4-1 1-4-2 1-5 1-6-1 1-6-2	-21.4	3.73	0.37	9.9
5	C-1-3	1-7 1-8-1 1-8-2 1-9 1-10-1 1-10-2 1-11	-26.5	3.93	0.38	12.1
4	C-1-4	1-12 1-13 1-14 1-15 1-16 1-17	-25.7	4.81	0.37	15.2
3	C-1-5	1-18 1-19-1 1-19-2	-	-	-	-

Table 19 con't

Layer from center	Sample	Laminae included	$\delta^{13}C_{org}$	C	N	C/N
			‰ vs. VPDB	Weight percent		
		1-20-1 1-20-2 1-21-1 1-21-2				
2	C-1-6	1-22-1 1-22-2	-20.1	3.15	0.61	7.1
1	C-1-7	1-23-1 1-23-2 1-24 1-25 1-26-1 1-26-2 1-27 1-28 1-29	-22	4.18	0.48	10.2
Avg.			-22.1			10.6

Microbialite LN-13-5						
Layer from Center	Sample	Laminae included	$\delta^{13}C_{org}$	C	N	C/N
			‰ vs. VPDB	Weight percent		
10	C-5-1	5-1 5-2	-	-	-	-
9	C-5-2	5-3-1 5-3-2	-17.3	3.50	0.37	11.0
8	C-5-3	5-4 5-5-1 5-5-2 5-6 5-7-1 5-8-1 5-8-2	-18.5	4.38	0.58	8.8

Table 19 con't

Layer from Center	Sample	Laminae included	$\delta^{13}C_{org}$	C	N	C/N
7	C-5-4	5-9 5-10-1 5-10-2 5-11	‰ vs. VPDB -19.7	Weight percent 5.20	 0.80	7.6
6	C-5-5	5-12	-18.9	4.73	0.60	9.2
5	C-5-6	5-13 5-14-1 5-14-2 5-15-1	-	-	-	-
4	C-5-7	5-16 5-17 5-18-1 5-18-2	-21.8	2.78	0.20	16.2
3	C-5-8	5-19 5-20 5-21 5-22	-	-	-	-
2	C-5-9	5-23 5-24	-20.2	8.0	2.96	9.3
1	C-5-10	-				
Avg.			-19.4			10.4

Table 19 con't

Microbialite LN-13-10						
Layer from center	Sample	Laminae included	$\delta^{13}C_{org}$	C	N	C/N
			‰ vs. VPDB	Weight percent		
4	C-10-1	10-1 10-2 10-3	-21.6	4.16	0.41	11.8
3	C-10-2	10-4 10-5 10-6 10-7-1 10-7-2 10-8 10-9 10-10 10-11 10-12 10-13 10-14 10-15 10-16-1 10-16-2 10-17	-26.9	4.63	0.41	13.2
2	C-10-3	10-18 10-19 10-20 10-21 10-22 10-23-1 10-23-2	-	-	-	-
1	C-10-4	10-24 10-25 10-26 10-27 10-28	-21.3	3.18	0.46	8.1
Avg.			-23.3			11.0

Table 19 con't

Microbialite LN-13-13						
Layer from center	Sample	Laminae included	$\delta^{13}C_{org}$	C	N	C/N
			‰ vs. VPDB	Weight percent		
9	C-13-9	-	-	-		-
8	C-13-1	13-TOR 13-1 13-2	-25.4	2.77	0.17	19.0
7	C-13-2	13-3 13-4 13-5-1 14-5-2 13-6	-24.3	0.02	-	-
6	C-13-3	13-7 13-8-1 13-8-2	-19.8	3.35	0.43	10.5
5	C-13-4	13-9	-	-	-	-
4	C-13-5	13-10-1 13-10-2 13-11-1 13-11-2 13-12-1 13-12-2 13-13-1 13-13-2	-	-	-	-
3	C-13-6	13-13-3 13-14 13-15 13-16 13-17-1 13-17-2 13-18 13-19-1 13-19-2 13-20 13-21	-24.7	4.05	0.18	26.3

Table 19 con't

Layer from center	Sample	Laminae included	$\delta^{13}C_{org}$	C	N	C/N
			‰ vs. VPDB	Weight percent		
		13-22-3				
2	C-13-7	13-23-1 13-23-2 13-23-3 13-24 13-25-1 13-25-2 13-26 13-27 13-28	-19.8	3.35	0.43	9.1
1	C-13-8	13-29	-	-	-	-
Avg.			-22.5			16.5

Microbialite LN-13-20						
Layer from center	Sample	Laminae included	$\delta^{13}C_{org}$	C	N	C/N
			‰ vs. VPDB	Weight percent		
6	C-20-Black	-	-19.5	5.47	0.51	12.5
5	C-20-1	20-1 20-2 20-3	-26.9	9.47	0.29	38.1
4	C-20-2	20-4	-	-	-	-
3	C-20-3	20-5 20-6 20-7-1 20-7-2 20-7-3 20-8-1 20-8-2 20-8-3	-21.4	3.75	0.48	9.1

Table 19 con't

Layer from center	Sample	Laminae included	$\delta^{13}C_{org}$	C	N	C/N
			‰ vs. VPDB	Weight percent		
		20-9 20-10 20-11 20-12 20-13				
2	C-20-4	20-14 20-15 20-16 20-17 20-18 20-19-1 20-19-2 20-20-1 20-20-2 20-21 20-23 10-24 20-25 20-26-1 20-26-2 20-27	-	-	-	-
1	C-20-5	20-28 20-29 20-30 20-31 20-32-1 20-32-2 20-33 20-34 20-35 20-36 20-38 20-37	-19.5	5.47	0.51	15.5
Avg.			-22.1			18.8

Table 19 con't

Microbialite LN-13-28						
Layer from center	Sample	Laminae included	$\delta^{13}C_{org}$	C	N	C/N
			‰ vs. VPDB	Weight percent		
9	C-28-1	28-1-1 28-1-2	-	-	-	-
8	C-28-2	28-2	-	-	-	-
7	C-28-3	28-3 28-4 28-5	-	-	-	-
6	C-28-4	28-6-1 28-6-2 28-7	-	-	-	-
5	C-28-5	28-7-R 28-8-1 28-8-2	-26.6	4.91	0.17	33.7
4	C-28-6	28-9-1 28-9-2 28-10	-25.9	1.68	0.03	65.4
3	C-28-7	28-11-1 28-11-2 28-12 28-13 28-14	-25.6	3.53	0.14	29.4
2	C-28-8	28-15 28-15-I 28-16 28-17 28-18	-26.3	2.16	-	-
1	C-28-9	28-20-1 28-20-2	-	-	-	-
Avg.			-26.1			42.8

Appendix F: XRD Spectra

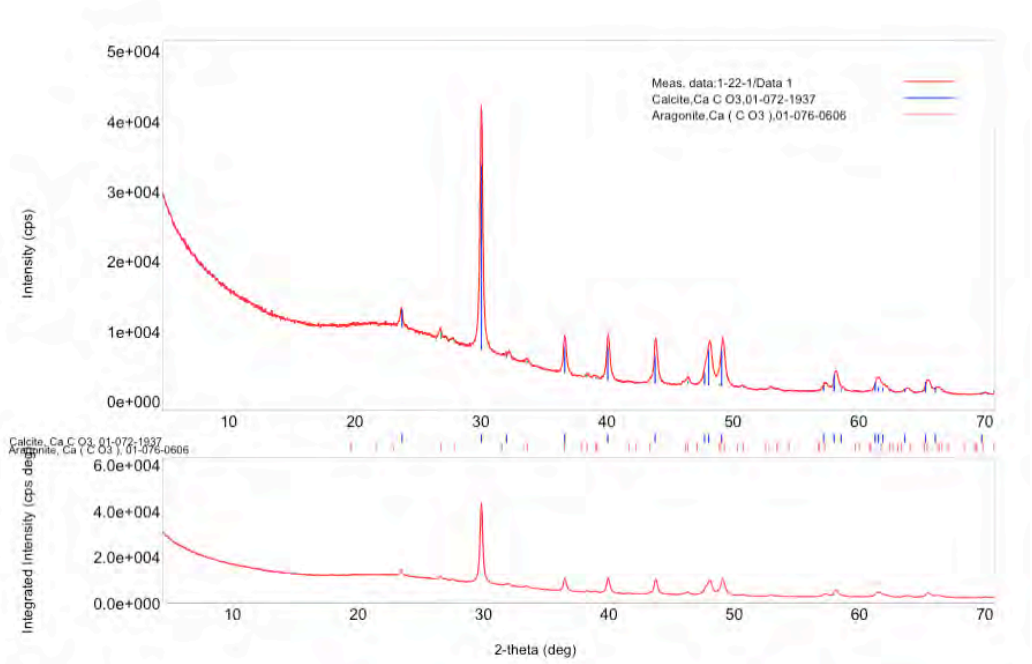

Figure 37: XRD spectra for lamina 22-1 of microbialite LN-13-1.

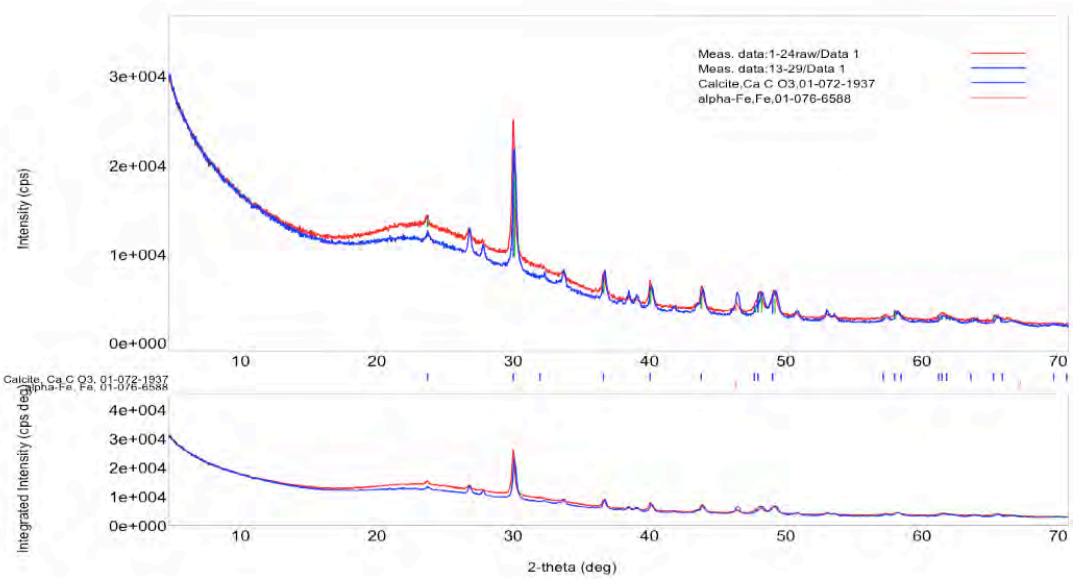

Figure 38: XRD spectra for lamina 29 of microbialite LN-13-13.

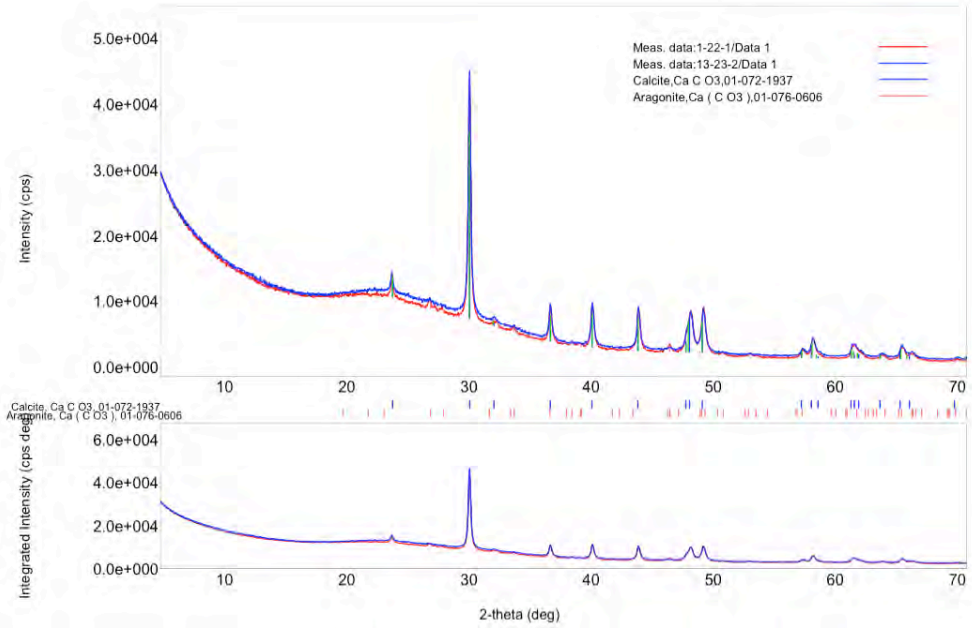

Figure 39: XRD spectra for lamina 23-2 of microbialite LN-13-13.

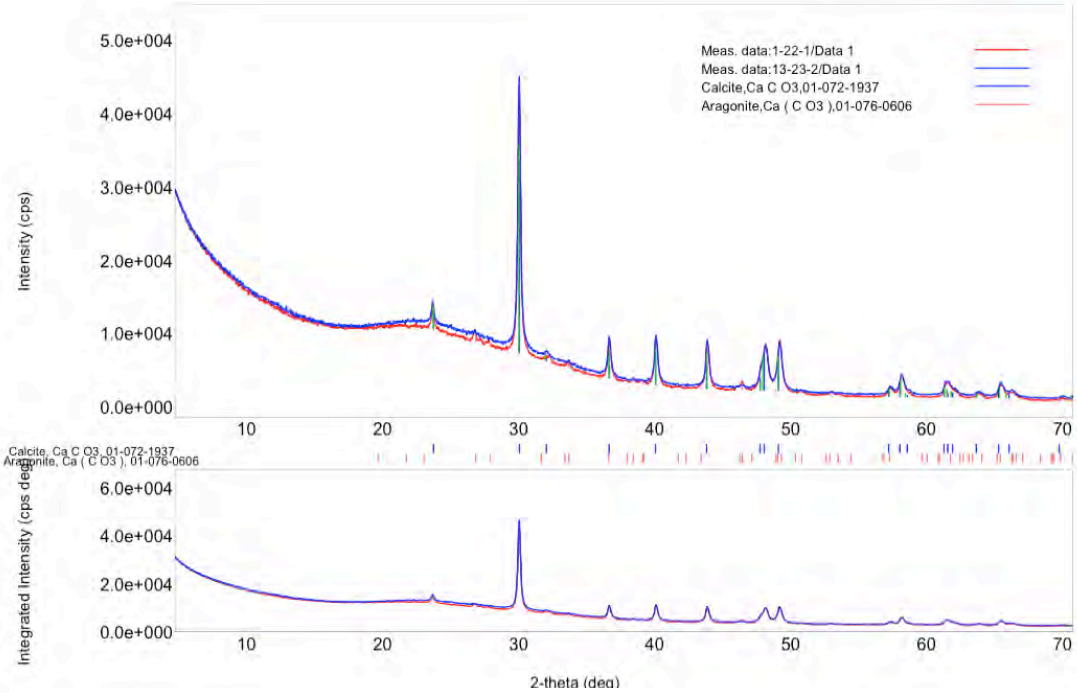

Figure 40: XRD spectra for lamina 24 of microbialite LN-13-1.

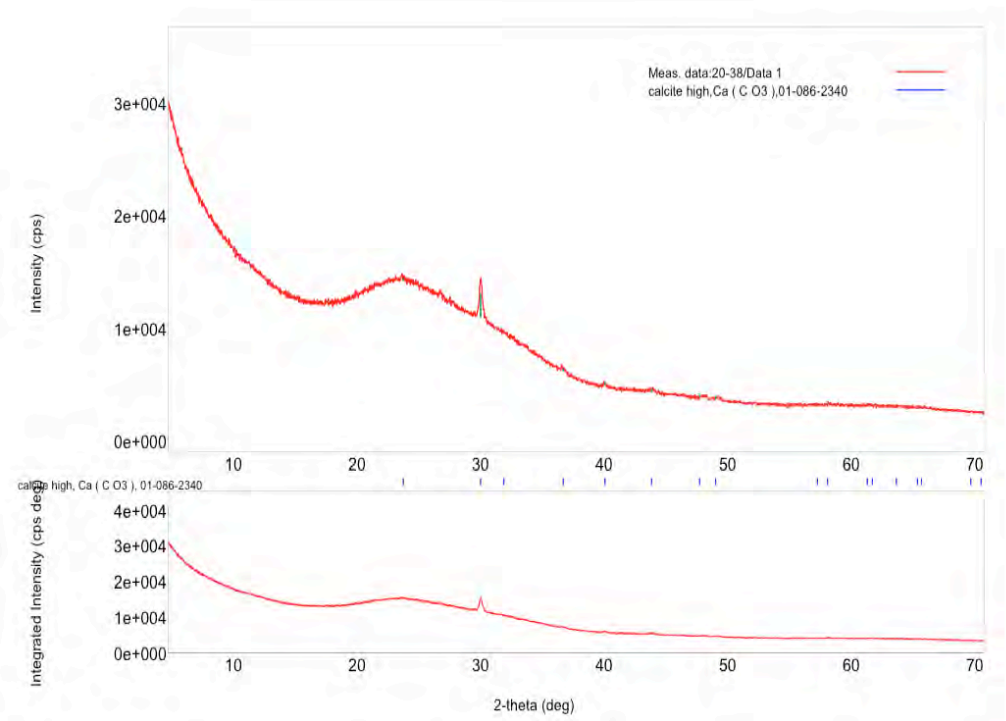

Figure 41: XRD spectra for lamina 38 of microbialite LN-13-28.

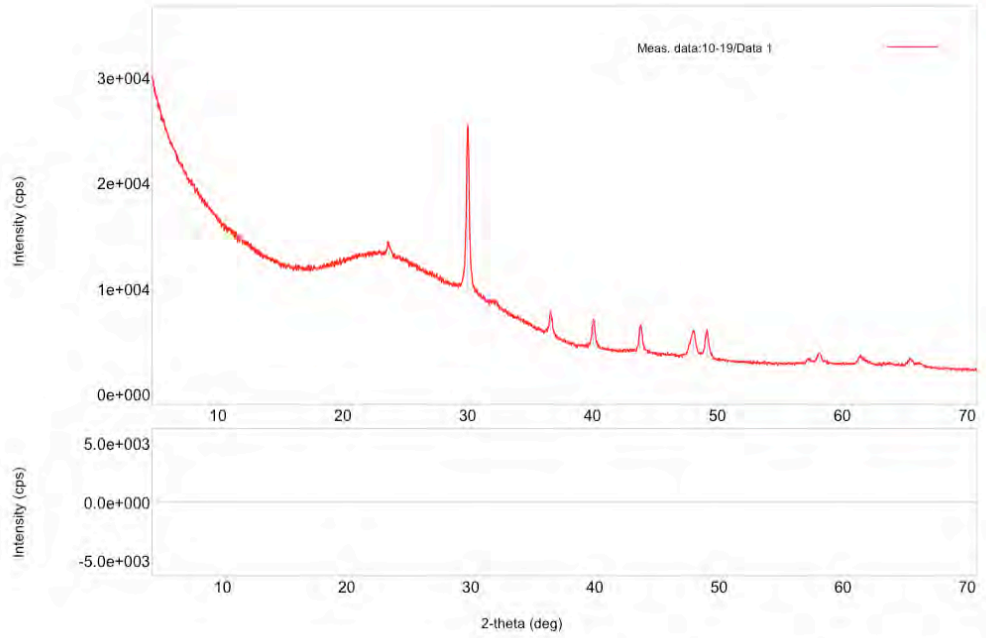

Figure 42: XRD spectra for lamina 19 of microbialite LN-13-10.

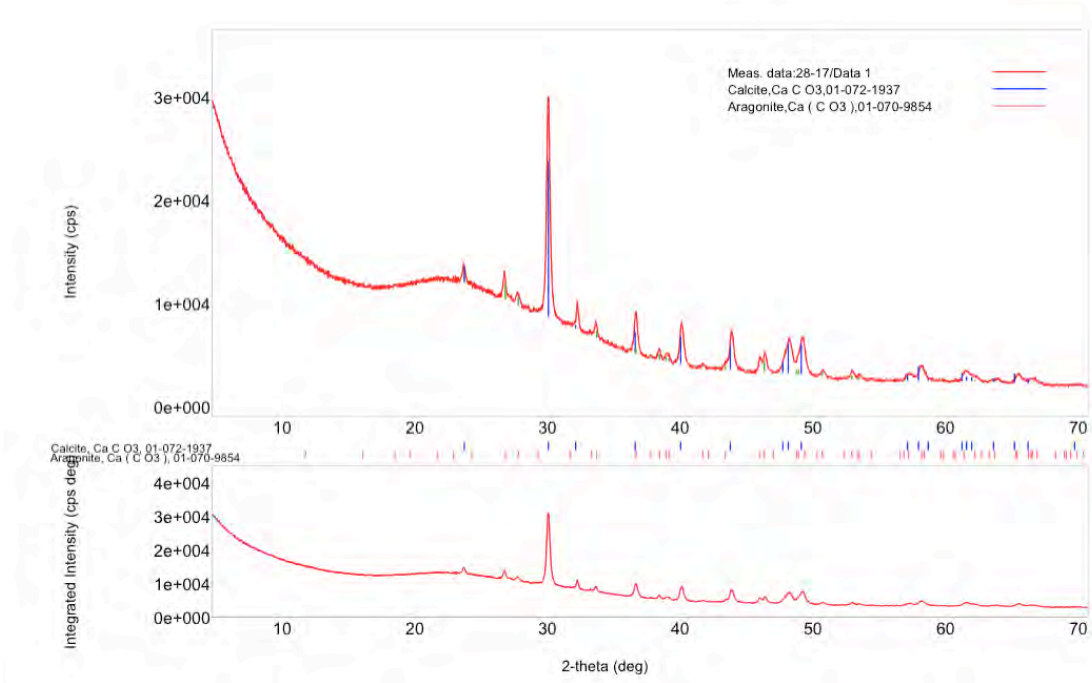

Figure 43: XRD spectra for lamina 17 of microbialite LN-13-28.

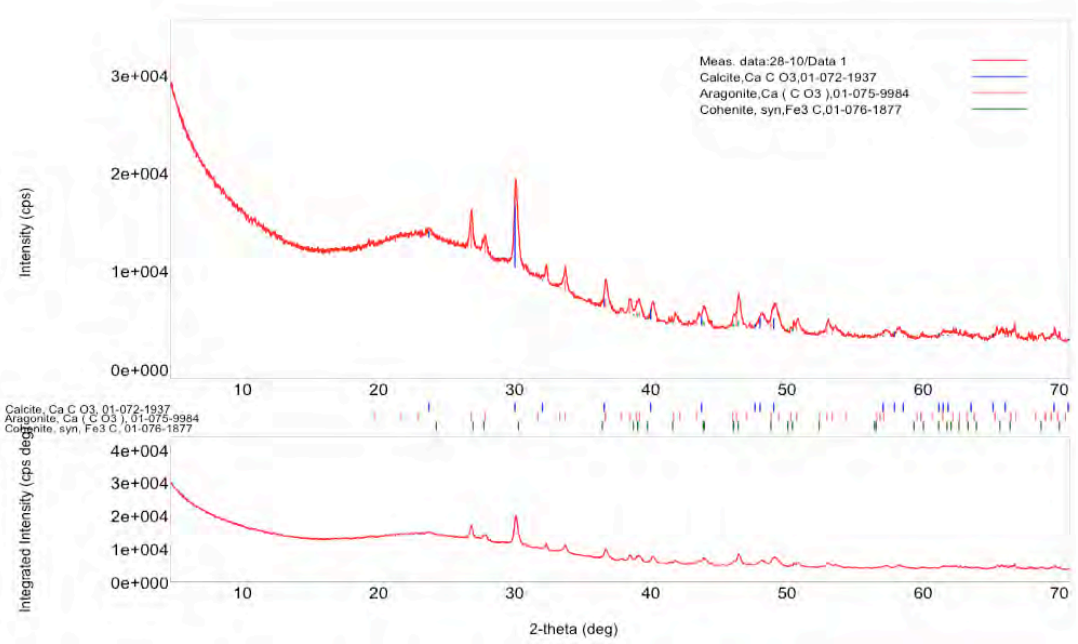

Figure 44: XRD spectra for lamina 10 of microbialite LN-13-28.

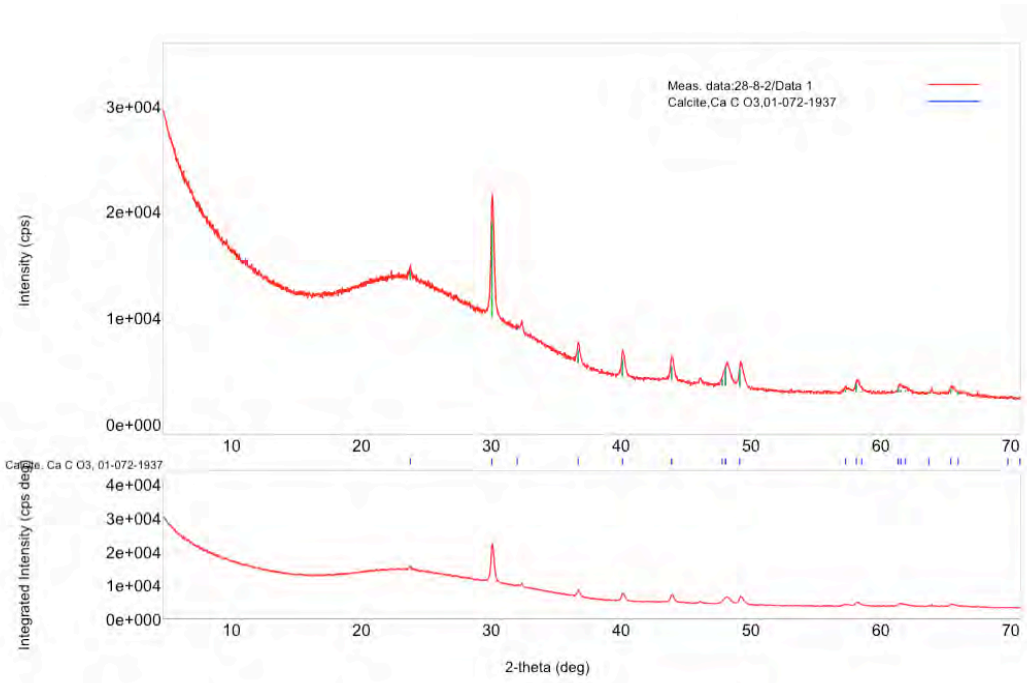

Figure 45: XRD spectra for lamina 8-2 of microbialite LN-13-28.

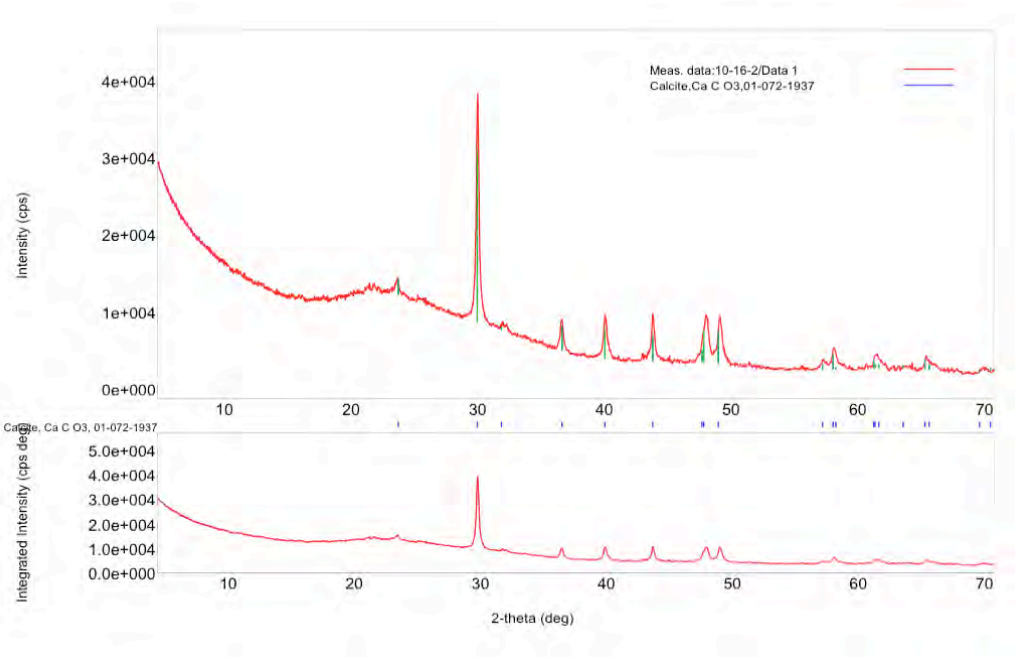

Figure 46: XRD spectra for lamina 16-2 of microbialite LN-13-10.

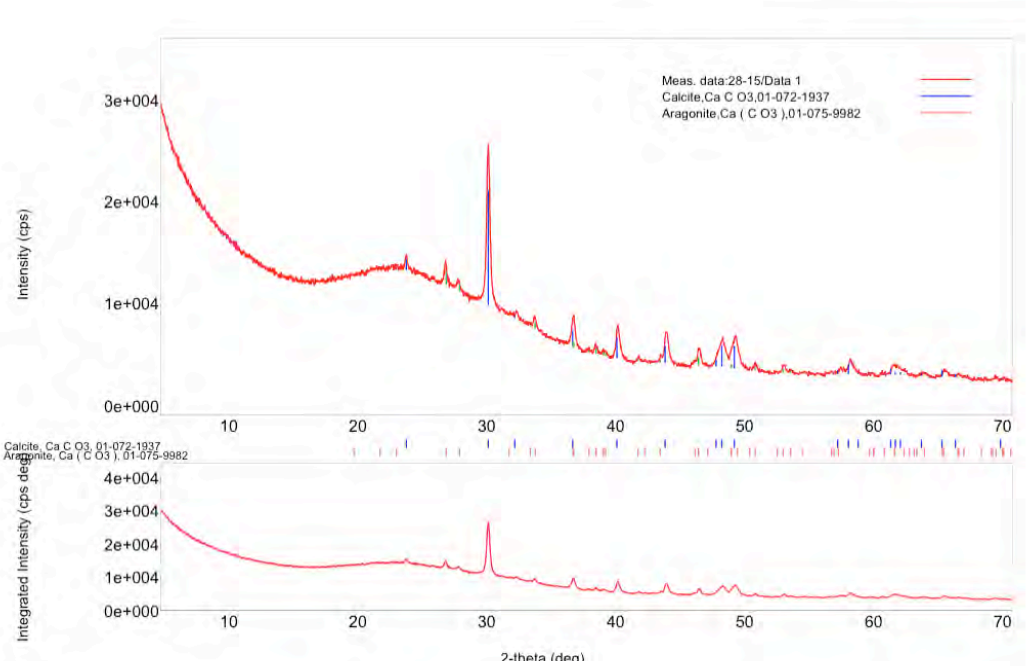

Figure 47: XRD spectra for lamina 15 of microbialite LN-13-28.

Appendix G: Tukey Testing

In order to determine if are statistically significant differences in observed isotopic compositions between the center-most and outter-most laminae, Tukey range testing was conducted on pseudo-replicates. The Tukey method is a single-step statistical test that compares means through a combination of ANOVA and pair-wise comparison of means. For this study, in lieu of standard replicate data which required large amounts of sample, we used the combination of four successive laminae as replicates. It is crucial to note, however, that use of this technique with psuedo-replicates carries the connotation of a genetic relationship between grouped laminae, which is not necessarily the case. Tukey testing was applied as an additional means to corroborate the qualitatively observed trend in isotope data with a quantiative approach.

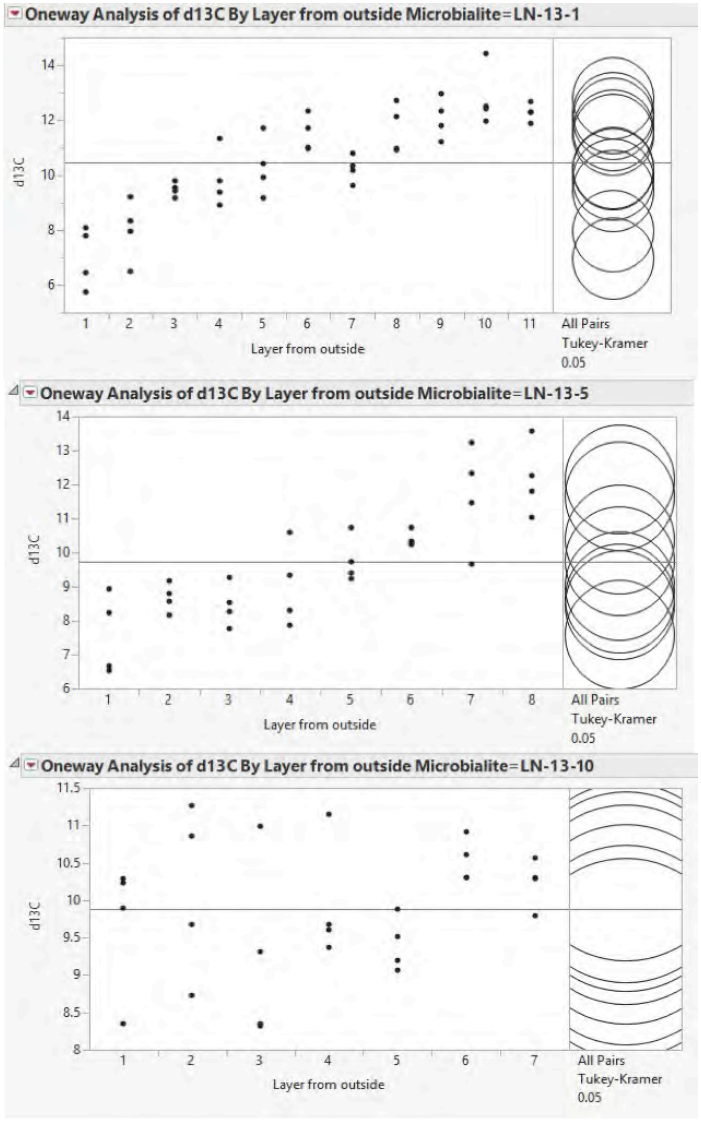

Figure 48: Screen shots of Tukey range testing of significant differences in observed carbon isotope values in microbialites LN-13-1, LN-13-5, and LN-13-10 using JMP software. Circles in right pane correspond to the mean values for laminae grouped as layers. Circles that are not touching are statistically significant at the 95% confidence interval.

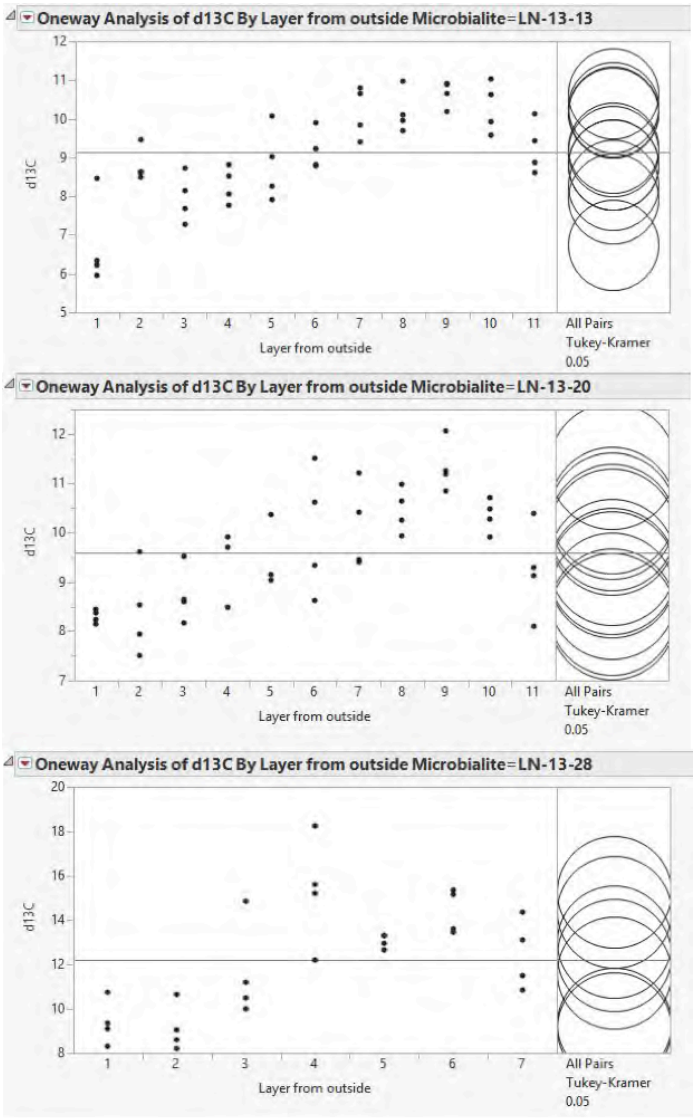

Figure 49: Screen shots of Tukey range testing of significant differences in observed carbon isotope values in microbialites LN-13-13, LN-13-20, and LN-13-28 using JMP software. Circles in right pane correspond to the mean values for laminae grouped as layers. Circles that are not touching are statistically significant at the 95% confidence interval.

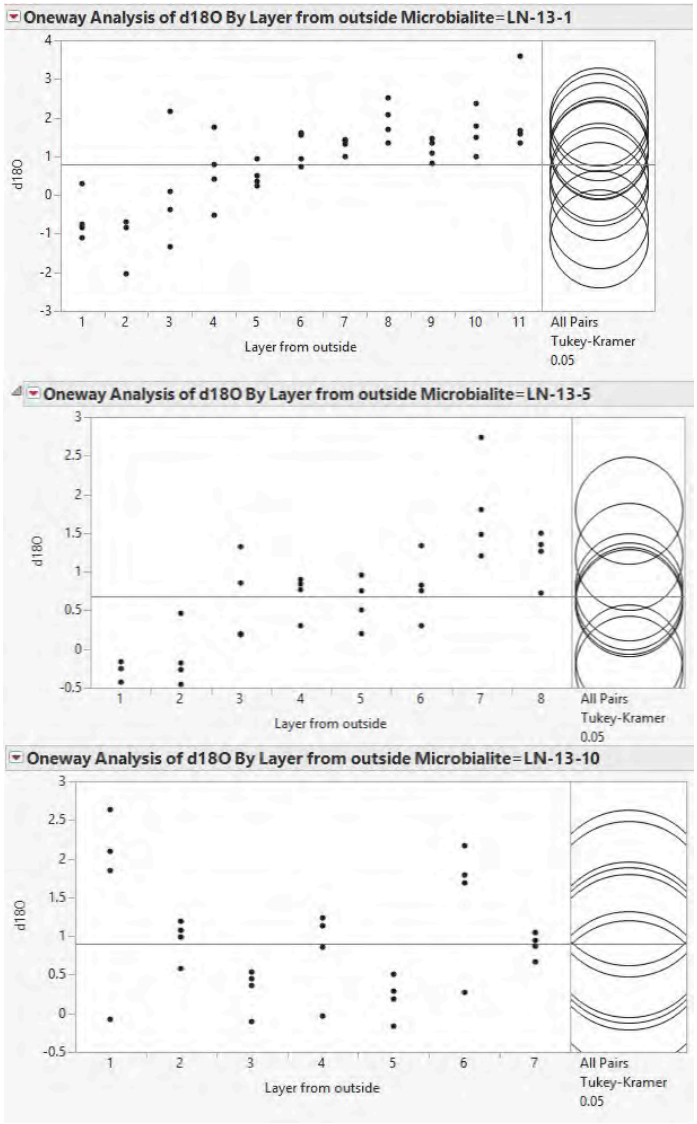

Figure 50: Screen shots of Tukey range testing of significant differences in observed oxygen isotope values in microbialites LN-13-1, LN-13-5, and LN-13-10 using JMP software. Circles in right pane correspond to the mean values for laminae grouped as layers. Circles that are not touching are statistically significant at the 95% confidence interval.

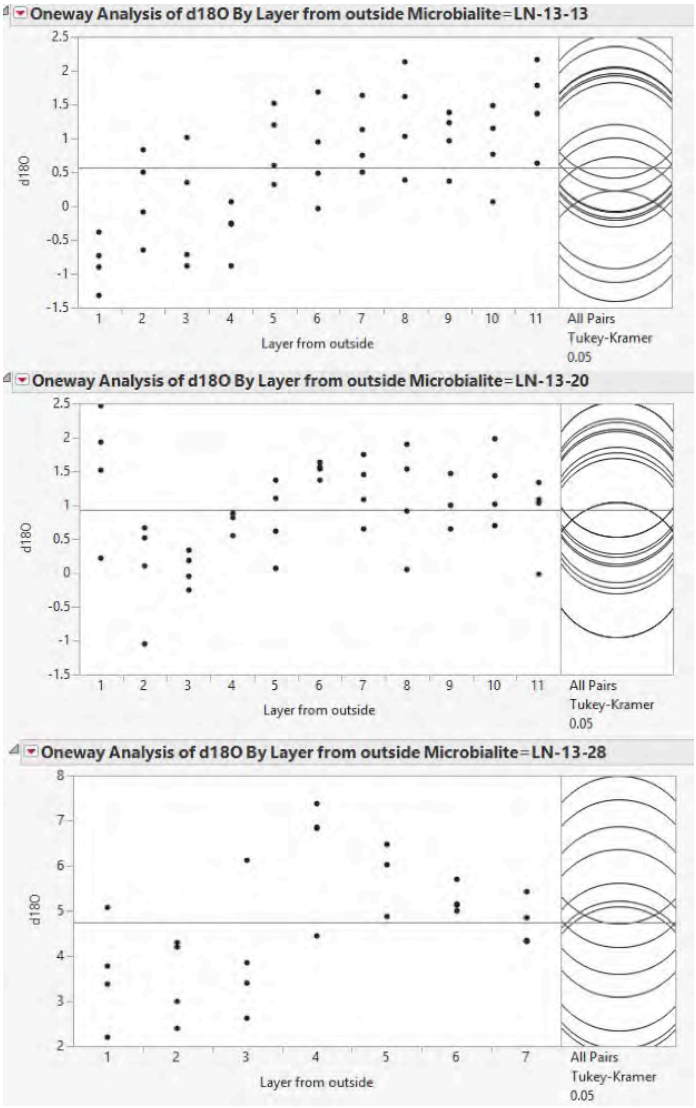

Figure 51: Screen shots of Tukey range testing of significant differences in observed oxygen isotope values in microbialites LN-13-13, LN-13-20, and LN-13-28 using JMP software. Circles in right pane correspond to the mean values for laminae grouped as layers. Circles that are not touching are statistically significant at the 95% confidence interval.

Connecting Letters Report

LN-13-1

Level		Mean
10	A	12.822857
11	A B	12.273645
9	A B	12.074126
8	A B C	11.672500
6	A B C D	11.507884
5	B C D	10.300384
7	B C D	10.233152
4	C D E	9.863517
3	D E	9.477500
2	E F	8.007500
1	F	7.015335

Connecting Letters Report

LN-13-13

Level		Mean
9	A	10.670283
10	A B	10.298204
8	A B	10.182500
7	A B	10.175981
11	A B C	9.270339
6	A B C	9.184162
5	B C	8.826353
2	B C	8.812500
4	C D	8.298358
3	C D	7.957500
1	D	6.743172

Connecting Letters Report

LN-13-5

Level		Mean
8	A	12.163038
7	A B	11.680188
6	A B C	10.397462
5	B C D	9.772500
4	C D	9.033069
2	C D	8.683181
3	C D	8.460690
1	D	7.595000

Connecting Letters Report

LN-13-20

Level		Mean
9	A	11.345643
8	A B	10.457128
10	A B	10.348890
7	A B C	10.126745
6	A B C D	10.022910
5	B C D	9.396977
11	B C D	9.229332
4	B C D	9.144159
3	B C D	8.728407
2	C D	8.392077
1	D	8.296062

Connecting Letters Report

LN-13-10

Level		Mean
6	A	10.534426
7	A	10.239372
2	A	10.133320
4	A	9.953436
1	A	9.692500
5	A	9.417500
3	A	9.241937

Connecting Letters Report

LN-13-28

Level		Mean
4	A	15.315000
6	A B	14.382500
5	A B	13.047413
7	A B C	12.456235
3	B C	11.631602
1	C	9.375000
2	C	9.135000

Figure 52: Connecting letter report for carbon isotopes. Levels are layers from outside, composed of groupings of four laminae. Levels not connected by the same letter are statistically different.

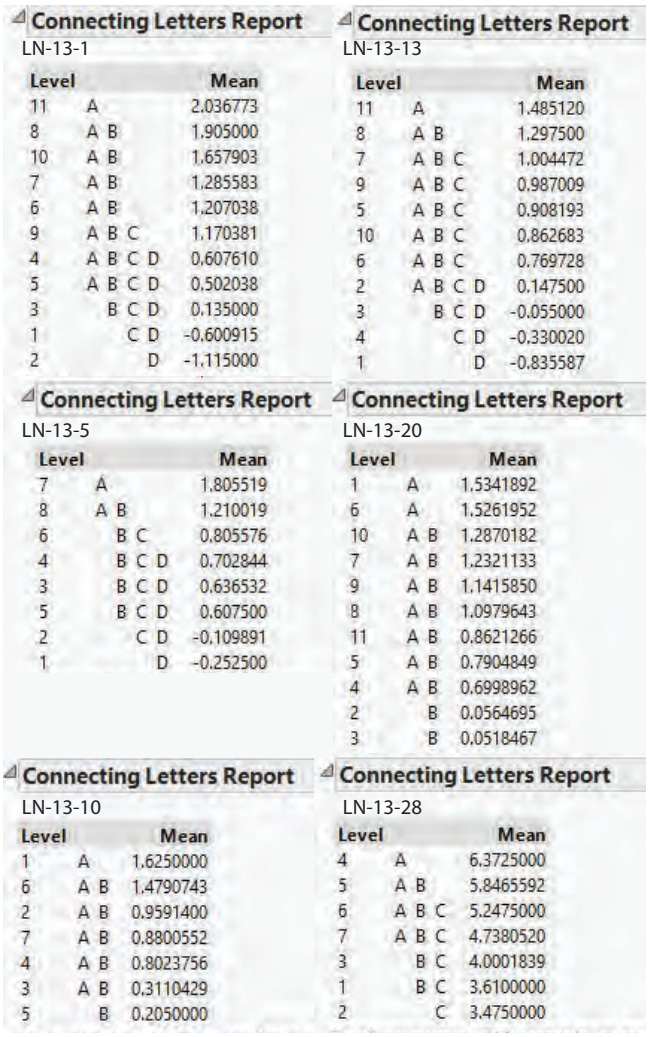

Connecting Letters Report

LN-13-1

Level					Mean
11	A				2.036773
8	A	B			1.905000
10	A	B			1.657903
7	A	B			1.285583
6	A	B			1.207038
9	A	B	C		1.170381
4	A	B	C	D	0.607610
5	A	B	C	D	0.502038
3		B	C	D	0.135000
1			C	D	-0.600915
2				D	-1.115000

Connecting Letters Report

LN-13-13

Level					Mean
11	A				1.485120
8	A	B			1.297500
7	A	B	C		1.004472
9	A	B	C		0.987009
5	A	B	C		0.908193
10	A	B	C		0.862683
6	A	B	C		0.769728
2	A	B	C	D	0.147500
3		B	C	D	-0.055000
4			C	D	-0.330020
1				D	-0.835587

Connecting Letters Report

LN-13-5

Level					Mean
7	A				1.805519
8	A	B			1.210019
6		B	C		0.805576
4		B	C	D	0.702844
3		B	C	D	0.636532
5		B	C	D	0.607500
2			C	D	-0.109891
1				D	-0.252500

Connecting Letters Report

LN-13-20

Level					Mean
1	A				1.5341892
6	A				1.5261952
10	A	B			1.2870182
7	A	B			1.2321133
9	A	B			1.1415850
8	A	B			1.0979643
11	A	B			0.8621266
5	A	B			0.7904849
4	A	B			0.6998962
2		B			0.0564695
3		B			0.0518467

Connecting Letters Report

LN-13-10

Level					Mean
1	A				1.6250000
6	A	B			1.4790743
2	A	B			0.9591400
7	A	B			0.8800552
4	A	B			0.8023756
3	A	B			0.3110429
5		B			0.2050000

Connecting Letters Report

LN-13-28

Level					Mean
4	A				6.3725000
5	A	B			5.8465592
6	A	B	C		5.2475000
7	A	B	C		4.7380520
3		B	C		4.0001839
1		B	C		3.6100000
2			C		3.4750000

Figure 53: Connecting letter report for oxygen isotopes. Levels are layers from outside, composed of groupings of four laminae. Levels not connected by the same letter are statistically different.

Appendix H: Principal Component Analysis

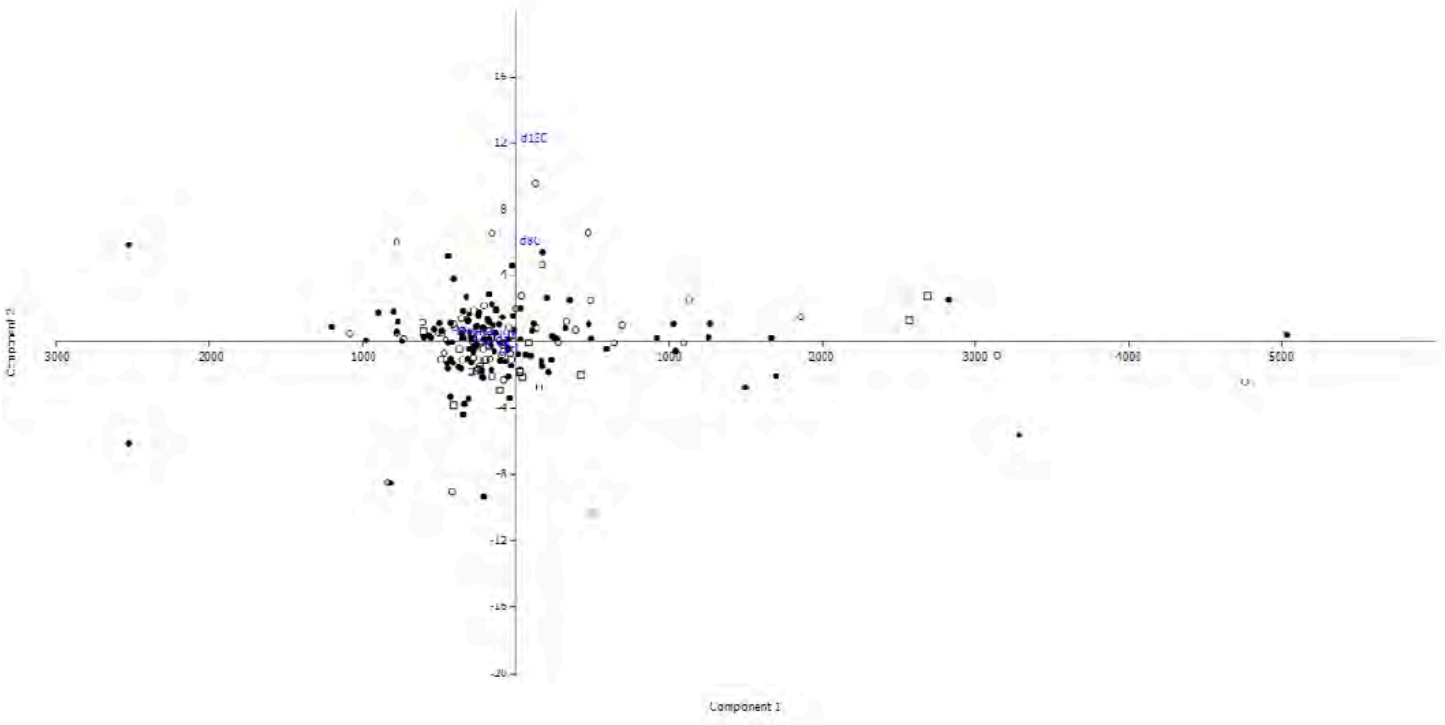
Component 2
Component 1
d13C
d18O
16
12
8
4
-4
-8
-12
-16
-20
3000
2000
1000
1000
2000
3000
4000
5000

Vita

Joy Buongiorno was born on November 7th, 1989 in Brooklyn, New York and later moved to middle Tennessee where she attended middle and high school. Despite hardships at home, she maintained excellent grades at Hendersonville High School, where she was the president of the National Honor Society and graduated within the top ten percent of her class. At age 17, she enrolled in Tennessee Technological University to study biology. While pursuing her Bachelor of Science degree, she received several academic awards, was inducted into multiple honor societies, instructed laboratories, supervised the biology department's live herpetological collection, and was a model with the Wilhelmina agency in Nashville. After graduating *summa cum laude* in biology, she moved to east Tennessee to pursue a Master's degree in geology at the University of Tennessee. She has been awarded several small grants from outside of the university to fund her research that she has presented at national and international conferences. In 2014, she was accepted into the microbiology graduate program at the University of Tennessee and was awarded the Chancellor's award to pursue a doctoral degree.